CHAPTER 4

RESULTS AND DISCUSSIONS

This chapter describes the dynamic hysteresis behaviors and power-law scaling relations in form of hysteresis area $< A >$ as a function of frequency f and electric field E_0 expressed as

$$< A > \propto f^m E_0^n \tag{4.1}$$

where $< A >$ is hysteresis area, f is frequency, E_0 is field amplitude, m and n are exponents dependent on the dimensionality and symmetry of the system. The investigations are observed under the influence of frequency, electric field, temperature, and field-waveform in some ferroelectric materials; i.e. BaTiO$_3$ single crystal, BaTiO$_3$ bulk ceramic, $0.7Pb(Mg_{1/3}Nb_{2/3})O_3–0.3PbTiO_3$ single crystal, and $(1-x)Pb(Zr_{1/2}Ti_{1/2})O_3-(x)Pb(Zn_{1/3}Nb_{2/3})O_3$ ceramic systems (where $x = 0.1, 0.2, 0.3, 0.4,$ and 0.5). The domain structure and field-waveform-dependent hysteresis properties and scaling relations of these ferroelectric materials are presented and discussed in the following sections.

4.1   The dynamic hysteresis properties at room temperature

4.1.1 BT system

BT single crystals

The P-E hysteresis loops at different f but fixed E_0 (6.0 kV/cm), and at different E_0 but fixed f (100 Hz) are shown in Figure 4.1(a)-(b), respectively. The $<A>$, P_r, and E_C decrease with an increase of frequency, as shown in Figure 4.1(a). As

shown in Figure 4.1(b), for applied fields lower than the coercive field (E_C), the loop does not saturate. With further increase in E_0 beyond E_C, the loop area $<A>$, remnant polarization (P_r), and coercive field (E_C) increase until well saturated loop is achieved. Similar observations have been reported in ferroelectric thin films and bulk ceramics [7, 9, 13, 16-17, 127].
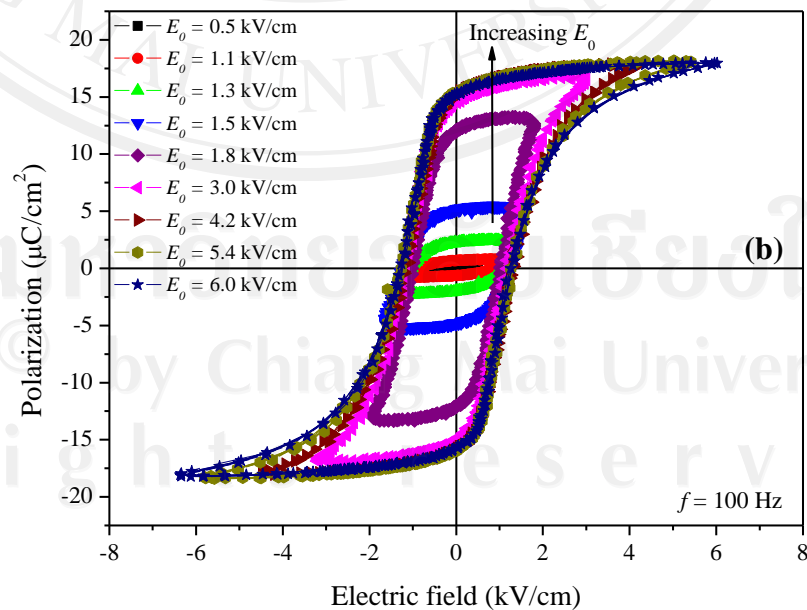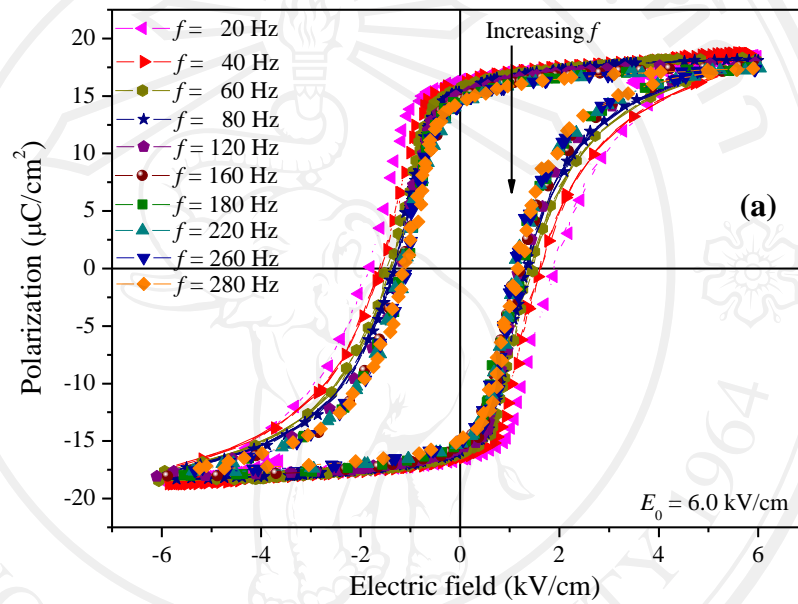
Figure 4.1 The *P-E* hysteresis loops for {100}-BaTiO$_3$ single crystal (a) at various *f* fixed E_0 = 6.0 kV/cm, and (b) at various E_0 fixed *f* = 100 Hz [24]

The profiles of hysteresis area < *A* > confirming decrease with increasing frequency *f* and increase with increasing field amplitude E_0 are shown in Figure 4.2(a)-(b).
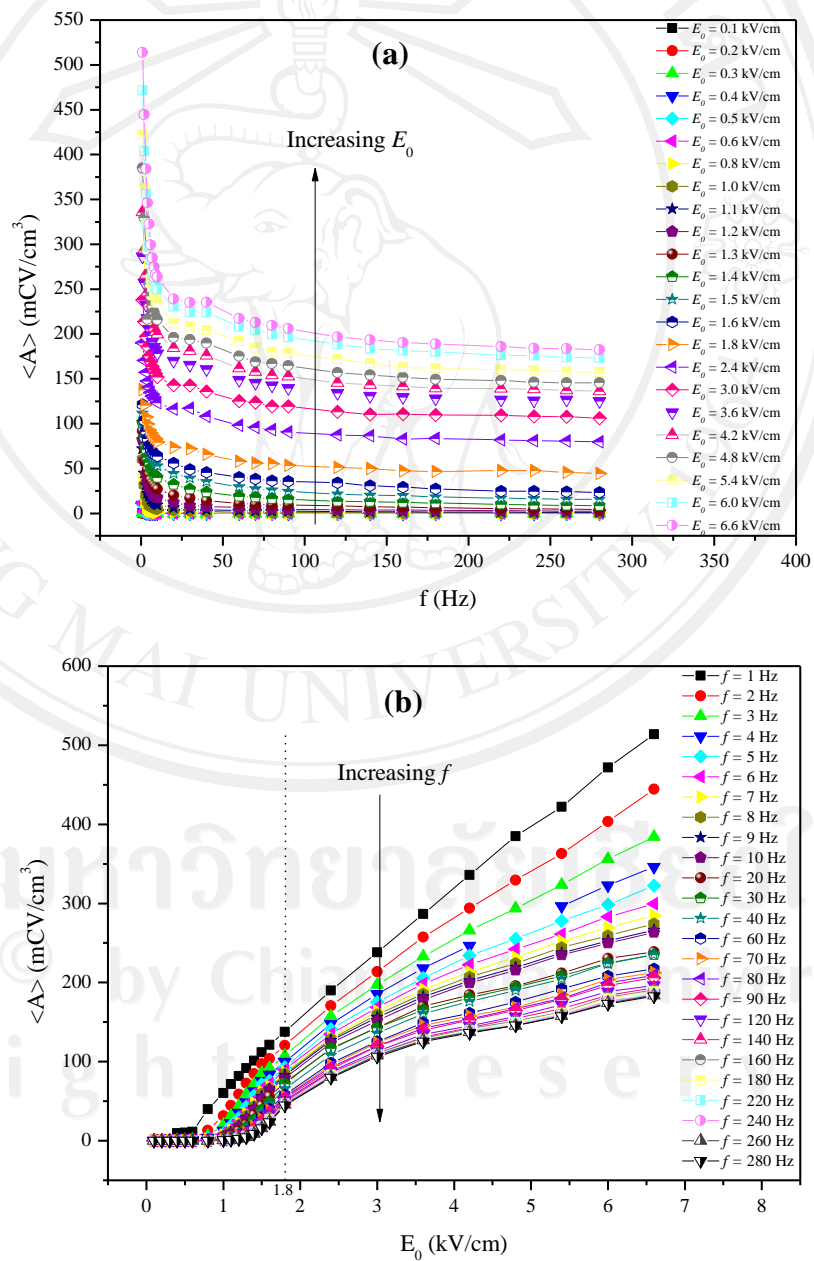
Figure 4.2 The hysteresis area $< A >$ profiles with evolutions of (a) frequency f, and (b) field amplitude E_0

As already established in previous investigations [16-17, 127], the scaling relations can be divided into two distinct regimes corresponding to sub-coercive field and saturated field condition which possess different domain switching mechanisms. The reversible 180° domain switching mechanism is responsible for changes occurring in sub-coercive field condition ($E_0 < E_C$) whereas the irreversible non-180° domain switching mechanism dominates in saturated field condition ($E_0 > E_C$) [24]. The same can be applied for the case of the $BaTiO_3$ single crystals, as seen in Figure 4.3(a)-(b) that the change in $< A >$ with E_0 follows two distinctly different trends with the applied field amplitude $E_0 = E_C$ (1.7 kV/cm) [121, 131] being a critical turning point. It should be noted that the E_C is generally frequency dependent [$E_C(f)$], but in this case the measuring frequency range is not too extensive to cause large variation in E_C, as seen in Figure 4.3(b). Thus, the fixed E_C of 1.7 kV/cm can be used effectively.

Thus, to obtain the scaling relations for the $BaTiO_3$ single crystals, one can fit the data with Equation (4.1) where exponents m and n are determined directly from the experimental data. By plotting $\log < A >$ against $\log f$ at fixed E_0, one obtains the exponent m. On the other hand, the exponent n can be obtained from plotting $\log <A>$ against $\log E_0$ at fixed f. In conjunction with the least square-fitting method, the methodology outlined above is applied to obtain the exponents m and n for the saturated loop ($E_0 > E_C$) and the minor loop ($E_0 < E_C$) data.
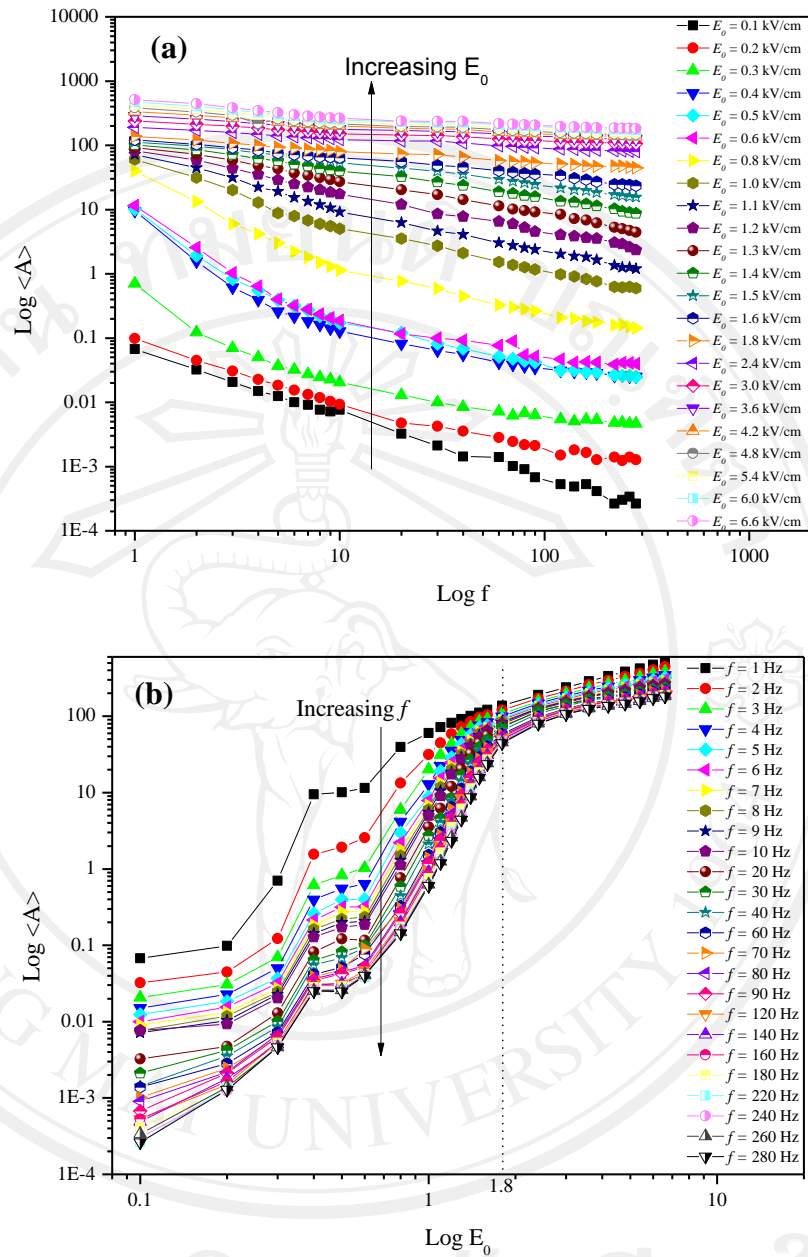
**Figure 4.3** Logarithmic plots between (a) log < A > and log f, and (b) log <A> and log E_0

In describing the physical meaning of scaling exponents, the f-exponent m refers to how quickly the domain can switch corresponding to frequency f of electric field switching. A higher negative magnitude for exponent m implies longer switching time where the ferroelectric domains cannot follow the applied ac electric field.

Several variables may cause the delay in domain switching including charged defects and space charges [138]. The polarization and hysteresis area $< A >$ decrease rapidly with increase of negative coefficient of m. On the other hand, if exponent m has lower negative coefficient, this implies that the switching time is short. The ferroelectric domains can follow the applied ac electric field, so the polarization and hysteresis area $< A >$ decreases slowly. The E_0-exponent n refers to the ease of domain wall motion. The high exponent n value refers to the ability of domain in following the applied electric field direction, so that hysteresis parameters ($< A >$, P_r, E_C) increase sharply with increasing E_0. Conversely, the low exponent n refers to the poor ability of domain switching in following the direction of applied electric field, so hysteresis parameters increase slowly [139].

Figures 4.4(a)-(b) show a variation in exponent m with E_0 and a variation in exponent n with f, respectively. Evidently, the two exponents depend slightly on the frequency f and significantly on the field amplitude E_0, with $E_0 = E_C$ being the critical turning point. The variations in both exponents obtained here are in strong contrast to most of the previous investigations [4-8, 10, 13, 18, 22, 132-134] in which the scaling exponents are normally treated as constant and depend only on the dimensionality and symmetry of the system, not the frequency f and field amplitude E_0, as stated previously in Equation (4.1).

From Figure 4.4(a), two linear relations can be obtained for the variation in f-exponent m with E_0. With $E_0 < E_C$, a strong field-dependent relation $m = (1.667)E_0 - 2.804$ (with $R^2 \sim 0.97$) is obtained, while a much weaker field-dependent relation $m = -(8.07 \times 10^{-3})E_0 - 0.163$ (with $R^2 \sim 0.93$) is attained at $E_0 > E_C$.

Furthermore, as displayed in Figure 4.4(b), two very weak frequency-dependent relations are obtained for the variation in E_0-exponent n with f, e.g., $n = (6.105 \times 10^{-4})f + 4.065$ (with $R^2 \sim 0.94$) and $n = (3.730 \times 10^{-4})f + 0.894$ (with $R^2 \sim 0.95$) for $E_0 < E_C$ and $E_0 > E_C$, respectively. It is important to point out that not only the complex scaling behaviors of a ferroelectric prototype BaTiO$_3$ single crystal are revealed but the relations expressed above also provide useful and critical information in understanding the scaling behaviors in other ferroelectric materials previously reported.
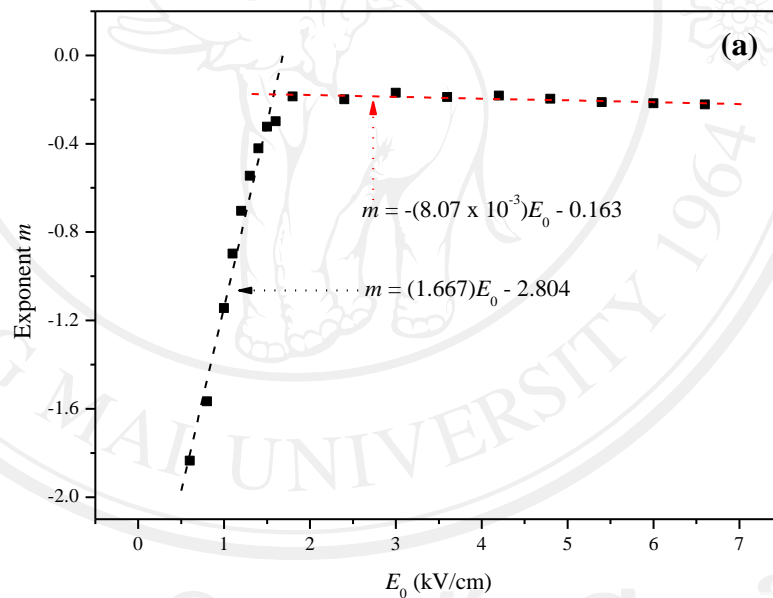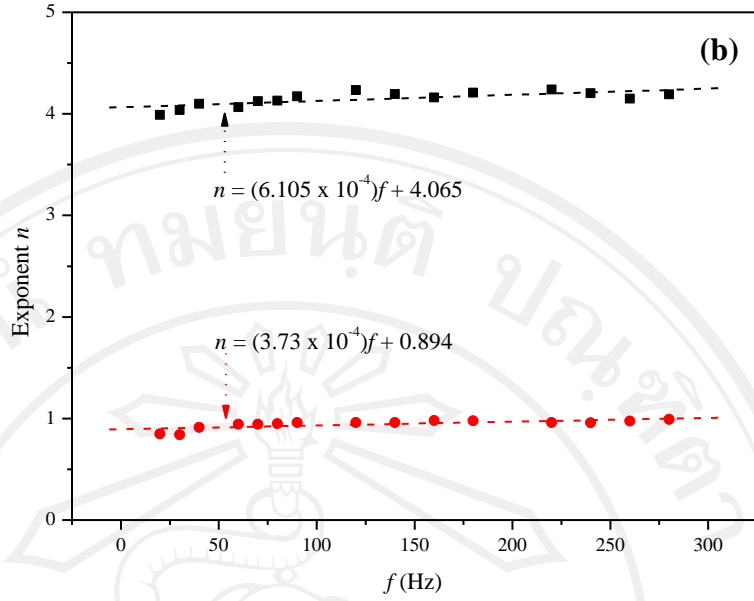
Figure 4.4 (a) Variation of f-exponent m with E_0, and (b) variation of E_0-exponent n with f in sub-coercive field $(E_0 < E_C)$ and saturated field $(E_0 > E_C)$ conditions. The dotted lines represent linear fitting [24]

Obviously, with very small coefficients to E_0 and f terms (for the whole range of E_0 and f used in this study), one can estimate the exponents $n = 4.157 \pm 0.092$ and $m = (1.667)E_0 - 2.804$ has to be used due to its strong field dependent nature when $E_0 < E_C$. As plotted in Figure 4.5(a), it is revealed that the minor loop data can be fitted very well ($R^2 \sim 0.99$), within the measured uncertainty, by

$$< A > \propto f^{1.667E_0 - 2.804} E_0^{4.157} \tag{4.2}$$

On the other hand, for the case of $E_0 > E_C$ the exponent $n = 0.950 \pm 0.056$ and $m = -0.195 \pm 0.016$ are estimated. Therefore, the scaling relation for the saturated loops of the BaTiO$_3$ single crystals takes the form of

$$< A > \propto f^{-0.195} E_0^{0.950} \tag{4.3}$$

which fitted reasonably well ($R^2 \sim$ 0.92) with the saturated loop data at each E_0, as plotted in Figure 4.5(b).
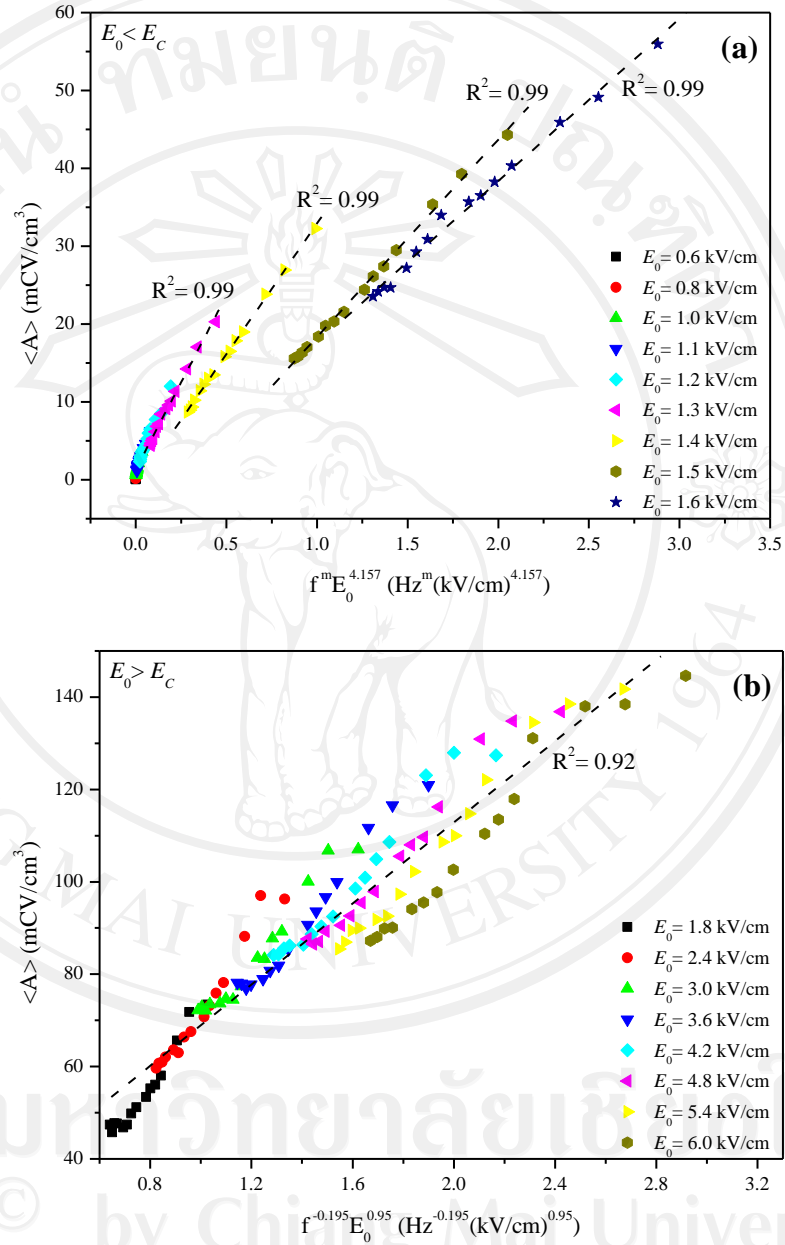
Figure 4.5 Power-law scaling relations of hysteresis for {100}-BaTiO$_3$ single crystals (a) $< A >$ against $f^{\,m}E_0^{\,4.157}$ for sub-coercive field ($E_0 < E_C$), and (b) $< A >$ against $f^{\,-0.195}E_0^{\,0.95}$ for saturated field ($E_0 > E_C$) conditions. The dotted lines represent linear fitting [24]

The scaling relation obtained in Equation (4.3) for the saturated loops of BaTiO$_3$ single crystals indicates that $< A >$ decays more slowly with f and grows more slowly with E_0 than the theoretical prediction from $(\Phi^2)^2$ and $(\Phi^2)^3$ models, as well as most of the other ferroelectric materials in both thin-film and bulk forms, as compared in Table 4.1. In the saturated loop case, when comparing the E_0-exponent n listed in Table 4.1, it is very interesting to observe that the n value (approximately 1) in our present study on BaTiO$_3$ single crystal is similar to those obtained earlier for the bulk ceramics and that directly estimated from Monte Carlo method based on Q-state planar Potts model [13], while it is much lower than those derived from $(\Phi^2)^2$ and $(\Phi^2)^3$ models and ferroelectric thin films ($n \sim 2$–3). A qualitative explanation for the difference may come from the polarization-interaction terms as considered in the $(\Phi^2)^2$ and $(\Phi^2)^3$ models, in which the polarization flip just has one contribution, i.e., polarization reversal [4-5]. Similarly, as explained thoroughly in our previous reports [16, 18], main polarization switching contribution in thin films would also be from the 180° domain reversal. Hence, a similar polarization switching kinetics is expected in the two cases. On the other hand, in the single crystals and bulk ceramics, there are influences of many depolarizing effects [16] arisen from domain walls, boundaries, space charges, immobile defects, etc., which may retard the external field. Consequently, the energy barrier is very much higher, which leads to slower polarization-flip kinetics. Therefore, a lower exponent for the E_0 term is expected in these types of materials. A more quantitative approach to explain a near linear dependence of hysteresis area with electric field amplitude E_0 can be drawn upon the domain reversal nature through the nucleation and growth concept [135], which is theoretically established very nicely for BaTiO$_3$ materials [6-7]. Here the domain

reversal can be characterized by an effective characteristic time [combining simultaneous contributions from both the new domain nucleation rate ($\tau_n \propto E_0^{-2/3}$) and the domain boundary motion velocity ($\tau_v \propto E_0^{-4/3}$)] $\tau' = \sqrt{\tau_n \tau_v} \propto E_0^{-1}$ [133-136]. If this effective characteristic time represents the response of the domain reversal to the varying external field at a given frequency, it should be inversely proportional to the hysteresis area $< A >$. Therefore, it can be assumed that $< A > \propto E_0$, which is in very good agreement with the present study. Furthermore, in the case of saturated loops, the f-exponent m of $BaTiO_3$ single crystal is smallest in absolute value among those listed in Table 4.1. In our previous reports, the depolarizing effects, acting as a buffer to polarization reversal mechanism, are already discussed as the reason of a relatively weaker dependence on f in bulk ceramics than that observed in thin films and predicted from theoretical models [16-17]. As for the smallest response to f in the single models [16-17]. As for the smallest response to f in the single crystals, an explanation may simply be a result of a near saturation of polarization in the single crystals under the applied field beyond its coercive field, as shown in Figure 4.1(b), under which the crystal is nearly in a single-domain-like state, unlike in thin films and bulk ceramics with multidomain states [137-138]. This has resulted in a relatively weaker dependence on f than those observed in most of the other ferroelectric thin films and bulk ceramics. It should also be noted here that a deviation of the experimentally obtained scaling relations from the theoretical prediction may be due to the fact that the models [4-5] are relevant to the insulating defect-free single domain samples with very low dielectric anisotropy and low electro-elastic coupling, which clearly is not the case for the $BaTiO_3$ single crystals with a well-known large dielectric anisotropy [121, 137-138]. For the minor loop scaling relation in Equation

(4.2) and as listed in Table 4.1, the E_0-exponent n (~4.157) in the BaTiO$_3$ single crystals is approximately in the same order (3–4) as to that in PZT thin film [7, 13], as well as those in minor loops of PZT and PZN-modified PZT bulk ceramics [16-17, 127]. As explained in our previous investigations [16-17], this is attributed to the fact that the main polarization orientation mechanism in thin films and in sub-coercive field condition for single crystals and bulk ceramics is likely from the reversible 180° domain rotation (which also occurs at much faster rate than the irreversible process), as the irreversible non-180° domain switching is normally accompanied with mechanical strain, it occurs at higher E-field than 180° domain rotation does. Therefore, under low E-fields, one would expect the 180° domain rotation to occur first [23, 139-143]. This explains why the scaling behavior of the single crystals and bulk ceramics at low E fields is similar to that of thin films and why the response to E_0 at sub-coercive field occurs at much faster response (n ~2–4) than that at higher field amplitude (n ~1). It should also be noticed that the n = 4.157 obtained experimentally in this study agrees very well with the n value of 4 obtained from the previous simulation study using Monte Carlo method based on Q-state planar Potts model [13]. Another important implication of this study is the fact that the f-exponent m is strongly field dependent in sub-coercive field condition, as seen in Figure 4.4(a). This may provide a hint to explain such variation in the m value, as listed in Table 4.1, which may be caused from an experimental limitation to fully achieve the saturation state in most of the previous high-field dynamic hysteresis studies available in literature. In fact, the m value for all previous investigations falls between -0.195 (that of saturated loop of BaTiO$_3$ obtained here, believed to be the upper limit of the f exponent) and -1 [theoretically obtained from $(\Phi^2)^2$ and $(\Phi^2)^3$ models for non-

saturated loops]. The upper limit of the m value is believed to be related to available domain states in the material, previously proposed in our investigations [17, 127], or growth dimension in growth kinetics model proposed by Ishibashi and Orihara [144-145 based on Kolmogorov-Avrami model. Nonetheless, more investigations are clearly required to support this hypothesis. It should also be noticed that the scaling relations obtained in this current study is only applicable to high frequency limit. This is because at lower frequency range(< 1 Hz) another set of scaling relations must be formulated, as seen in both previous theoretical and experimental works that $< A >$ is rapidly increasing, then turning to zero at much lower frequency. In addition, the high frequency limit in prior investigations in thin films is usually in the range of 1–100 kHz, the maximum frequency of 300 Hz used in this study may not be viewed as a high frequency limit as compared to those cases. The range of excitation parameters in this study is limited by equipment used. The field amplitude used here is reasonable as saturated P-E loops are already obtained. Therefore, while the higher field amplitude could be obtained, no new information is revealed. The major limitation in this current study is probably the frequency range of 1–300 Hz, which seems rather narrow, as compared to previous investigations in thin films. However, this can be explained very easily. All of the previous investigations on scaling behavior of ferroelectric materials are on thin films. Therefore, it is much easier to apply only 1–10 V to obtain saturated P-E loops and most of the function generators can provide this voltage in very wide frequency range (0.0001 Hz to > 1 MHz). As a result, most of the previous investigations are carried out in boarder range, as compared to current study in much thicker samples. Since this work is carried out on single crystal plates with nearly 1 mm thick, the amplifier can only provide high electric field (6 kV/cm)

up to 300 Hz. Based on the arguments mentioned, the scaling relations are considered applicable within the range of the experimental conditions. Nevertheless, it is interesting to point out that, through extrapolation of the scaling relations presented in Figure 4.4 for exponents *m* and *n* to the range of field amplitude of 10–50 kV/cm and frequency of 1–10 kHz used in the case of many previous thin-film studies, one could easily obtain the exponents *m* and *n* close to those previously reported as listed in Table 4.1. For instance, with E_0 of 25 kV/cm and *f* of 5 kHz, the exponents *m* and *n* of -0.365 and 2.759 (as compared to -0.33 and 2–3 for thin films) can be obtained.
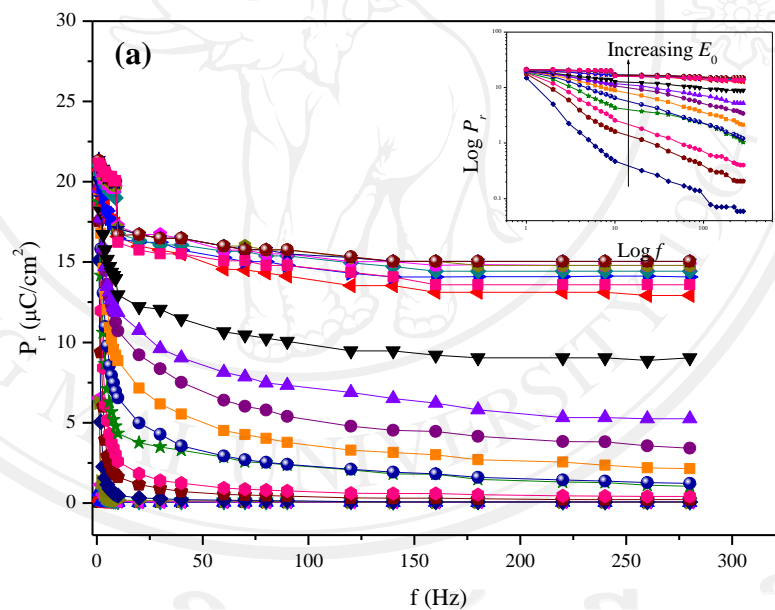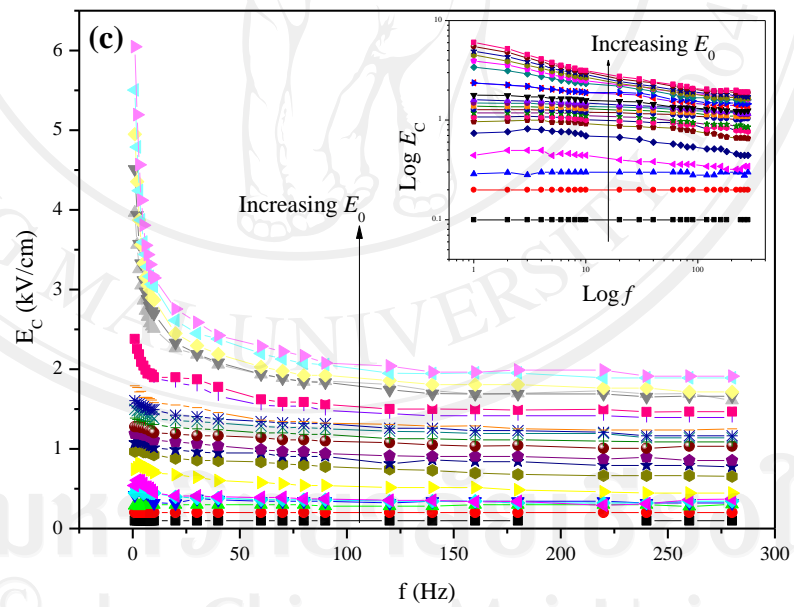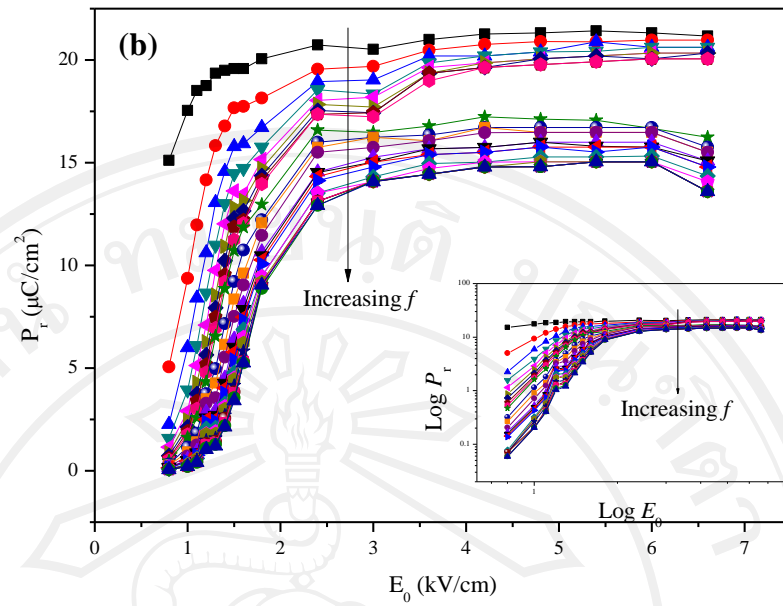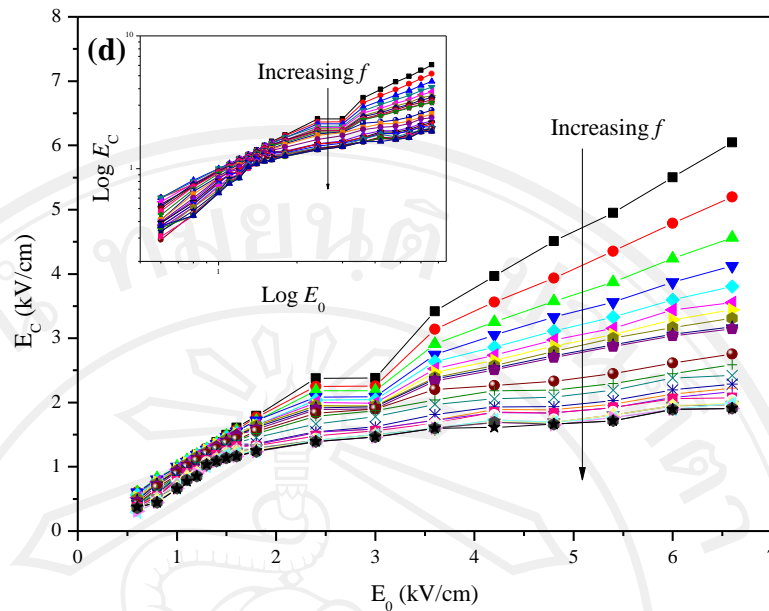
Figure 4.6 (a and b) The remnant polarization (P_r) profiles with evolutions of frequency f and field amplitude E_0, respectively, with insets of logarithmic plots, (c and d) the coercive field (E_C) profiles with evolutions of frequency f and field amplitude E_0, respectively, with insets of logarithmic plots [24]

More importantly, it should still be emphasized that the scaling relations obtained in this study is mostly applicable within the range of excitation parameters mentioned above. Finally, we look at the measured P_r and E_C as functions of f and E_0, as plotted in Figure 4.6. One can observe decaying of both P_r and E_C with f, while both parameters increase to saturation with E_0, as seen in Figure 4.6. As the frequency of the applied field increases, it is expected for P_r to decrease because some of the domains cannot follow the applied field. Hence, it takes lower electric field to force the polarizations to become zero, hence lower coercive field is observed. It is important to note that both P_r and E_C will not increase indefinitely as $f \rightarrow 0$. As reported in many previous investigations [6-7, 10, 13, 132-133, 145], the two parameters reach maxima at certain f, then begin to decrease to finite values (usually

called static P_r and E_C) as $f \rightarrow 0$. However, due to an equipment limitation such very low f range could not be performed in this study. Nonetheless, the measured P_r and E_c as functions of f seen in Figure 4.6 imply power-law relations between the two parameters and f, as also widely reported in literature [144-145]. On the other hand, as seen from Figure 4.6 rather complex relations with E_0 are obtained, hence will not be discussed here. Therefore, with least-square fitting method with $R^2 > 0.95$ (with some variation), the power law scaling of $P_r(f)$ and $E_C(f)$ for saturated loop data ($E_0 > 1.7$ kV/cm) takes the forms of

$$P_r \propto f^{0.079} \tag{4.4}$$

$$E_C \propto f^{0.164} \tag{4.5}$$

Since approaching saturation the hysteresis area can be roughly estimated with $(2P_r)(2E_C)$ [18, 146],so an empirical relation $< A > \propto f^{-0.243}$ is available from Equations (4.4) and (4.5). Although at fixed E_0 this relation is not too far from Equation (4.14) with $< A > \propto f^{-0.195}$, the difference in the f-exponent could arrive from the complex relations between P_r, E_C, and E_0, as displayed in Figure 4.6 and discussed above. Nonetheless, these two scaling methods seem to agree reasonably well [115, 147]. So once the scaling of area to the frequency is found, it is possible to guess how the E_C would scale with f if the scaling relation between P_r and f is known or vice versa.

Table 4.1 Scaling exponents in different ferroelectric materials [24]

| System	m	n
$(\Phi^2)^2$ and $(\Phi^2)^3$ models	-1	2
Q-state Potts model		
Saturated Loops	-	1
Minor Loops	-	4
Nd-doped $Bi_4Ti_3O_{12}$ thin-film	-0.33	2
$SrBi_2Ta_9O_4$ thin-film	-0.33	3
$Pb(Zr,Ti)O_3$ thin-films	-0.33	1
$PbTiO_3$/polymer Composite	-1	2
Soft PZT bulk ceramic		
Saturated Loops	-0.25	1
Minor Loops	-0.33	3
Hard PZT bulk ceramic		
Saturated Loops	-0.28	0.89
Minor Loops	-0.43	3.19
$Na_{0.5}Bi_{0.5}TiO_3$ ceramic		
Minor Loops	-0.39	2.63
{001}-$BaTiO_3$ single crystals		
Saturated Loops	-0.195±0.016	0.950±0.056
Minor Loops	$(1.667)E0$-2.804	4.157±0.092

BT bulk ceramics

The *P–E* hysteresis profiles with various E_0 (0-15 kV/cm) but fixed f (100 Hz) and various f (1-100 Hz) but fixed E_0 (15.0 kV/cm) for tetragonal BaTiO$_3$ bulk ceramic at room temperature are shown in Figure 4.7(a)-(b), respectively [126].
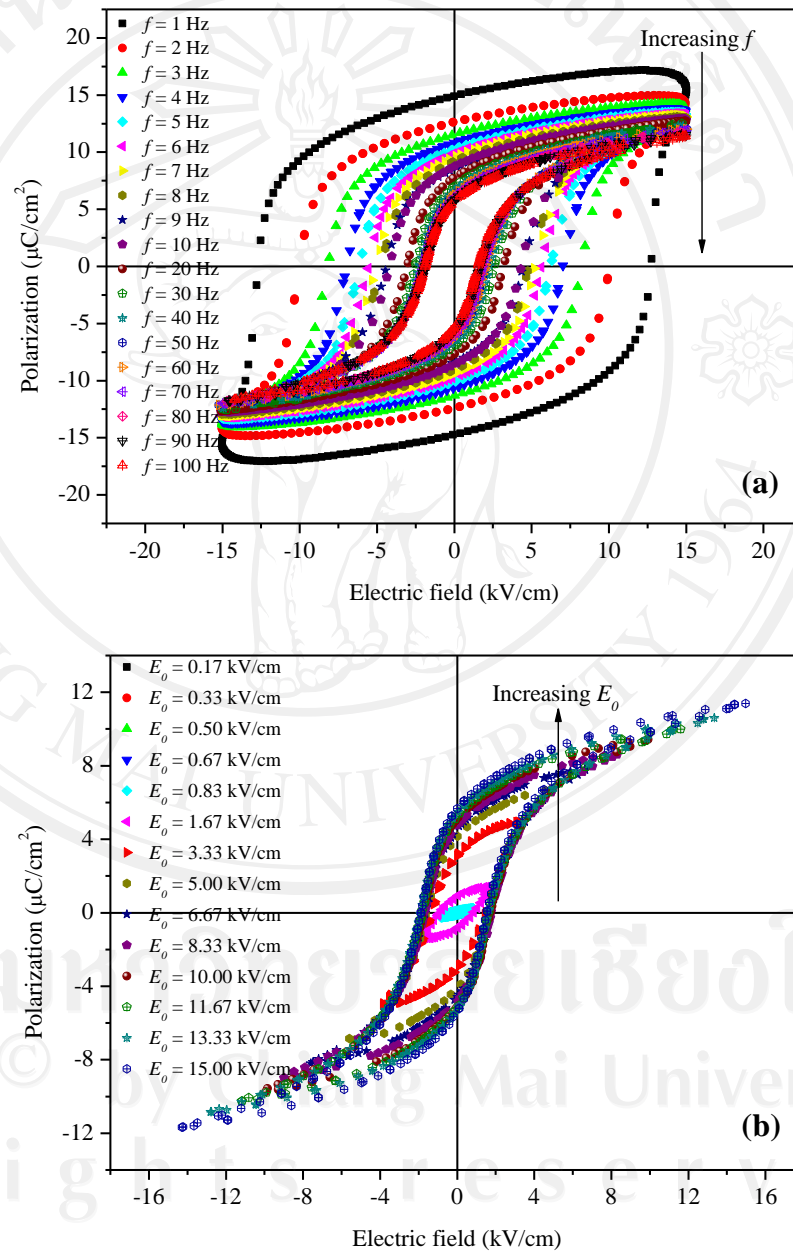

Figure 4.7 The *P-E* hysteresis loops for polycrystalline BaTiO$_3$ bulk ceramics (a) at various f fixed E_0 = 15 kV/cm, and (b) at various E_0 fixed f = 100 Hz [126]

At fixed E_0, remnant polarization (P_r) coercive field (E_C) and hysteresis area $<A>$ decrease with increasing frequency f due to the increase of the delayed response of the polarization reversal [148], as shown in Figure 4.7(a) and 4.8(a). At fixed f, for applied field lower than the coercive field (E_C), the loop does not saturate. With further increase in E_0 beyond E_C, remnant polarization (P_r), coercive field (E_C), and hysteresis area $< A >$ increase until well-saturated loop is achieved due to enlargement of electrical driving force, as shown in Figure 4.7(b) and 4.8(b). Similar observations have been reported in ferroelectric single crystals, thin-films, and bulk ceramics [7, 9, 13, 16-17, 24, 149].
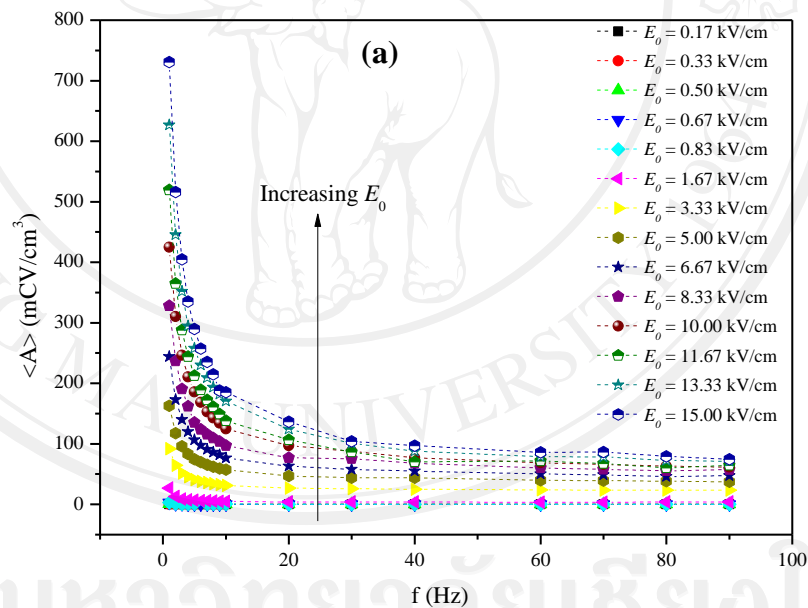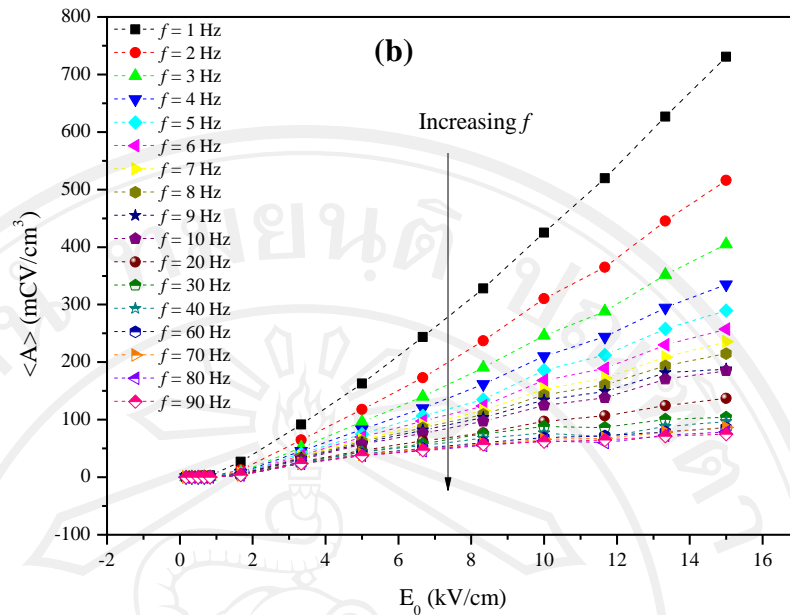
Figure 4.8 The hysteresis area $< A >$ profiles with evolutions of (a) frequency f, and (b) field amplitude E_0

As already established in previous investigations [16-17, 149], the scaling behavior can be divided into two distinct regimes; that for the saturated loops ($E_0 > E_C$) and the other for the minor loops ($E_0 < E_C$). The same can be applied for the case of the BaTiO$_3$ bulk ceramics, as seen in Figure 4.9(a)-(b) that there are two distinctly different trends with the applied field amplitude.

From Figure 4.9(b), it is reasonable to estimate $E_C = 3.33$ kV/cm as a critical turning point for BaTiO$_3$ bulk ceramics (as opposed to 1.67 kV/cm for BaTiO$_3$ single crystals) [24]. Thus, to obtain the scaling relations for the polycrystalline BaTiO$_3$ bulk ceramics, one can fit the data with Equation (4.1) where exponent m and n are determined directly from the experimental data. By plotting $\log < A >$ against $\log f$ at fixed E_0, one obtains the exponent m. On the other hand, the exponent n can be obtained from plotting $\log < A >$ against $\log E_0$ at fixed f [16-17]. In conjunction with

the least square-fitting method, the methodology outlined above is applied to obtain the exponents m and n from the saturated loop ($E_0 > E_C$) and the minor loop ($E_0 < E_C$) data.
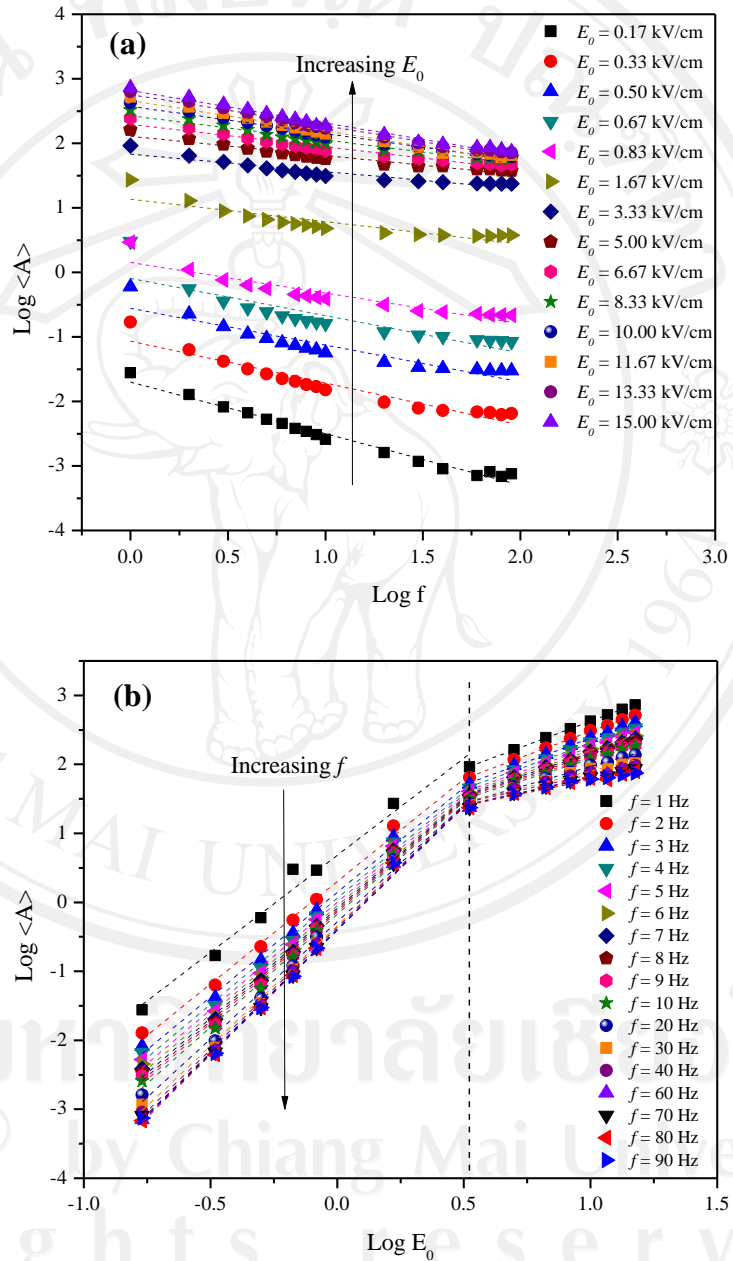

Figure 4.9 Logarithmic plots between (a) log $< A >$ and log f, and (b) log $<A>$ and log E_0. The dotted lines represent linear fitting

Figure 4.10(a)-(b) shows a variation of exponent m with E_0, and a variation of exponent n with f, respectively. Evidently, the two exponents depend slightly on the frequency f and significantly on the field amplitude E_0 with $E_0 = E_C$ being the critical turning point. The variations of both exponents obtained here are in strong contrast to most of the previous investigations [4-5, 7-8, 10, 13, 16-18, 127, 134], in which the scaling exponents are normally treated as constant and depend only on the dimensionality and symmetry of the system, not the frequency f and field amplitude E_0.

From Figure 4.10(a), two linear relations can be obtained for the variation of f-exponent m with E_0. With $E_0 < E_C$, $m = -0.593 + 0.112E_0$ is obtained, while $m = -0.184 - 0.022E_0$ is attained at $E_0 > E_C$. On the other hand, as displayed in Figure 4.10(b), two weak frequency-dependent non-linear relations are obtained for the variation of E_0-exponent n with f for both $E_0 < E_C$ and at $E_0 > E_C$. It is important to point out that, not only the complex scaling behaviors of a ferroelectric prototype BaTiO$_3$ bulk ceramics are revealed, but the relations expressed above also provide useful and critical information in understanding a variation in the scaling behaviors in other ferroelectric materials previously reported.

The variation of E_0-exponents n with f obtained here is similar to that in BaTiO$_3$ single crystals [24], while the f-exponent m variation with E_0 shows a little discrepancy with that of BaTiO$_3$ single crystals [24]. The slopes of the linear relations are noticeably different from BaTiO$_3$ single crystals [24].
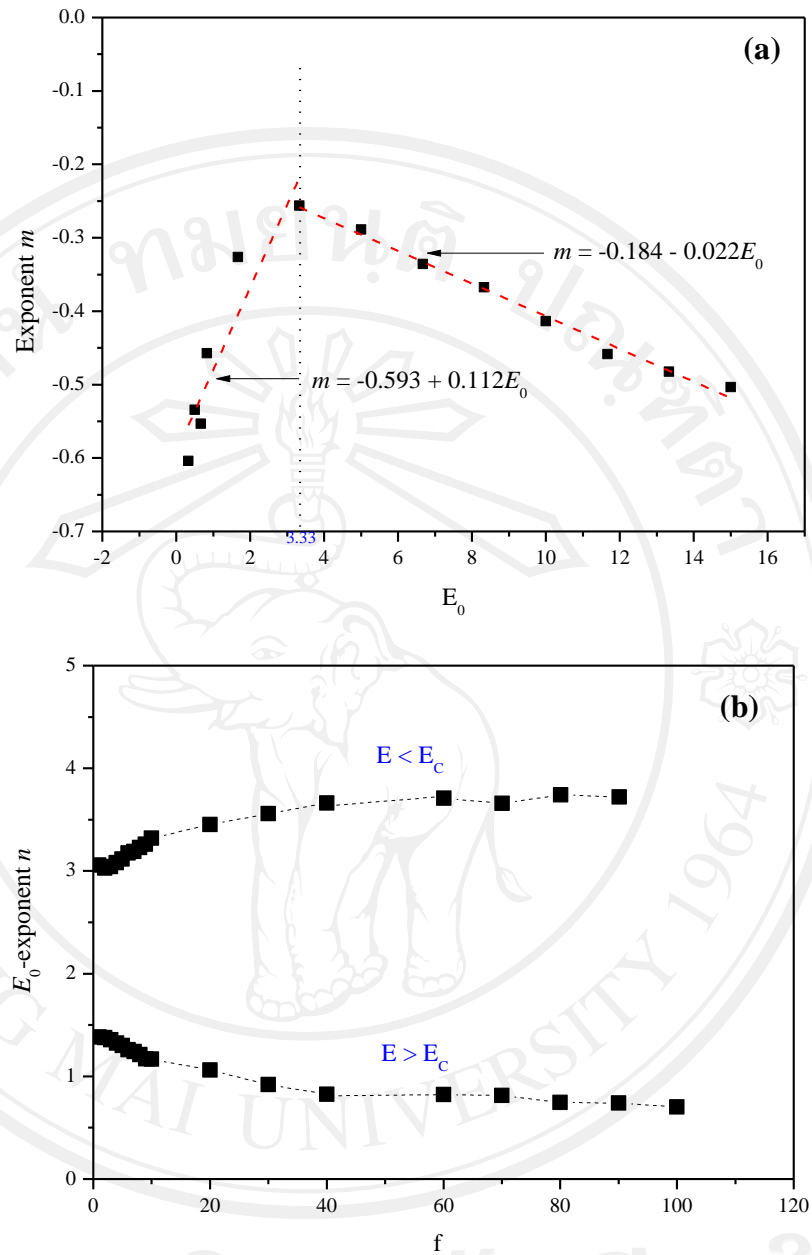
Figure 4.10 (a) Variation of f-exponent m with E_0, and (b) variation of E_0-exponent n with f under sub-coercive field ($E_0 < E_C$) and beyond coercive field ($E_0 > E_C$) conditions. The dotted lines represent data linear fitting in each range [126]

For a better comparison, approximations of exponent values of both f-exponent m and E_0-exponent n are obtained. At $E_0 < E_C$, the exponents m are averaged to a mean value of -0.55 and n of 3.40. As plotted in Figure 4.11(a), it is revealed that

the minor loop data can then be fitted reasonably well ($R^2 \sim 0.97$), within the measured uncertainty, by

$$< A > \propto f^{-0.55} E_0^{3.40} \qquad \text{for} \qquad E_0 < E_C \qquad (4.6)$$

Additionally, for the case of $E_0 > E_C$, the exponents $n = 1.06$ and $m = -0.39$ are attained from approximation. Therefore, the scaling relation for the saturated loops of the polycrystalline $BaTiO_3$ bulk ceramics takes the form of

$$< A > \propto f^{-0.39} E_0^{1.06} \qquad \text{for} \qquad E_0 > E_C \qquad (4.7)$$

which can be fitted well ($R^2 \sim 0.96$) with the saturated loop data, as plotted in Figure 4.11(b). In the saturated loop case, it is very interesting to observe that the E_0-exponent n value for the polycrystalline bulk ceramics is very similar to that for the single crystals [24]. On the other hand, the f-exponent m is significantly higher, about two times in absolute value, than that of the $BaTiO_3$ single crystals. The difference may be results of a near saturation of polarization in the single crystal under the applied field beyond the coercive field, and of the depolarizing effects in polycrystalline bulk ceramics acting as a buffer to polarization-reversal mechanism resulting in slower domain switching [18, 127]. For the minor loop scaling relation, the E_0-exponent m (3.40) in the $BaTiO_3$ bulk ceramics is approximately the same as in $BaTiO_3$ single crystals [24]. As explained in previous investigations [18, 127], this is attributed to the fact that the main polarization orientation mechanism in thin-films and in sub-coercive field condition for bulk ceramics is likely from the reversible 180º domain rotation (which also occurs at much faster rate than the irreversible process), as the irreversible non-180º domain switching is normally accompanied with

mechanical strain, it occurs at higher E-field than reversible 180° domain rotation does. Therefore, under low E-fields, one would expect the reversible 180° domain rotation to occur first. This explains why the scaling behavior of the bulk ceramics at low E-fields is similar to that of thin-films and why the response to E_0 at sub-coercive field occurs at much faster response ($n \sim$ 2–4) than that at higher field amplitude ($n \sim$ 1). However, even $n = 3.40$ can be roughly considered as the same as that of BaTiO$_3$ single crystal, but these values still have some discrepancy. This may be an influence of many depolarizing effects [127], arisen from domain walls, boundaries, space charge, immobile defects, etc., which may restrain the external field. Consequently, the energy barrier is very much higher, which leads to slower polarization-flip kinetics [24]. Therefore, a lower exponent for the E_0 term is expected in polycrystalline BaTiO$_3$ bulk ceramics. More interestingly, when compared with previous studies in bulk ceramic materials such as commercial soft and hard PZTs, the exponents n obtained for both regimes are comparable to those of previously studied systems. On the contrary, the exponents m obtained in this study are noticeably different from those of previous ones for both regimes, as shown in Table 4.2. The possible cause may be the difference in measuring frequency range. Most of previous investigations are observed and established scaling relations in frequency range of 20–100 Hz, while this study scaling relation is performed in frequency range of 1–100 Hz. The different frequency ranges may cause different exponents m.
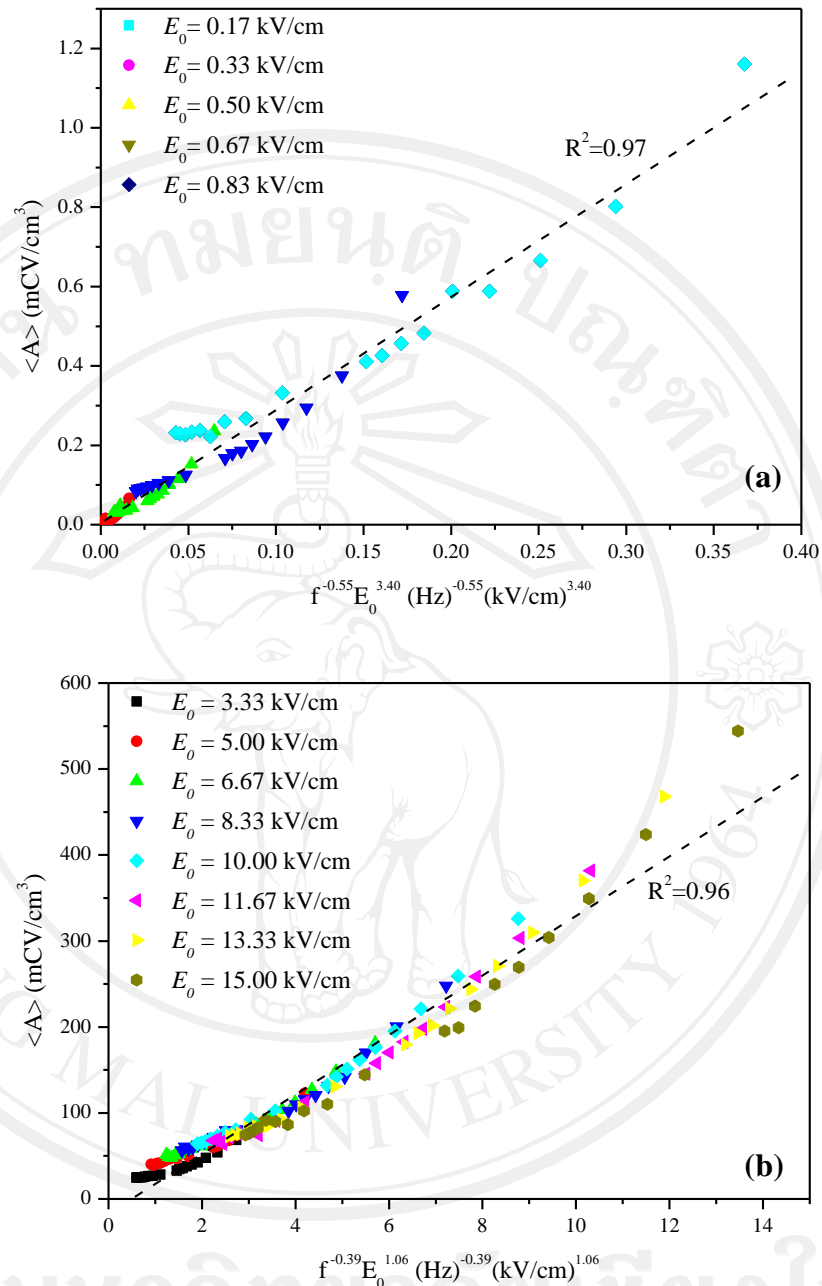
Figure 4.11 Power-law scaling relations of hysteresis for polycrystalline BaTiO$_3$ bulk ceramics (a) $< A >$ against $f^{-0.55}E_0^{3.40}$ for sub-coercive field ($E_0 < E_C$), and (b) $< A >$ against $f^{-0.39}E_0^{1.06}$ for saturated field ($E_0 > E_C$) conditions. The dotted lines represent linear fitting [126]

Hence, to confirm this hypothesis, the hysteresis behavior and scaling relations of the polycrystalline $BaTiO_3$ bulk ceramic are also examined in frequency range of 20–100 Hz. The f-exponent m and E_0-exponent n are extracted and shown variations in Figure 4.12(a)-(b).
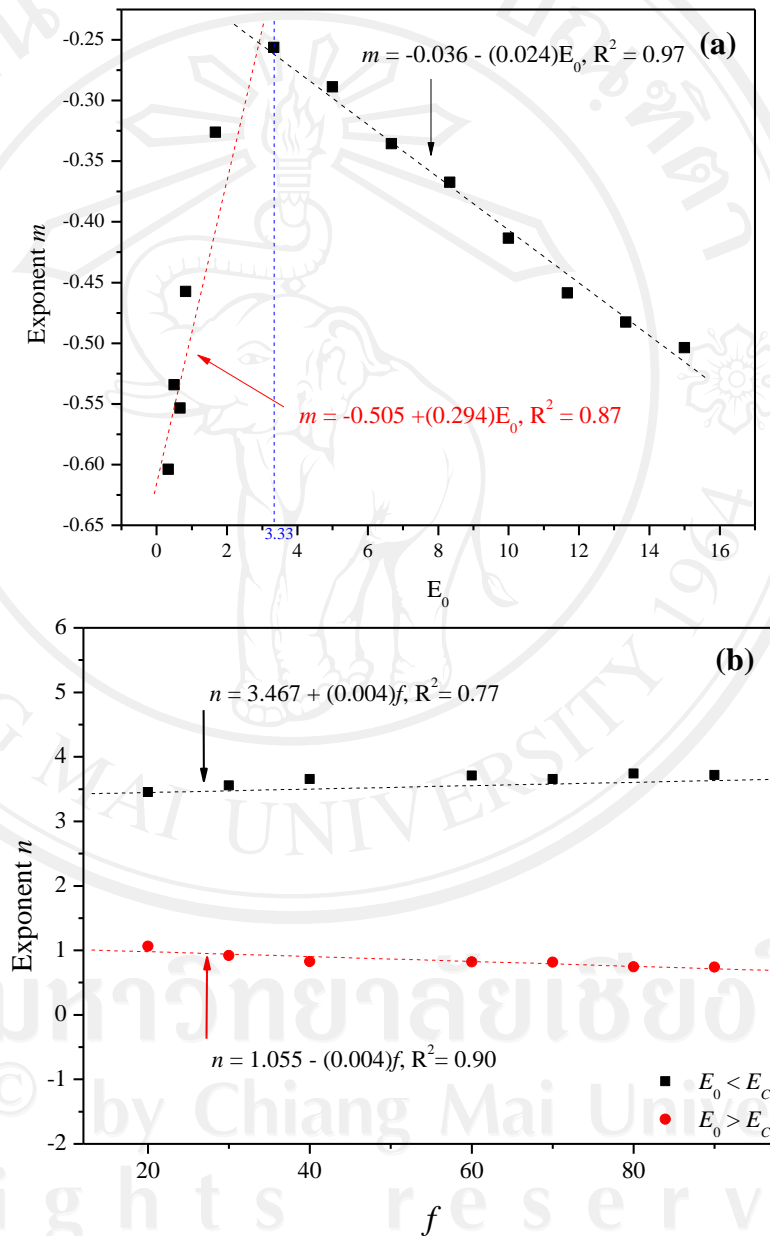
Figure 4.12 (a) Variation of f-exponent m with E_0, and (b) variation of E_0-exponent n with f under sub-coercive field ($E_0 < E_C$) and beyond coercive field ($E_0 > E_C$) conditions. The dotted lines represent data linear fitting in each range [176]

Based on the same methodology of exponent extraction, the exponents m and n in frequency range of 20–100 Hz are obtained for both minor and saturated loops. From Figure 4.12(a), two linear relations can be obtained for the variation of f-exponent m with E_0. With $E_0 < E_C$, $m = -0.505 + 0.294E_0$ is obtained, while $m = -0.036 - 0.024E_0$ is attained at $E_0 > E_C$. Furthermore, as displayed in Figure 4.12(b), two weak frequency-dependent relations are obtained for the variation of E_0-exponent n with f, e.g. $n = 3.467 + 0.004f$ and $n = 1.055 - 0.004f$ for $E_0 < E_C$ and $E_0 > E_C$, respectively.

Following Equation (4.1) and through first approximation, the scaling relations take the form of

$$<A> \propto f^{-0.32}E_0^{3.68} \qquad \text{for minor loop} \qquad (E_0 < E_C) \qquad (4.8)$$

and

$$<A> \propto f^{-0.25}E_0^{0.82} \qquad \text{for saturated loop} \qquad (E_0 > E_C) \qquad (4.9)$$

as seen in Figure 4.13(a)-(b). As expected, the obtained scaling relations are very similar to those of previous investigations, as summarized in Table 4.2. Consequently, this strongly suggests that the scaling relations depend significantly on the frequency range of observation.
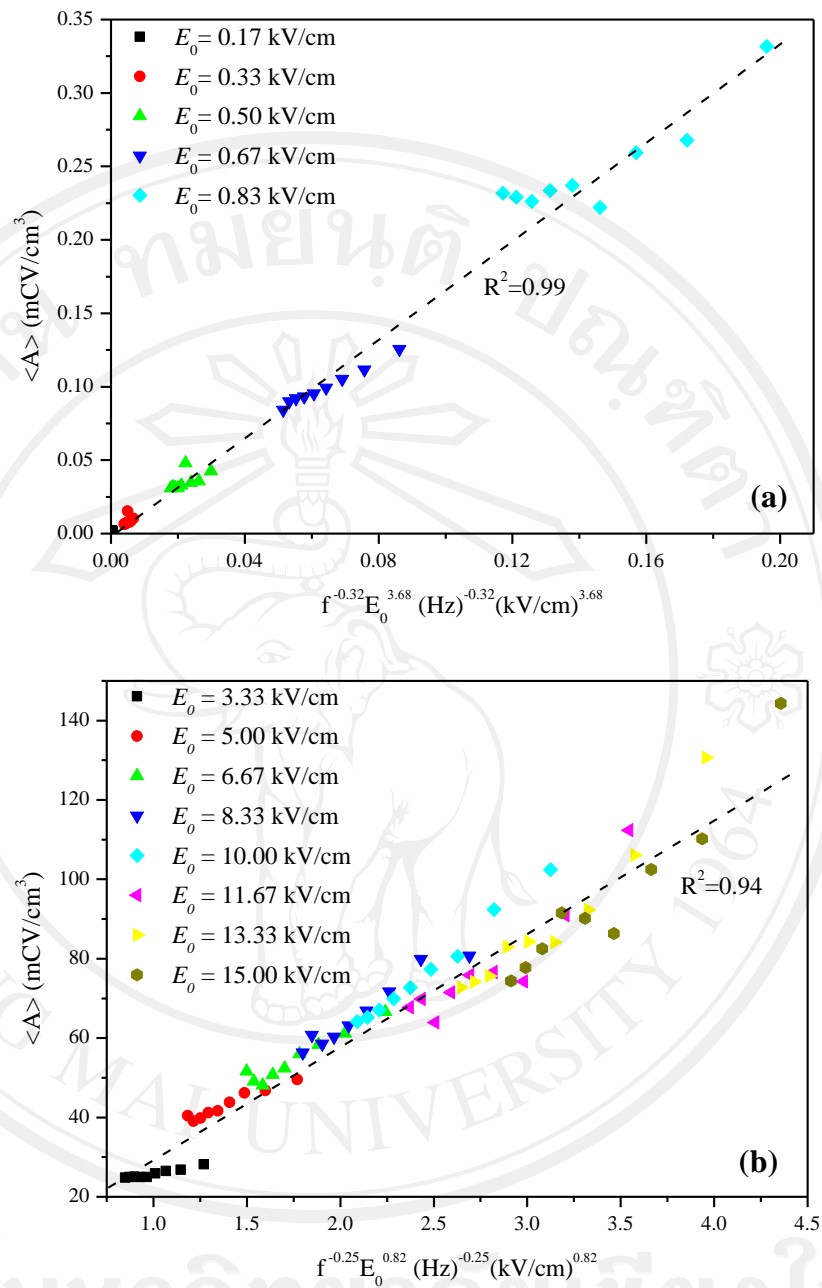
Figure 4.13 Power-law scaling relations for polycrystalline BaTiO$_3$ bulk ceramics with different observation f-range (a) scaling relations of $<A>$ against $f^{-0.32}E_0^{3.68}$ and (b) $<A>$ against $f^{-0.25}E_0^{0.82}$ for sub-coercive and saturated field conditions, respectively, with observed f-range of 20-100 Hz [126]

In addition to the scaling relations of hysteresis area $< A >$ against frequency f and electric field E_0, the scaling relations of the other hysteresis parameters: P_r and E_C, in the forms of

$$P_r \propto f^m E_0{}^n \tag{4.10}$$

and

$$E_C \propto f^m E_0{}^n \tag{4.11}$$

where m and n are exponents that depend on the dimensionality and symmetry of the system are also established to provide an additional dimension to the hysteresis behavior prediction through scaling relations. As seen in Figure 4.14, decaying of P_r and E_C with f can be observed. Both parameters increase to saturation with E_0. As the frequency of the applied field increases, it is expected for P_r to decrease because some of the domains cannot follow the applied field. Hence, it takes lower electric field to force the polarizations to become zero, so lower coercive field is observed [24].

Based on the same methodology, the exponent m and n for P_r-scaling relations are extracted by plotting $\log P_r$ against $\log f$ at fixed E_0 to obtain exponent m and plotting $\log P_r$ against $\log E_0$ at fixed f to obtain exponent n for both saturated and minor loops. Similarly, the exponent m and n for E_C-scaling relations are also extracted with the same methodology. Similar to the case of hysteresis area $< A >$, remnant polarization P_r and coercive field E_C also show the inter-correlation of f-exponent m with E_0 and E_0-exponent m with f, as displayed in Figure 4.15.
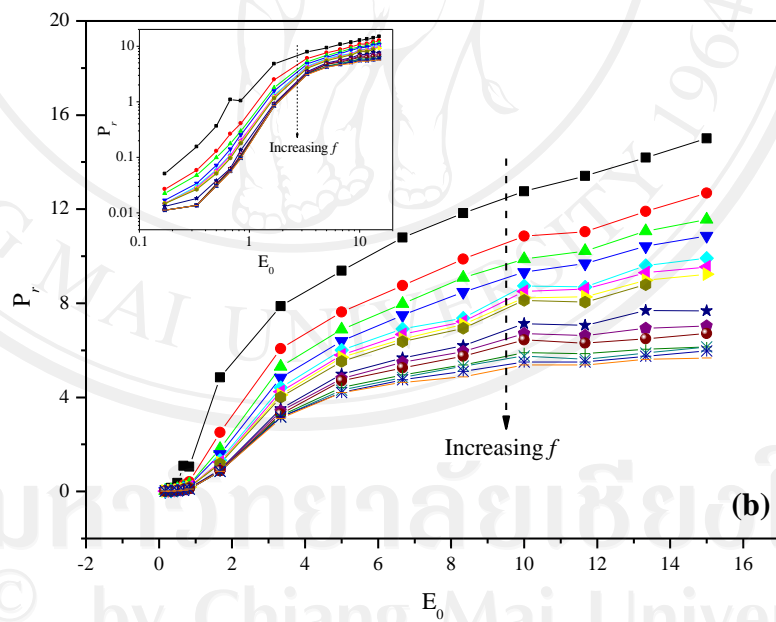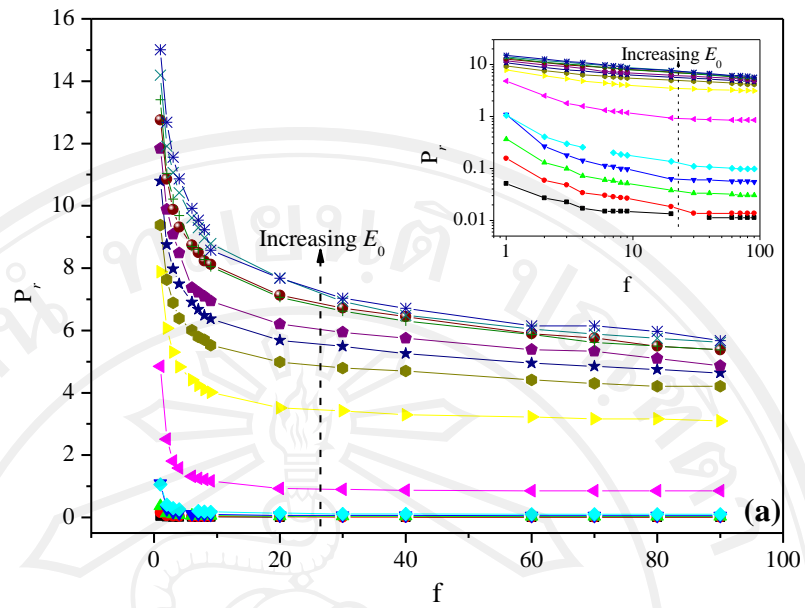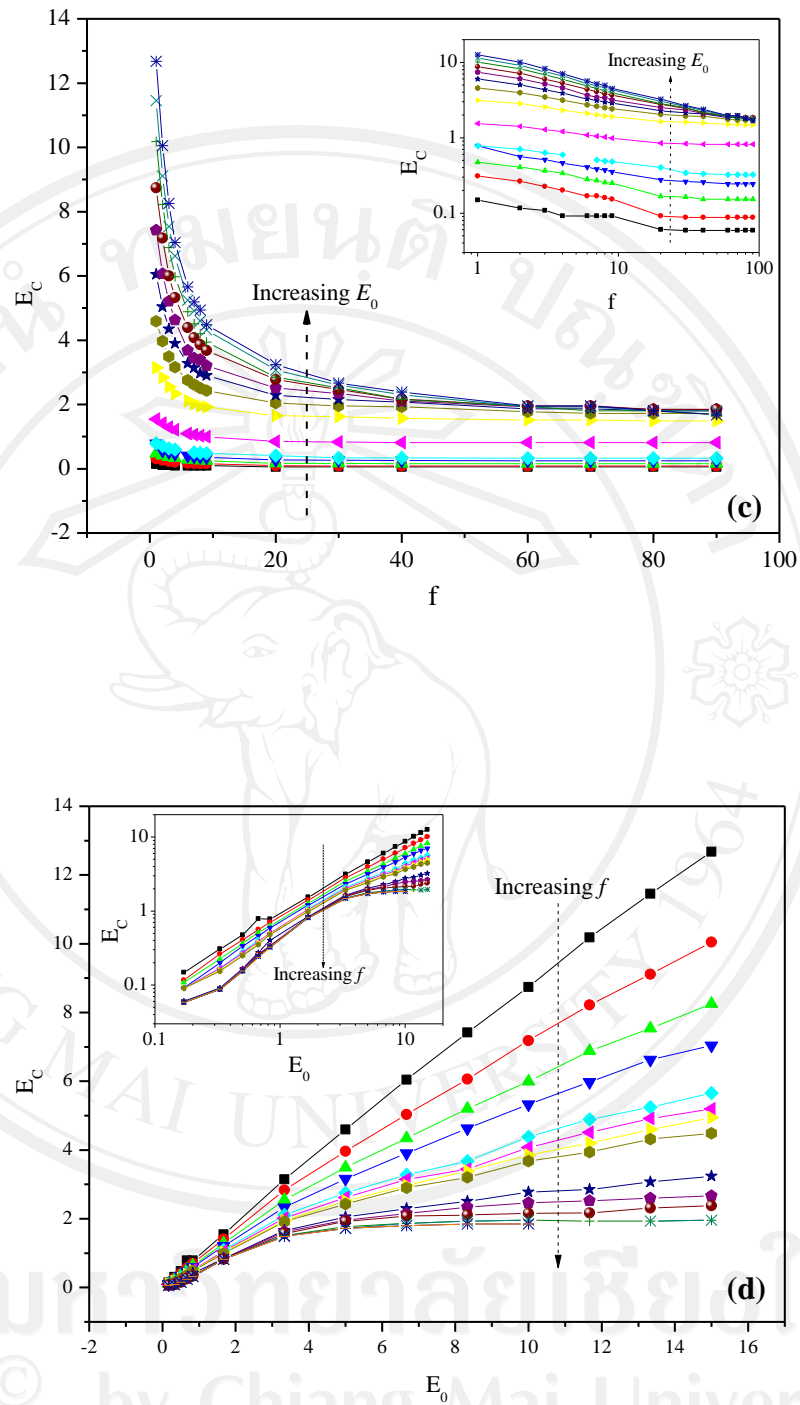
Figure 4.14 (a and b) The remnant polarization (P_r) profiles with evolutions of frequency f and field amplitude E_0, respectively, with insets of logarithmic plots, (c and d) the coercive field (E_C) profiles with evolutions of frequency f and field amplitude E_0, respectively, with insets of logarithmic plots

Figure 4.15 shows a variation of f-exponent m with E_0, and a variation of E_0-exponent n with f, respectively, for P_r- and E_C-scaling relations. Evidently, the exponent n of all scaling relations, P_r and E_C, depends slightly on the frequency f, while the exponent m depends significantly on the field amplitude E_0 with $E_0 = E_C$ being the critical turning point. From Figure 4.15(a)-(b), the linear relations can be obtained for the variation of f-exponent m with E_0. With $E_0 < E_C$ (3.33 kV/cm), strong field-dependent relations $m = (-0.524) + (0.028)E_0$ for P_r-scaling, and $m = (-0.301) + (0.054)E_0$ for E_C-scaling are obtained, while weaker field-dependent relations $m = (-0.146) + (-0.004)E_0$ for P_r-scaling, and $m = (-0.085) + (-0.027)E_0$ for E_C-scaling relations are attained at $E_0 > E_C$.

Furthermore, as displayed in Figure 4.15(b), the E_0-exponents n are slightly dependent on f for both regimes which can be explained by complex exponential relations that are not shown here. Notably, E_0-exponents n of each parameter relation are approaching a certain value at low frequency. These observations are very similar to those of BaTiO$_3$ single crystals [24]. Nonetheless, further experiments capable of very high frequency region will be needed to arrive at any conclusion. In addition, a variation of m and n relations in $E_0 < E_C$ and $E_0 > E_C$ regimes may be caused by the difference in polarization switching mechanisms, since a reversible 180° domain switching mainly controls the dynamic hysteresis in sub-coercive field condition [127, 150-157], while an irreversible non-180° domain switching is primarily responsible for above coercive field condition [127, 139, 152-157]. More importantly, Figure 4.15 clearly reveals that the f-exponent m is a function of E_0 and the E_0-exponent n is a function of f. The scaling relations can then be written in an inter-correlation form as $\langle A \rangle \propto f^{\,m(E_0)} E_0^{\,n(f)}$ for both $E_0 < E_C$ and $E_0 > E_C$ regimes. One can generally predict

hysteresis behavior in sub-coercive field and above coercive field from the scaling relations established in Figure 4.16.
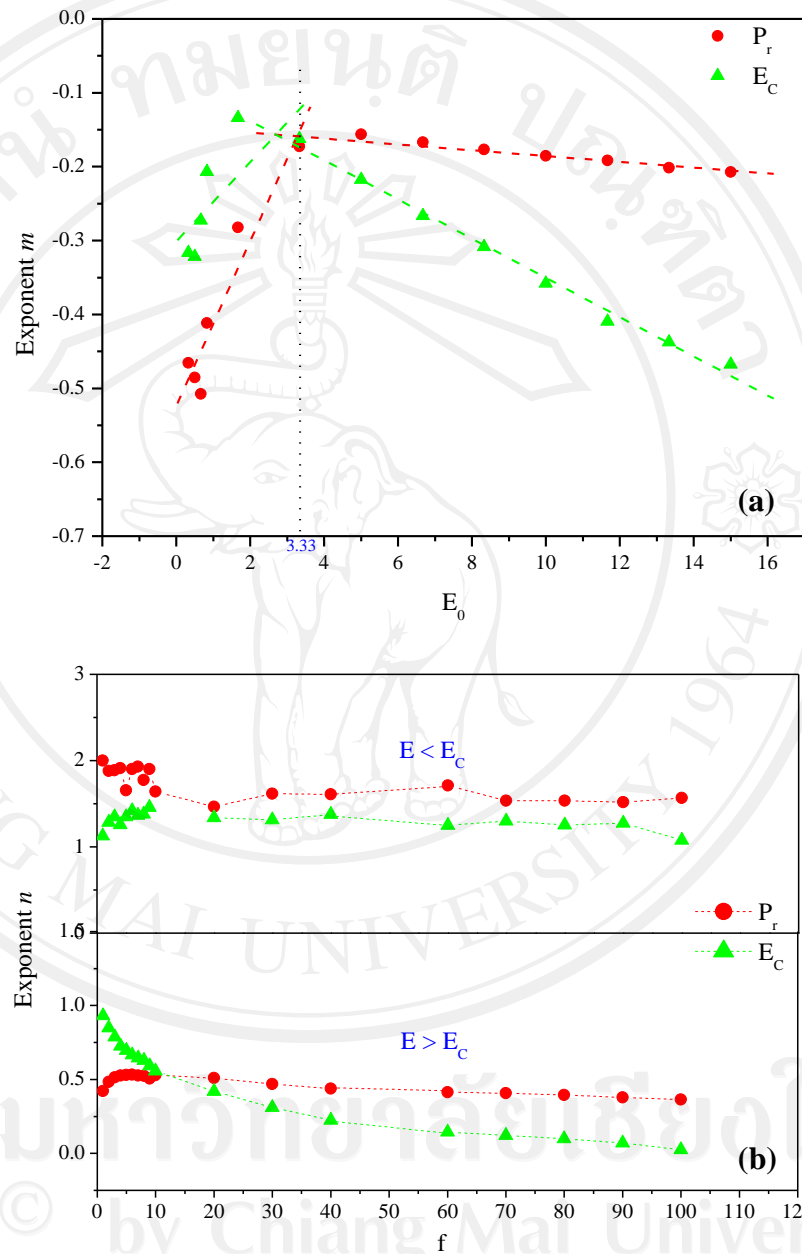
Figure 4.15 (a) Variation of f-exponent m with E_0, and (b) variation of E_0-exponent n with f under sub-coercive field ($E_0 < E_C$) and beyond coercive field ($E_0 > E_C$) conditions. The dotted lines represent linear fitting [126]

Through an approximation, the P_r-scaling relations for minor ($E_0 < E_C$) and saturated ($E_0 > E_C$) loops take a form of $P_r \propto f^{-0.43}E_0^{1.73}$ and $P_r \propto f^{-0.18}E_0^{0.47}$, respectively, as plotted in Figure 4.16(a)-(b). For E_C, the scaling relation takes the form of $E_C \propto f^{-0.27}E_0^{1.35}$ for the minor loop, while $E_C \propto f^{-0.33}E_0^{0.46}$ is obtained for the saturated loop, as plotted in Figure 4.16(c)-(d). Clearly, f-exponents m of P_r and E_C-scaling relations for saturated loop in this study, which are −0.18 and −0.33, are also about two times higher in absolute value than those of BaTiO$_3$ single crystal (−0.079 and −0.164) [24]. This is because, as mentioned previously, the depolarizing effects in polycrystalline bulk ceramics acting as a buffer to polarization reversal mechanism resulting in slower domain switching. So the higher absolute values of f-exponents m for both P_r- and E_C-scaling relations of polycrystalline BaTiO$_3$ bulk ceramic are obtained. Since empirical approximation of the hysteresis area $< A >$ can be estimated with $(2P_r)(2E_C)$ [18, 146], $< A > \propto f^{-0.70}E_0^{3.08}$ and $< A > \propto f^{-0.51}E_0^{0.93}$ are available from the P_r- and E_C-scaling relations obtained above for minor and saturated loops, respectively, through this empirical formula the relations. When compared with directly obtained scaling relations from experimental data in Equation (4.6) and (4.7), the exponents of the empirical relations are lower, yet comparable, than those obtained directly from the experiment in both regimes. It is noted that the empirical relation $(2P_r)(2E_C)$ is clearly based on the square-shape loop. Unlike the BaTiO$_3$ single crystal case [24] where the above-mentioned relations agreed very well, this empirical relation is clearly not suitable for estimation of the hysteresis area of polycrystalline BaTiO$_3$ bulk ceramics and other materials which do not have square-shape-like loop.
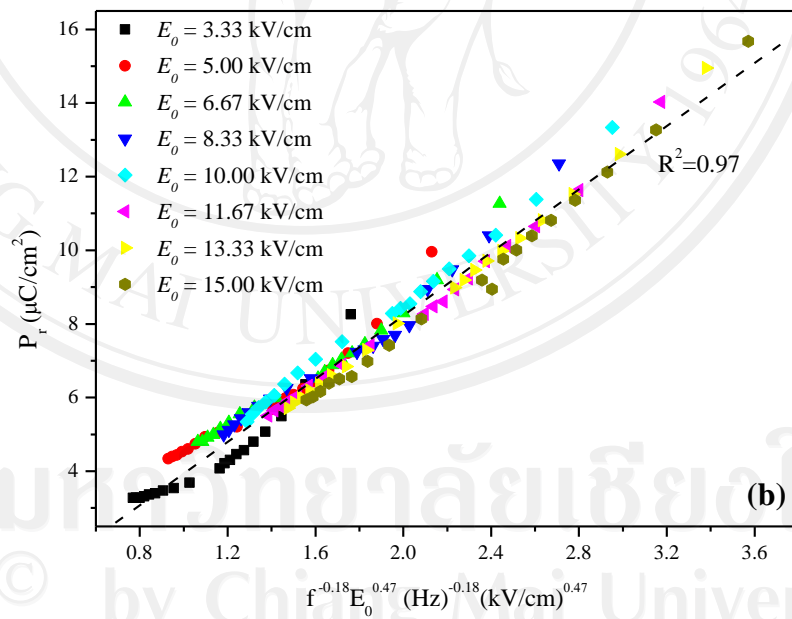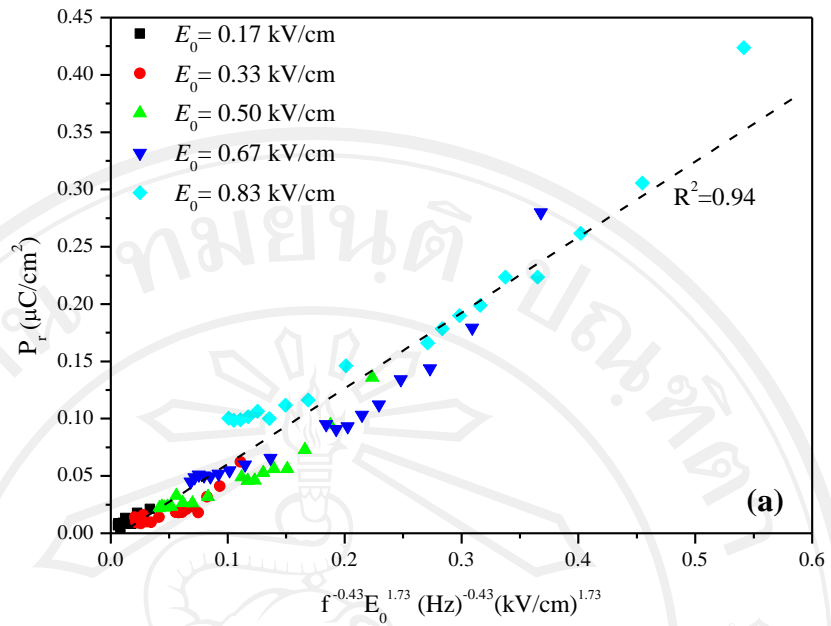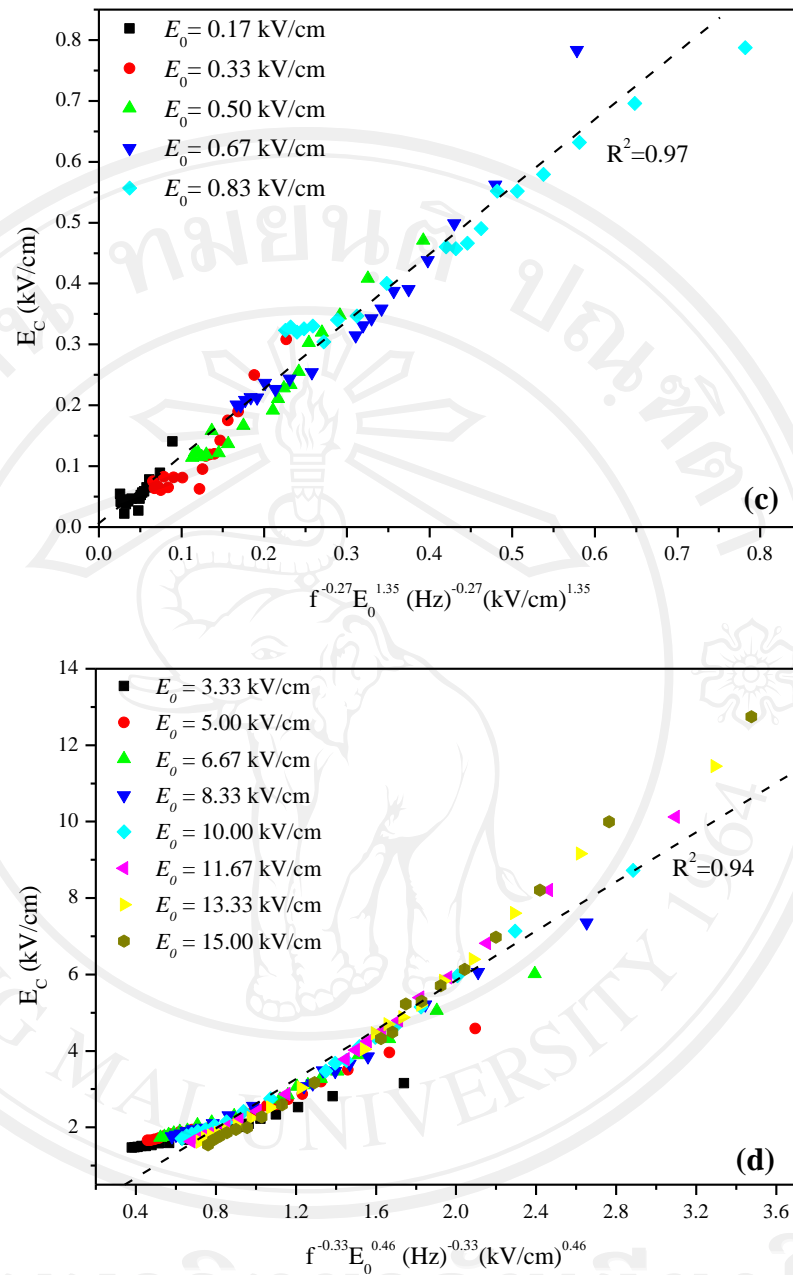
Figure 4.16 P_r- and E_C-power-law scaling relations for polycrystalline BaTiO$_3$ bulk ceramics with observed f-range of 1-100 Hz, (a and b) scaling relations of P_r against $f^{-0.43}E_0^{1.73}$ and P_r against $f^{-0.18}E_0^{0.47}$ for sub-coercive and saturated field conditions, respectively, (c and d) scaling relations of E_C against $f^{-0.27}E_0^{1.35}$ and E_C against $f^{-0.33}E_0^{0.46}$ for sub-coercive and saturated field conditions, respectively. The dotted lines represent linear fitting [126]

**Table 4.2** Scaling exponents in ferroelectric materials [177]

Systems	m	n
Nd-doped $Bi_4Ti_3O_{12}$ thin film	-0.33	2
$SrBi_2Ta_9O_4$ thin film	-0.33	3
$Pb(Zr,Ti)O_3$ thin film	-0.33	1
$PbTiO_3$/polymer composite	-1	2
Soft PZT bulk ceramic		
Saturated Loops	-0.25	1
Minor Loops	-0.33	3
Hard PZT bulk ceramic		
Saturated Loops	-0.28	0.89
Minor Loops	-0.43	3.19
$Na_{0.5}Bi_{0.5}TiO_3$ ceramic		
Minor Loops	-0.39	2.63
{001}-$BaTiO_3$ single crystals		
Saturated Loops	-0.195	0.95
Minor Loops	$(1.667)E_0$-2.804	4.157
$BaTiO_3$ bulk ceramic (20-100 Hz)		
Saturated Loops	-0.25	0.82
Minor Loops	-0.32	3.68
$BaTiO_3$ bulk ceramic (1-100 Hz)		
Saturated Loops	-0.39	1.06
Minor Loops	-0.55	3.40

Table 4.2 (continued) Scaling exponents in different ferroelectric materials

| Systems	m	n
P_r-scaling relations of BaTiO$_3$ bulk ceramic (1-100 Hz)		
Saturated Loops	-0.18	0.47
Minor Loops	-0.43	1.73
E_C-scaling relations of BaTiO$_3$ bulk ceramic (1-100 Hz)		
Saturated Loops	-0.33	0.46
Minor Loops	-0.27	1.35

4.1.2 0.7PMN-0.3PT single crystals

The dynamic *P-E* hysteresis profiles with sinusoidal waveform applied at different *f* (range of 1-200 Hz) but fixed $E_0 = 15$ kV/cm and different E_0 (up to 15 kV/cm) with fixed $f = 50$ Hz are shown in Figure 4.17(a)-(b), respectively.
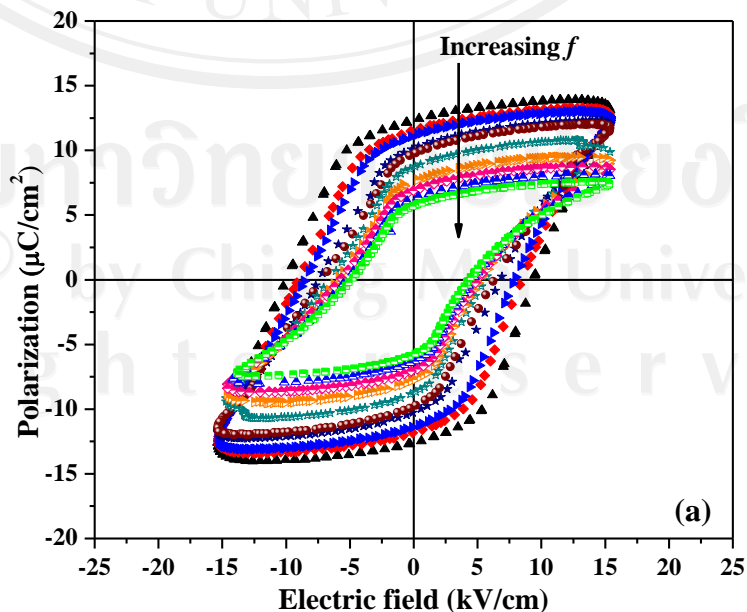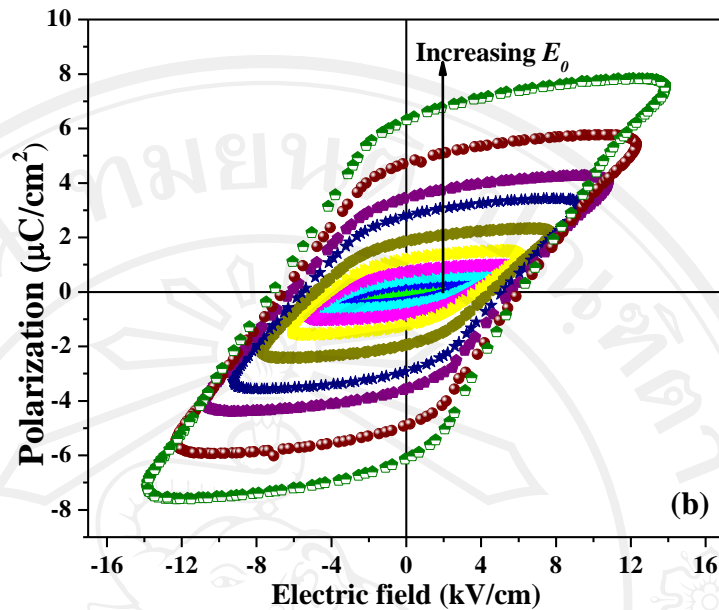
Figure 4.17 The *P-E* hysteresis loops for 0.7PMN-0.3PT single crystal (a) at various *f* fixed $E_0 = 15$ kV/cm, and (b) at various E_0 fixed *f* = 50 Hz

The development of hysteresis area $< A >$ scaling to *f* and E_0 are shown by Figure 4.18(a)-(b), respectively. At fixed *f*, hysteresis area $< A >$, remnant polarization (P_r) and coercive field (E_C) are found to increase with increasing E_0 while they are found to decrease with an increase of *f* at fixed E_0. Similar results have been observed in earlier studies [16-18].
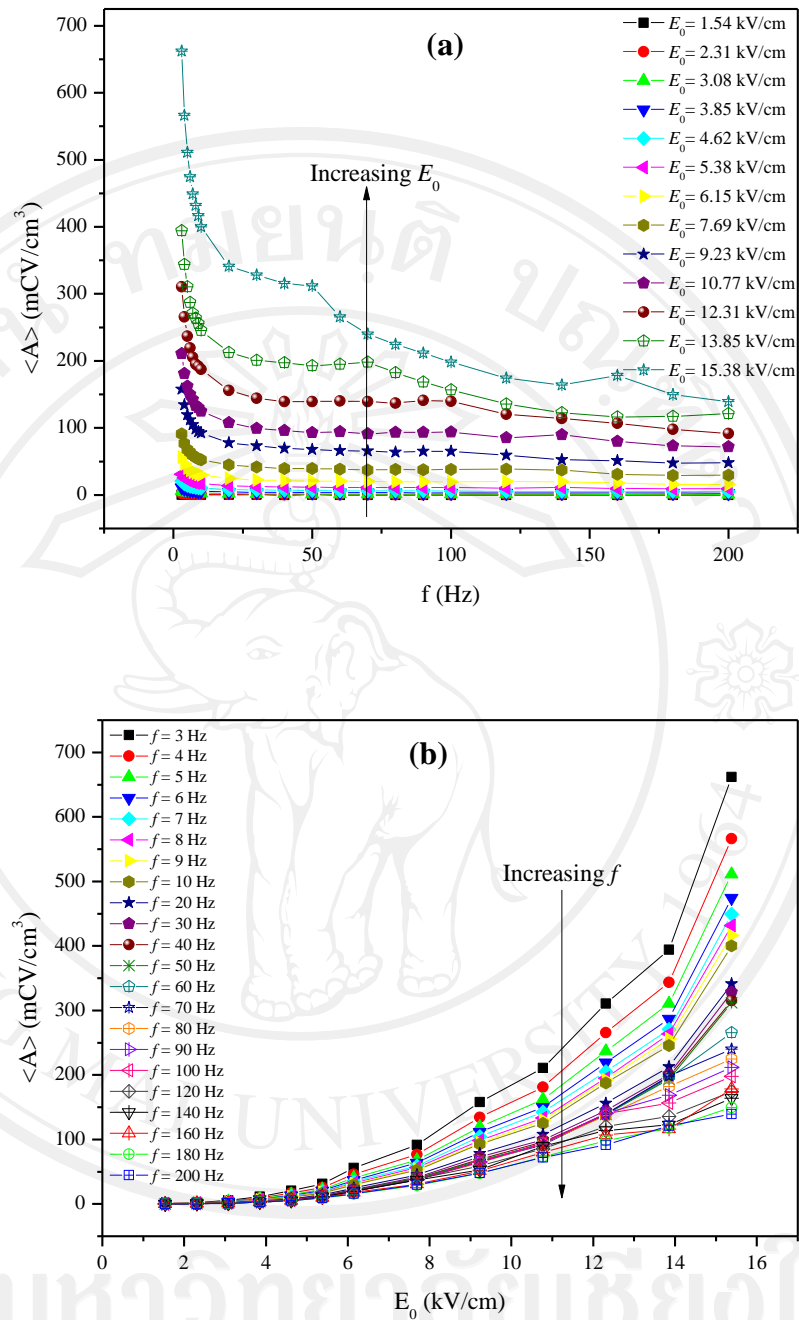
Figure 4.18 The hysteresis area $< A >$ profiles with evolutions of (a) frequency f, and (b) field amplitude E_0 for 0.7PMN-0.3PT single crystal

To obtain the suitable scaling relation for 0.7PMN-0.3PT single crystal, one can first follow the suggested scaling law given in Equation (4.1) to determine exponents m and n directly from the experimental data. By plotting $\log < A >$ against

log f at fixed E_0, one obtains the exponent m. In addition, the exponent n can be obtained from plotting log $< A >$ against log E_0 at fixed f, as shown in Figure 4.19(a)-(b). In conjunction with the least square-fitting method, the methodology outlined above is applied to obtain the exponents m and n for the sub-coercive field ($E_0 < E_C$) and saturated field ($E_0 < E_C$) data.
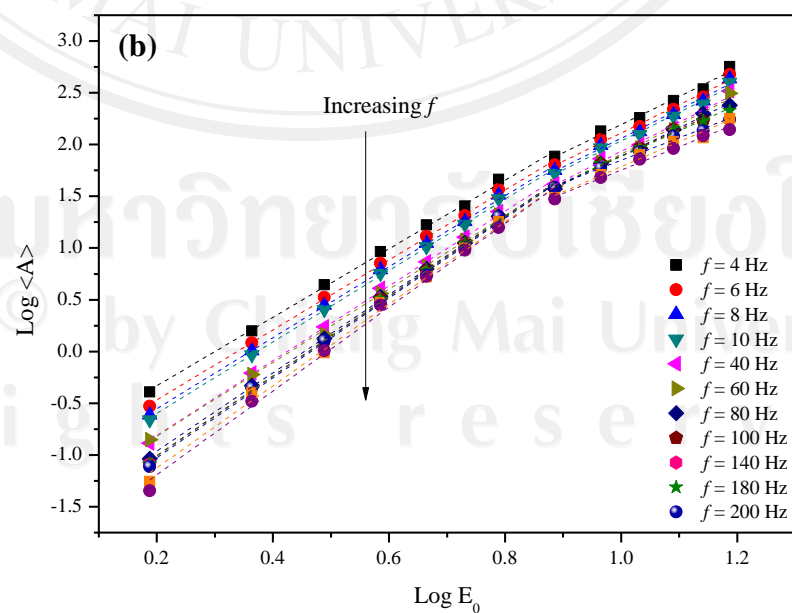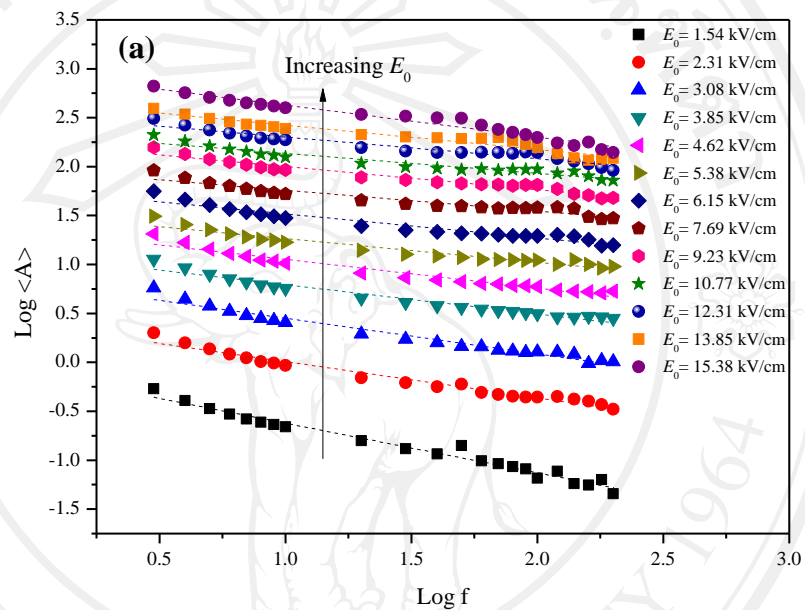
Figure 4.19 Logarithmic plots between (a) $\log < A >$ and $\log f$, and (b) $\log$ $<A>$ and $\log E_0$ for 0.7PMN-0.3PT single crystal. The dotted lines represent linear fitting

The variation of f-exponent m with E_0 and E_0-exponent n with f is revealed. It is found that both exponents m and n depend strongly on field amplitude E_0, and frequency f, respectively, as seen in Figure 4.20(a)-(b). The variations of both exponents obtained here are in strong contrast to most of the previous investigations [4-5, 7-8, 10, 13, 16-18, 127, 134], in which the scaling exponents are normally treated as constant and depend only on the dimensionality and symmetry of the system, not the frequency f and field amplitude E_0.
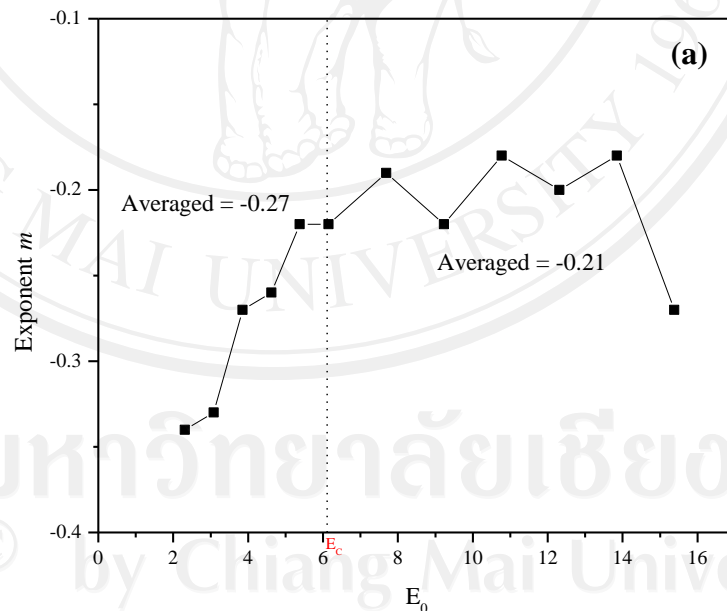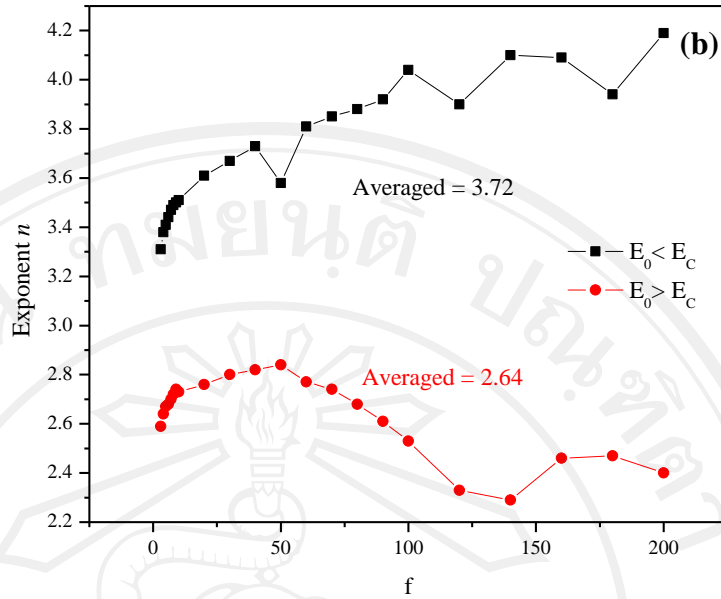
Figure 4.20 (a) Variation of f-exponent m with E_0, and (b) variation of E_0-exponent n with f in sub-coercive field ($E_0 < E_C$) and beyond coercive field ($E_0 > E_C$) conditions for 0.7PMN-0.3PT single crystal

Through first approximation, exponent $m = -0.27$ and exponent $n = 3.72$ are obtained for $E_0 < E_C$. The scaling relation for minor loop data can be fitted very well ($R^2 \sim 0.99$), within the measured uncertainty, by

$$<A> \propto f^{-0.27} E_0^{3.72} \tag{4.12}$$

While for $E_0 > E_C$, exponent $m = -0.21$ and exponent $n = 2.64$ are obtained and scaling relation for saturated loop data is fitted reasonably well ($R^2 \sim 0.97$) as

$$<A> \propto f^{-0.21} E_0^{2.64} \tag{4.13}$$

The scaling relations of $<A>$ against f and E_0 for sinusoidal waveform are shown in Figure 4.21.
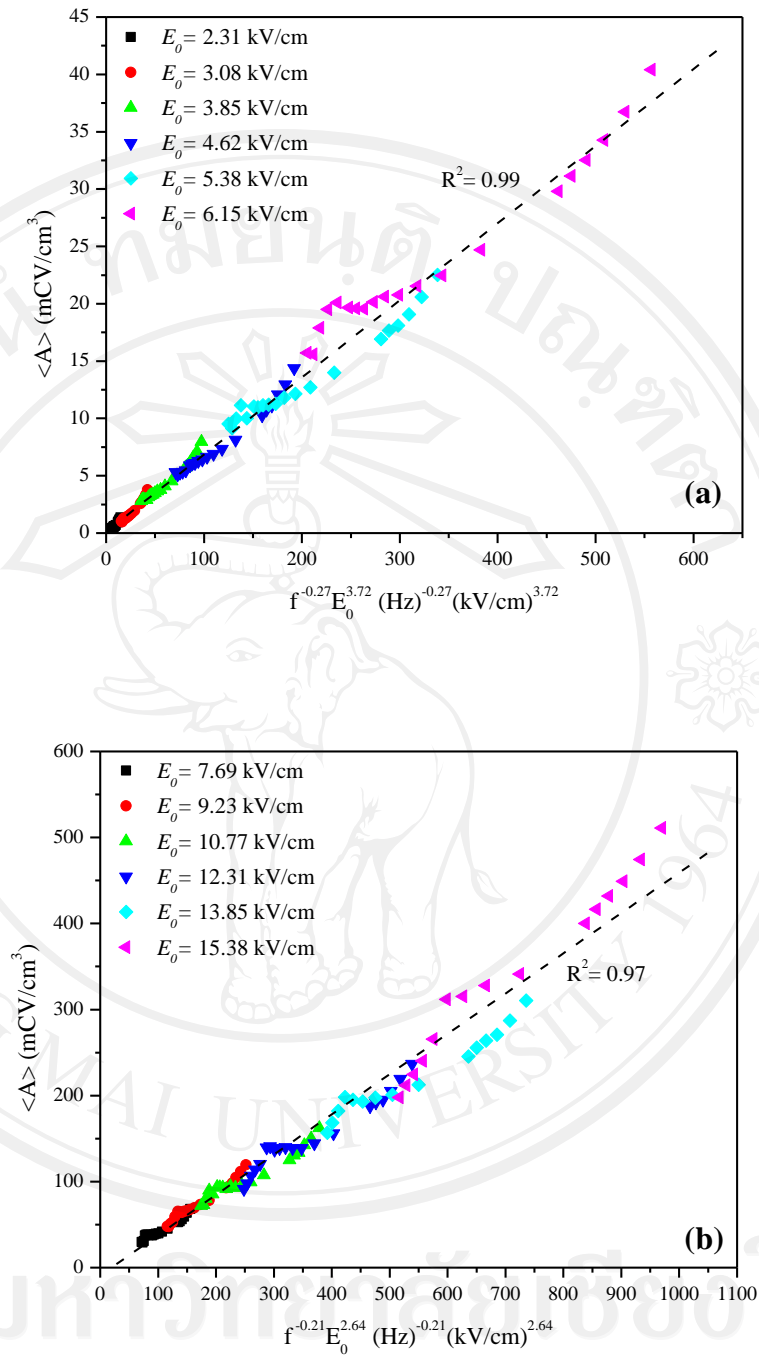
Figure 4.21 Power-law scaling relations of hysteresis for 0.7PMN-0.3PT single crystals (a) $<A>$ against $f^{-0.27}E_0^{3.72}$ for sub-coercive field ($E_0 < E_C$), and (b) $<A>$ against $f^{-0.21}E_0^{2.64}$ for saturated field ($E_0 > E_C$) conditions. The dotted lines represent linear fitting

Comparing with previous investigation in normal BaTiO$_3$ (BT) single crystal [24], for low field condition, E_0-exponent n of 0.7PMN-0.3PT single crystal (n = 3.72) is lower than that of BT single crystal (4.16) possibly due to existence of random fields in relaxor based ferroelectrics and difference in crystal structure which is rhombohedral for 0.7PMN-0.3PT single crystal while the structure is tetragonal for BT single crystal, as listed in Table 4.3. The relaxor state is believed to form because of quenched random fields due to defects/substitutents which are frozen-in from high temperatures [158-159]. Normal ferroelectrics often contain defects/substitutents that can also be randomly frozen-in, but the concentration of these defects is insufficient to result in the breakdown of long-range polar order, as in the case of a relaxor state [160-161]. In a relaxor state, random interactions between clusters result in polarization freezing and glass-like characteristics [162-163]. Hence, lower exponent n in 0.7PMN-0.3PT is reasonable. For f-exponent m, one obtained for BT single crystal varies significantly with E_0 as reported in Ref. # 24. The calculated f-exponent m became close to that of 0.7PMN-0.3PT single crystal (m = -0.27) at E_0 = 1.5 kV/cm (m = -0.29 for BT single crystal at 1.5 kV/cm).

**Table 4.3** The exponents of power-law scaling relation for systems

| System	Sub-coercive field		Saturated field	
	m	n	m	n
BT single crystal [24]	-0.29 at 15 kV/cm	4.16±0.09	−0.20±0.02	0.95±0.06
0.7PMN-0.3PT single crystal	-0.27±0.05	3.72±0.27	-0.21±0.03	2.64±0.16

For high field condition, E_0-exponent n of 0.7PMN-0.3PT single crystal is 2.64 while that of BT single crystal is 0.95. In addition, when compared to 0.7PMN-0.3PT film [21] which its exponent n is 0.67, these exponents are very different, possibly because the maximum applied field of 15 kV/cm does not produce full saturation in 0.7PMN-0.3PT single crystal.

4.1.3 (1-x)PZT-(x)PZN ceramic system

0.9PZT-0.1PZN; (x =0.1)

The *P-E* hysteresis loops with various frequencies *f* and field amplitudes E_0 for tetragonal 0.9PZT-0.1PZN ceramic are obtained. The loops at different *f* (2-100 Hz) fixed E_0 = 18.52 kV/cm and different E_0 (0-15 kV/cm) fixed *f* = 10 Hz are shown in Figure 4.22 (a)-(b), respectively [127].
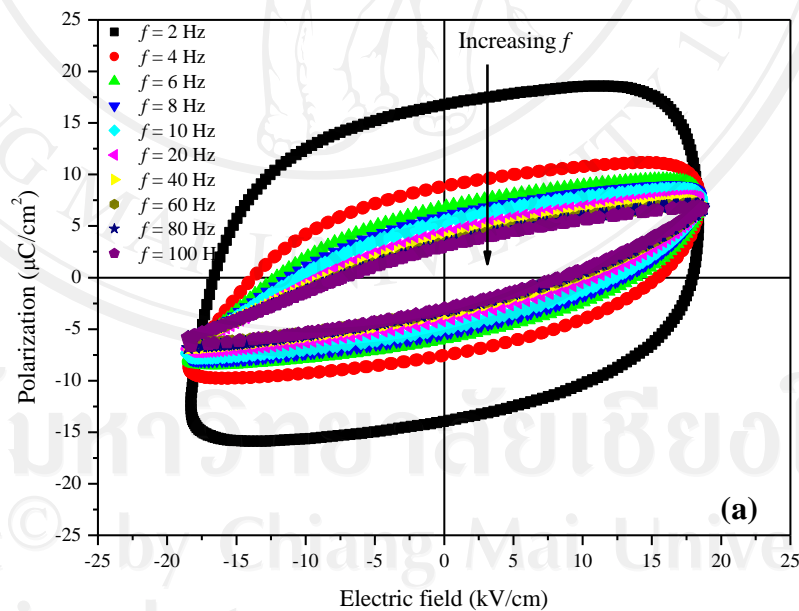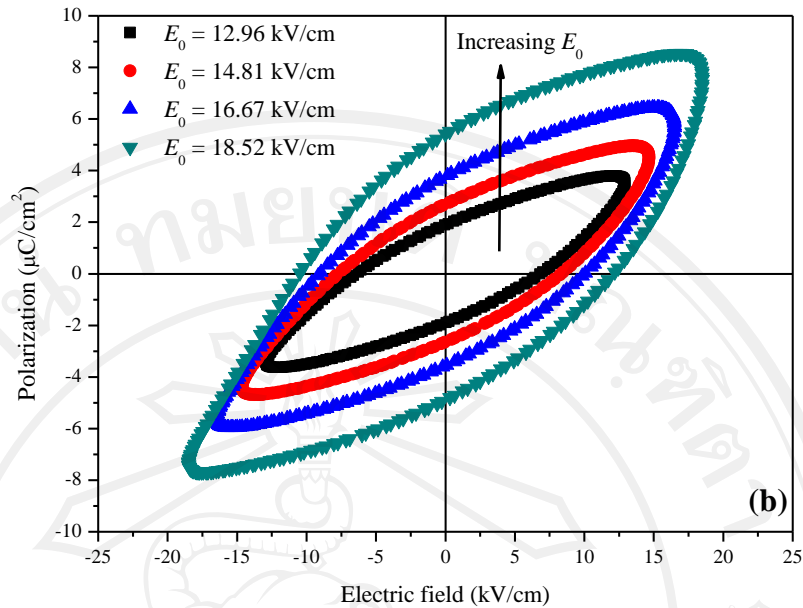
Figure 4.22 The *P-E* hysteresis loops under sub-coercive field condition for 0.9PZT-0.1PZN ceramic (a) at various *f* fixed E_0 = 18.52 kV/cm, and (b) at various E_0 fixed *f* = 10 Hz [127]

The dependence of the *P-E* hysteresis loop pattern and hysteresis area < *A* > on *f* and *E* are remarkable and shown in Figure 4.23(a)-(b). At fixed E_0, remnant polarization (P_r) decreases with increasing frequency *f* due to the increase of the delayed response of the spin reversal, as shown in Figure 4.22(a) [148]. Since coercive field (E_C) is defined as the magnitude of electric field required to bring remnant polarization back to zero so coercive field (E_C) decreases with increasing frequency *f* due to the decrease of remnant polarization. Effects of decrement of these parameters result in the decrease of hysteresis area < *A* >, the area within closed *P-E* loop, as shown in Figure 4.23(a). For the effect of field amplitude E_0, at fixed *f*, remnant polarization (P_r), coercive field (E_C) and hysteresis area < *A* > increase with an increase of field amplitude E_0, as shown in Figure 4.22(b) and 4.23(b). This is as

the larger E_0 provides higher level of electrical driving force, the polarization dissipation energy subjected to one full cycle of electric field application. The loop area is therefore directly related to volume involved in the switching process during the application of electric field [148, 164-165]. Similar observations have been reported in soft and hard PZT ceramics [19, 166-167, 129, 168-170].
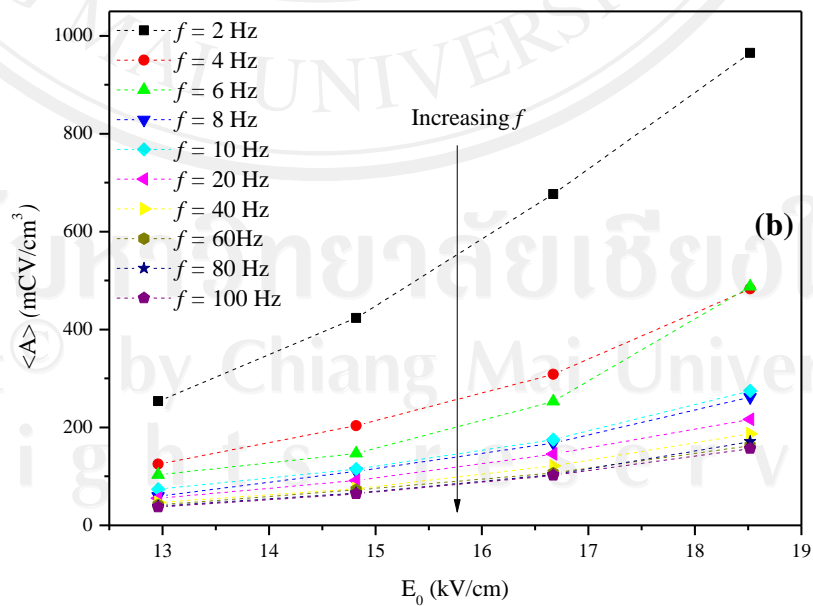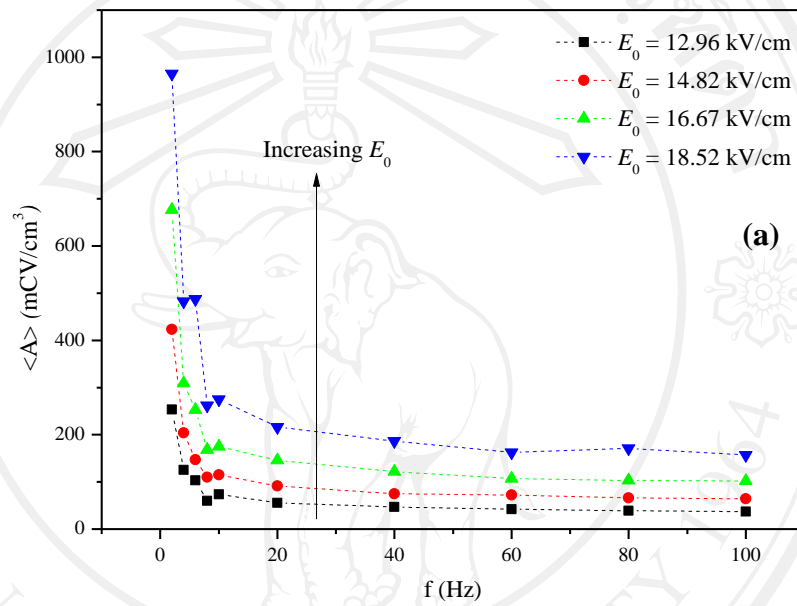
Figure 4.23 The hysteresis area $< A >$ profiles with evolutions of (a) frequency f, and (b) field amplitude E_0 under sub-coercive field condition for 0.9PZT-0.1PZN ceramic

To obtain the suitable scaling relation for the bulk ceramics, one can first follow the suggested scaling law in Equation (4.1) to determine exponent m and n directly from the experimental data. By plotting $< A >$ against f in log-log scale or the other way by plotting $\log < A >$ against $\log f$ at fixed E_0, in conjunction with linear least square-fitting, the exponent m can be obtained by the slope of fitted linear relation. Similarly, the exponent n can be obtained from plotting $\log < A >$ against $\log E_0$ or plotting $< A >$ against E_0 in log-log scale at fixed f and then by linear relation fitting, exponent n is obtained, as shown in Figure 4.24(a)-(b).

Note that to minimize the statistical errors contributing to each exponent, one should be emphasized of how to extract the exponents. Such an exponent (m and n), being applied as the exponent to the power law, should be averaged from all with the same kind. For example, all of f-exponent m, obtained from all of particularly fixed electric field, should be averaged into one constant value and then that value shall be applied as exponent m of power law. This method is also applied to obtain n exponents of power law.
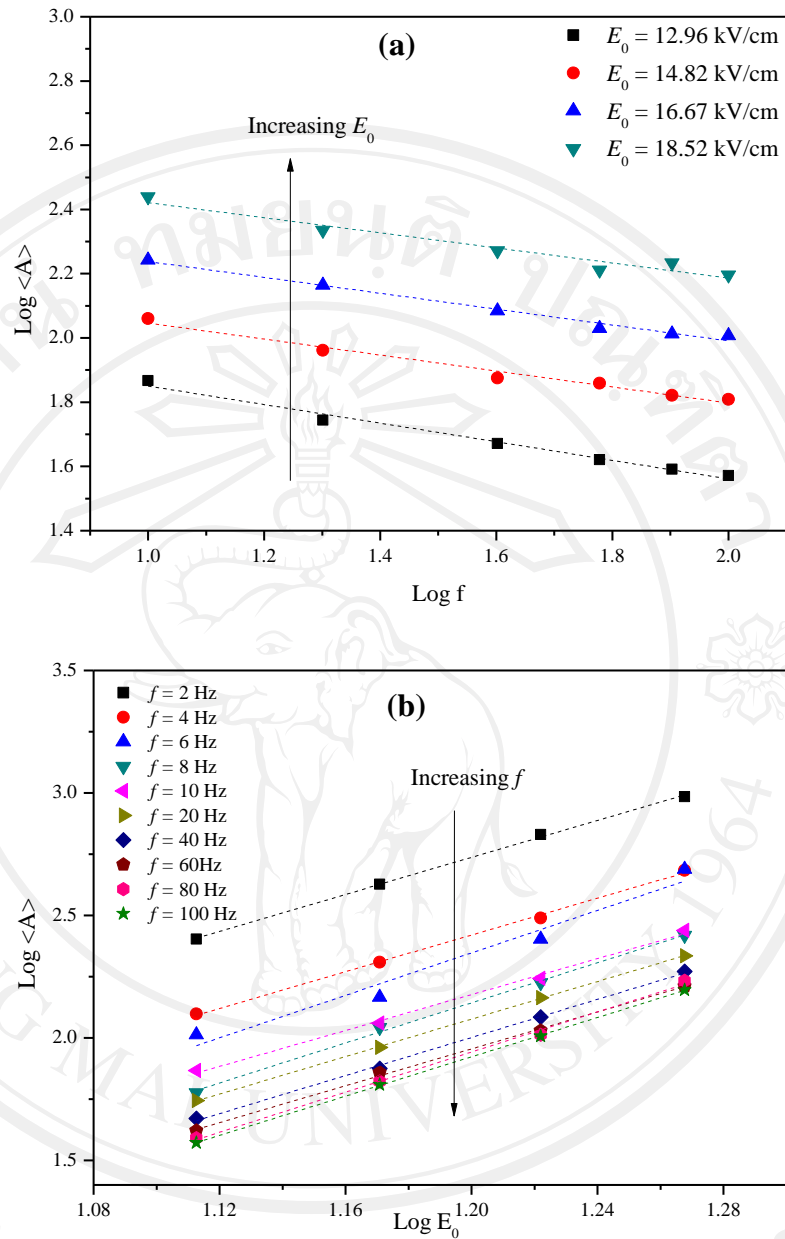
Figure 4.24 Logarithmic plots between (a) log $< A >$ and log f, and (b) log
$<A>$ and log E_0 under sub-coercive field condition for 0.9PZT-0.1PZN ceramic. The
dotted lines represent linear fitting

It is found that the f-exponent m depends strongly on the field amplitude E_0,
while the E_0-exponent n significantly depends on the frequency f in low f-range (2-10
Hz), but more slightly depends on the frequency f in high f-range (20-100 Hz), as seen

in Figure 4.25(a)-(b). The variations of both exponents obtained here are in strong contrast to most of the previous investigations [4-5, 7-8, 10, 13, 16-18, 127, 134], in which the scaling exponents are normally treated as constant and depend only on the dimensionality and symmetry of the system, not the frequency f and field amplitude E_0.
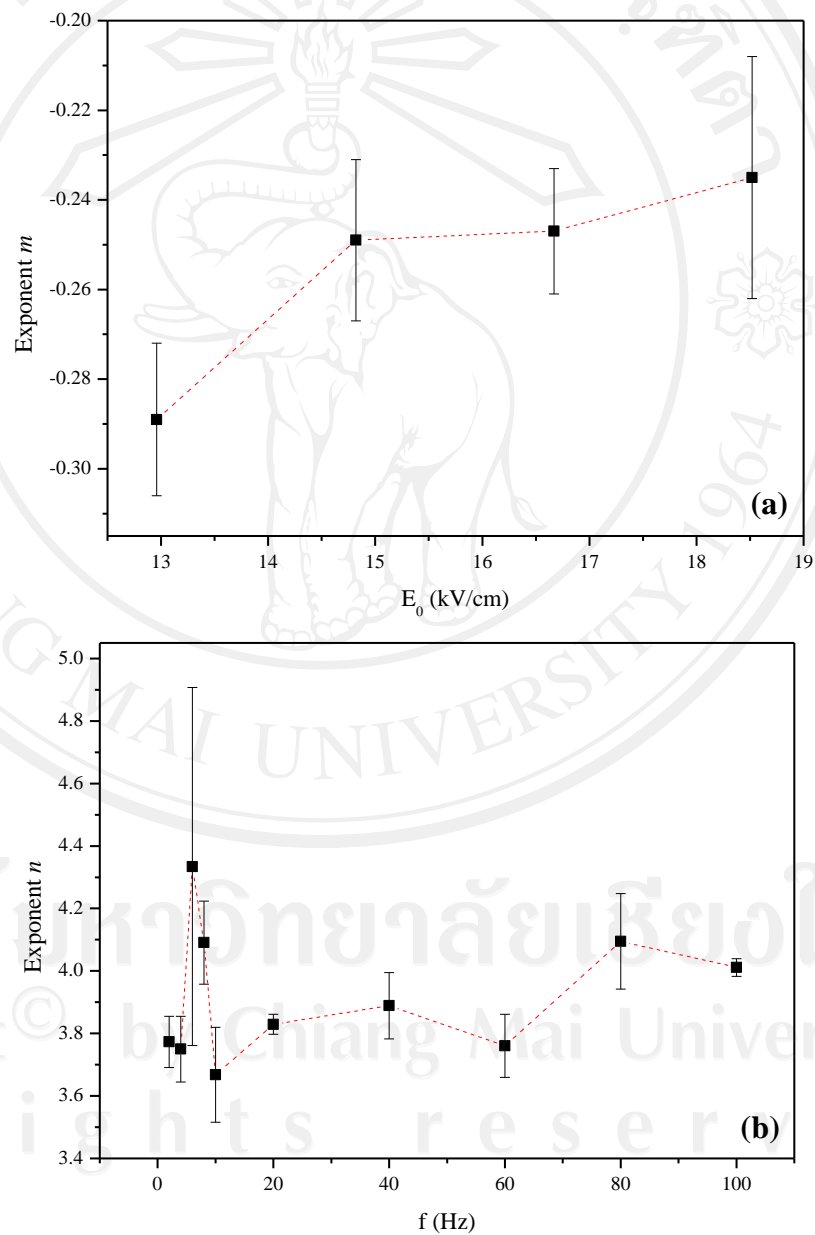
Figure 4.25 (a) Variation of f-exponent m with E_0, and (b) variation of E_0-exponent n with f under sub-coercive field condition for 0.9PZT-0.1PZN ceramic

Anyway, for better illustration, the simplification to establish power-law scaling relation is constructed. Both of f-exponent m and E_0-exponent n are approximated as constant values to be representatives to conduct power-law scaling relations. Through first approximation, the f-exponent $m = -0.42$ and the E_0-exponent $n = 3.65$ are obtained for scaling relation of 0.9PZT-0.1PZN ceramic under sub-coercive field condition. As plotted in Figure 4.26, it is revealed that the experimental data can be fitted very well (with $R^2 = 0.99$), within the measured uncertainty, by

$$< A > \propto f^{-0.42} E_0^{3.65} \tag{4.14}$$
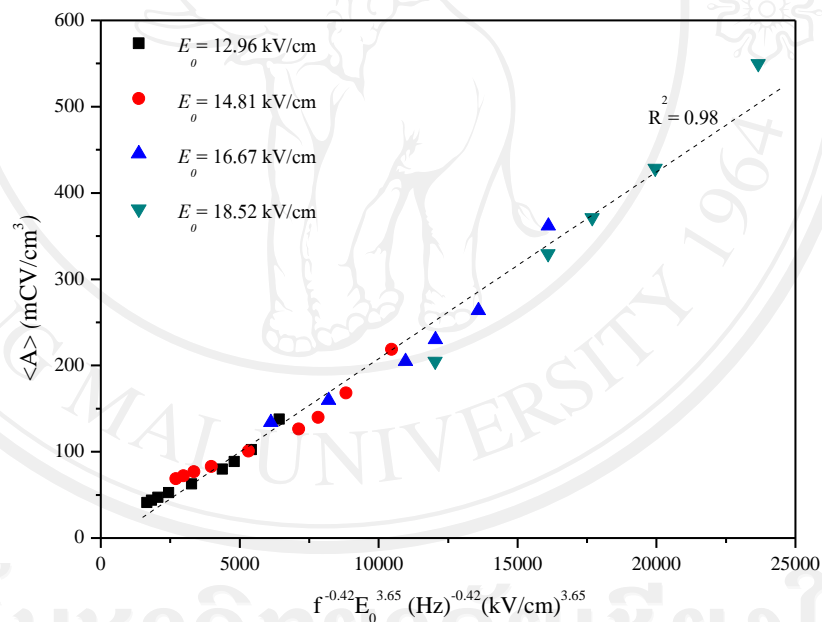

Figure 4.26 Power-law scaling relation of hysteresis area $< A >$ against $f^{-0.42} E_0^{3.65}$ for 0.9PZT-0.1PZN ceramic under sub-coercive field condition. The dotted lines represent linear fitting [127]

Here, the first interesting observation is that the minor loop scaling in PZN-modified PZT bulk ceramics is generally similar to that of PZT thin film [6-7] as well

as that of minor loop of PZT bulk ceramics [16-17]. As explained in previous literatures [16], this is attributed to the fact that main polarization orientation mechanism in thin films and in sub-coercive field condition for bulk ceramics likely is from the 180° domain reversal. This explains why the scaling behavior of PZT bulk ceramics at low E fields is similar to that of thin films. More importantly, the scaling relation obtained in Equation (4.14) indicates that $<A>$ more quickly decays with f and more quickly grows with E_0 than the minor-loop scaling relations obtained earlier for commercial soft PZT bulk ceramic with $<A> \propto f^{-0.33} E_0^3$ [16]. This clearly indicates the ease of the polarization orientation process in tetragonal 0.9PZT-0.1PZN ceramics with a clear regular lamellar 90° domain configuration [171] that leads to faster polarization orientation kinetics, as compared to complex domain structures of commercial PZT bulk ceramics which require higher energy barrier for the polarization orientation process.
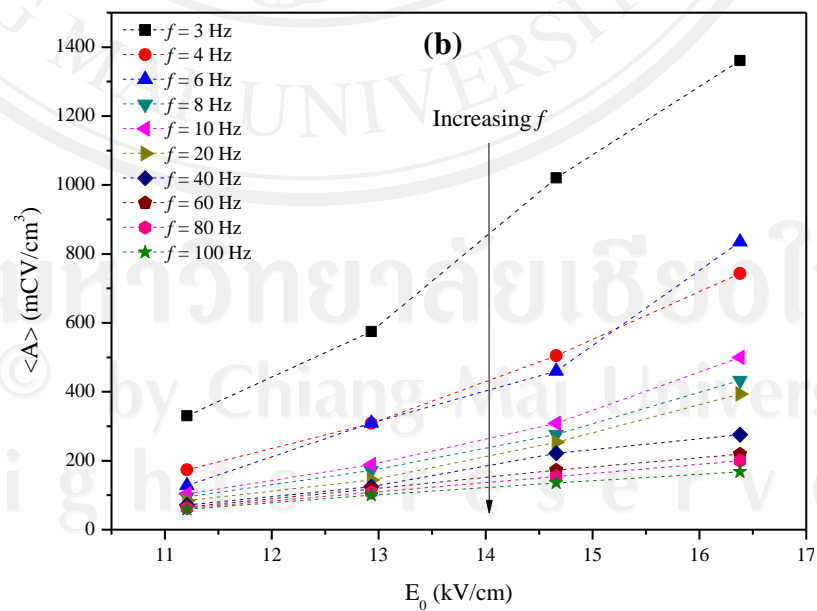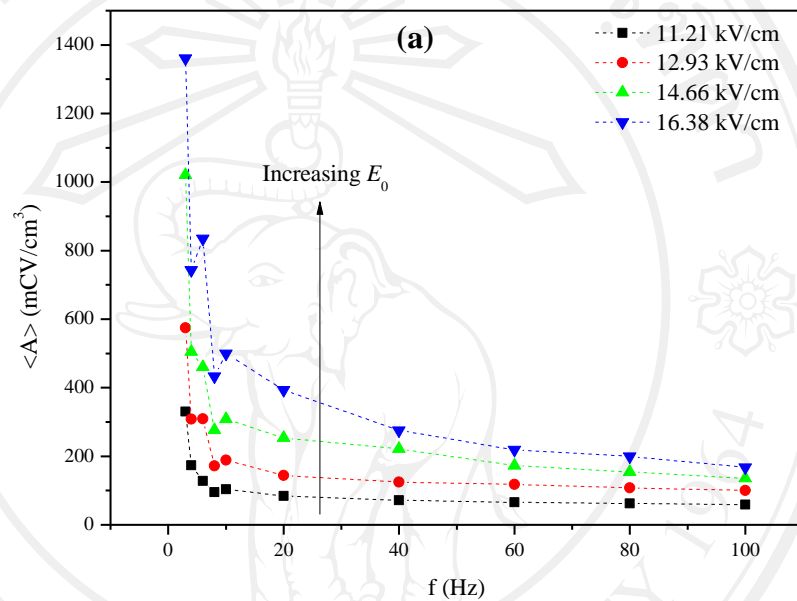
0.8PZT-0.2PZN; (x = 0.2)

The P-E hysteresis profiles with various frequencies f and field amplitude E_0 for mixing phases of rhombohedral and tetragonal 0.8PZT-0.2PZN ceramic are obtained. The hysteresis loops at different f but fixed E_0 (16 kV/cm) and at different E_0 but fixed f (10 Hz) are shown in Figure 4.27(a)-(b), respectively [128].
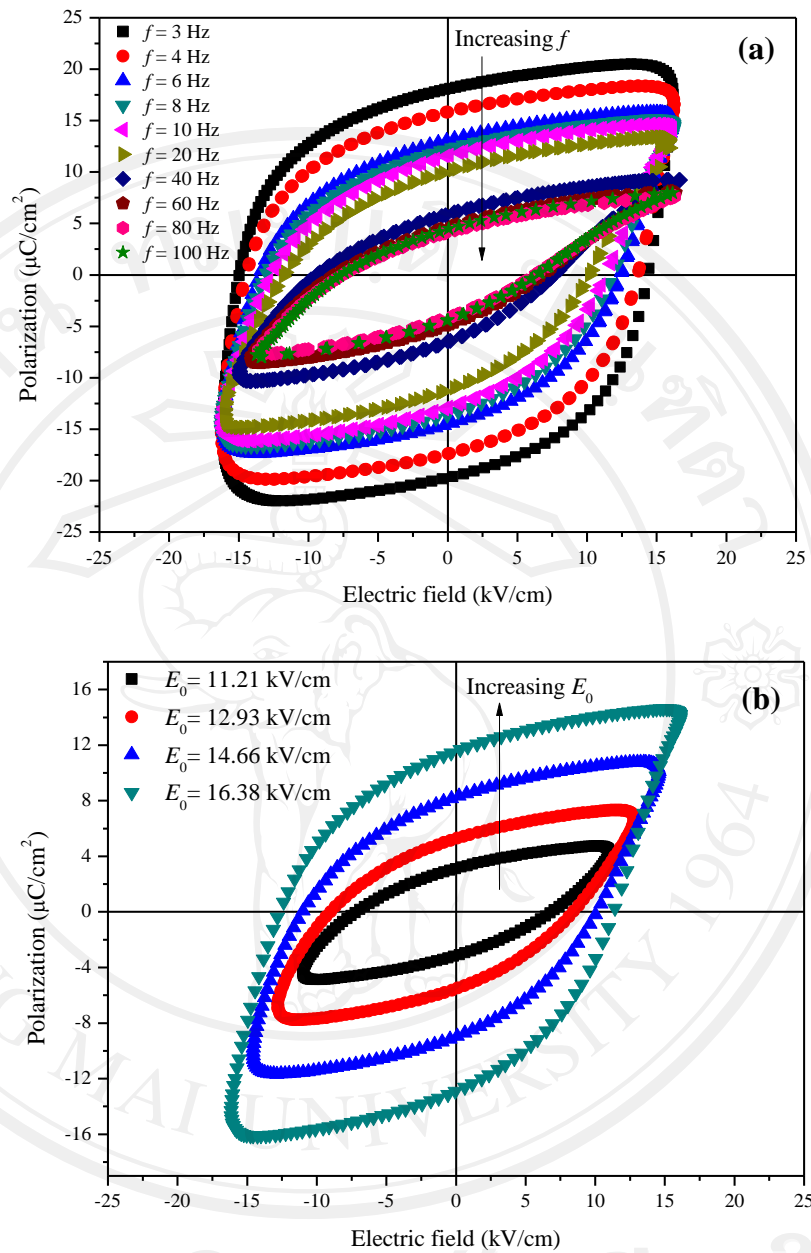
Figure 4.27 The *P-E* hysteresis loops under sub-coercive field condition for 0.8PZT-0.2PZN ceramic (a) at various *f* fixed E_0 = 16.38 kV/cm, and (b) at various E_0 fixed *f* = 10 Hz [128]

The dependence of the loop pattern and hysteresis area < *A* > on *f* and E_0 are shown in Figure 4.28(a)-(b). At fixed E_0, remnant polarization (P_r) coercive field (E_C) and hysteresis area < *A* > decrease with increasing frequency *f* due to the increase of

the delayed response of the spin reversal [148]. At fixed f, remnant polarization (P_r) coercive field (E_C) and hysteresis area $< A >$ increase with an increase of field amplitude E_0 due to enlargement of electrical driving force, as explained previously. Similar observations have also been reported in the other PZT–PZN compositions [19, 129, 166-167], as well as in soft and hard PZT ceramics [168-170].

Figure 4.28 The hysteresis area $< A >$ profiles with evolutions of (a) frequency f, and (b) field amplitude E_0 under sub-coercive field condition for 0.8PZT-0.2PZN ceramic

To obtain the suitable scaling relation for the bulk ceramics, one can first follow the suggested scaling law given in Equation (4.1) to determine exponent m and n directly from the experimental data. By plotting $\log < A >$ against $\log f$ at fixed E_0, one obtains the exponent m. In addition, the exponent n can be obtained from plotting $\log < A >$ against $\log E_0$ at fixed f, as shown in Figure 4.29(a)-(b).
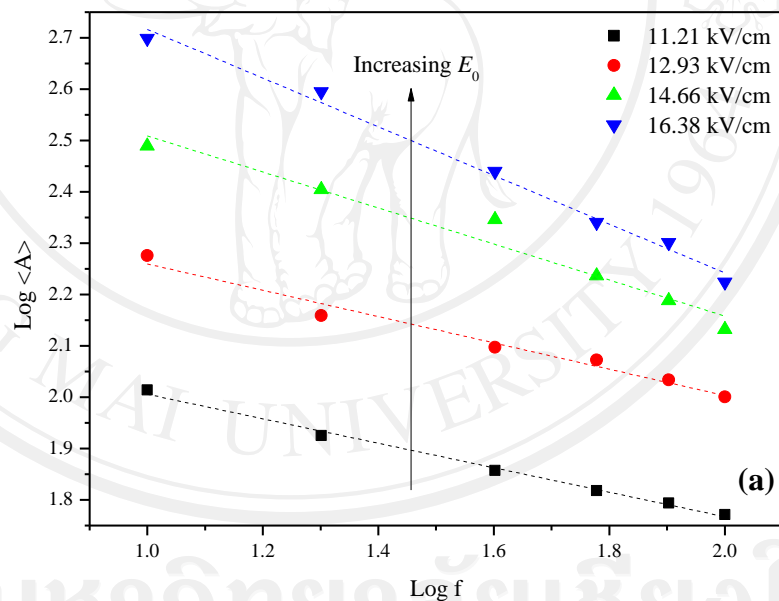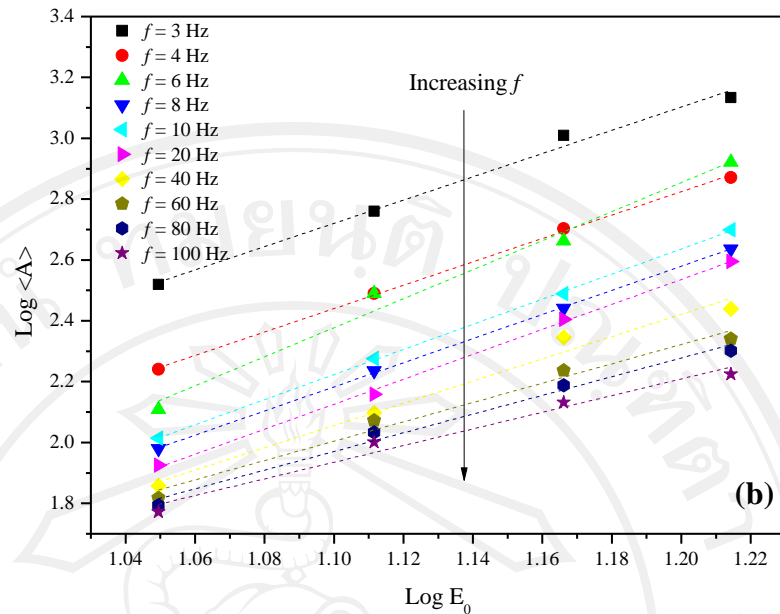
Figure 4.29 Logarithmic plots between (a) log $< A >$ and log f, and (b) log $<A>$ and log E_0 under sub-coercive field condition for 0.8PZT-0.2PZN ceramic. The dotted lines represent linear fitting

It is found that both f-exponent m and E_0-exponent n depend strongly on field amplitude E_0, and frequency f, respectively, as seen in Figure 4.30(a)-(b). The variations of both exponents obtained here are in strong contrast to most of the previous investigations [4-5, 7-8, 10, 13, 16-18, 127, 134], in which the scaling exponents are normally treated as constant and depend only on the dimensionality and symmetry of the system, not the frequency f and field amplitude E_0.
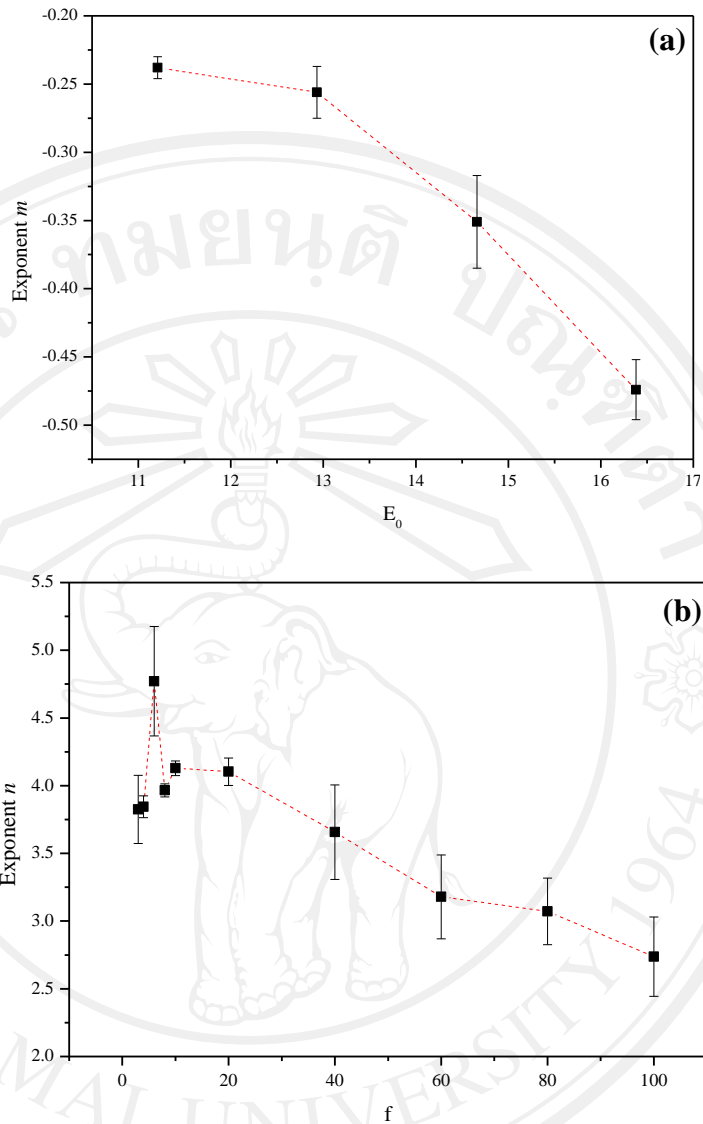
Figure 4.30 (a) Variation of f-exponent m with E_0, and (b) variation of E_0-exponent n with f under sub-coercive field condition for 0.8PZT-0.2PZN ceramic

For better illustration, the simplification to establish power-law scaling relation is constructed. Both of f-exponent m and E_0-exponent n are approximated as constant values to be representatives to conduct power-law scaling relations. Through first approximation, the f-exponent $m = -0.33$ and the E_0-exponent $n = 3.75$ are obtained for scaling relation of 0.8PZT-0.2PZN ceramic under sub-coercive field condition.

When applies f-exponent m and E_0-exponent n to Equation (4.1), the well scaling relation of hysteresis area $< A >$ against frequency (f) and field amplitude (E_0) can be obtained as

$$< A > \propto f^{-0.33} E_0^{3.75} \tag{4.15}$$

The plot of scaling law is shown in Figure 4.31.
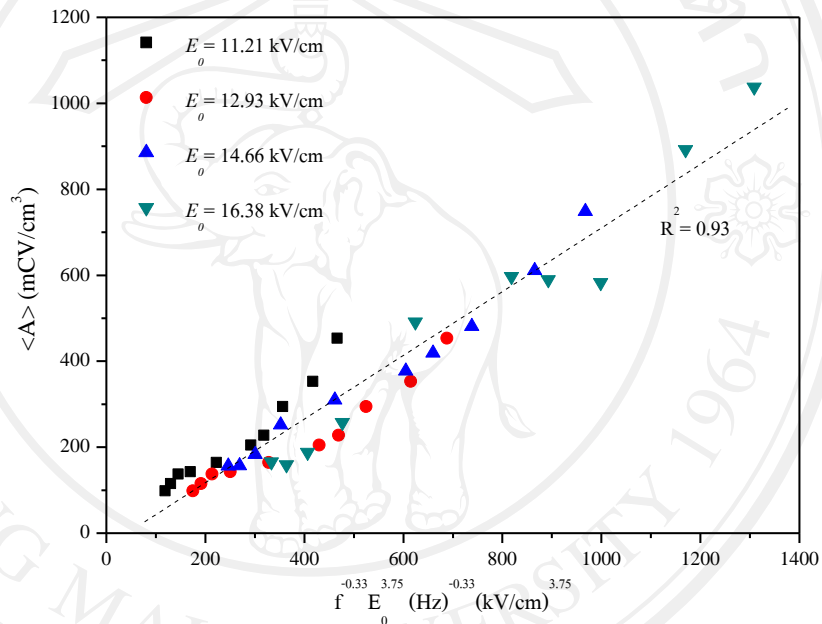
Figure 4.31 Power-law scaling relation of hysteresis area $< A >$ against $f^{-0.33} E_0^{3.75}$ for 0.8PZT-0.2PZN ceramic under sub-coercive field condition. The dotted lines represent linear fitting [128]

More importantly, it should first be mentioned that the scaling exponents m and n for this MPB composition ceramic are not significantly different from those obtained for the other PZT–PZN compositions reported previously [19, 129, 166-167]. Probably, this may be resulted from that the loop areas $< A >$ are calculated by integrating technique, summing all data points on P–E loops, including any noise information.

As a result, this technique probably averages out the existence of slightly different data on P–E loops arising from different domain states at the MPB composition so the differences of the scaling exponents (m and n) between the MPB composition (in this study) and other compositions of PZT–PZN cannot be clearly observed. To enhance exponent verification, the differential technique should be used simultaneously with the integrating technique. However, these similar scaling exponents suggest that the domain states existing in the ceramics play a key role in controlling the scaling behavior, not the ceramic compositions. It should also be noticed that scaling in 0.8PZT–0.2PZN bulk ceramics is generally similar to that of PZT thin film [6-7], as well as that of minor-loop of PZT bulk ceramics [16-17]. As explained in our previous investigation [16], this is attributed to the fact that main polarization orientation mechanism in thin-films and in sub-coercive field condition for bulk ceramics is likely from the 180° domain-reversal [23, 142-143, 150-151]. This explains why the scaling behavior of 0.8PZT–0.2PZN bulk ceramics at sub-coercive condition is similar to that of thin-films. In addition, one possible reason resulting the scaling of 0.8PZT–0.2PZN, PZT bulk ceramics and PZT thin films to be similar may be the similarity in their domain structures. PZT bulk ceramics and PZT thin films are in tetragonal phase structure (room temperature) while 0.8PZT–0.2PZN bulk ceramics are in MPB mixing of tetragonal/rhombohedral phase structure. Hence, the scaling relations obtained here do support our previously proposed hypothesis that the domain structures play major role in controlling dynamic hysteresis behavior of ferroelectric materials [16-17].
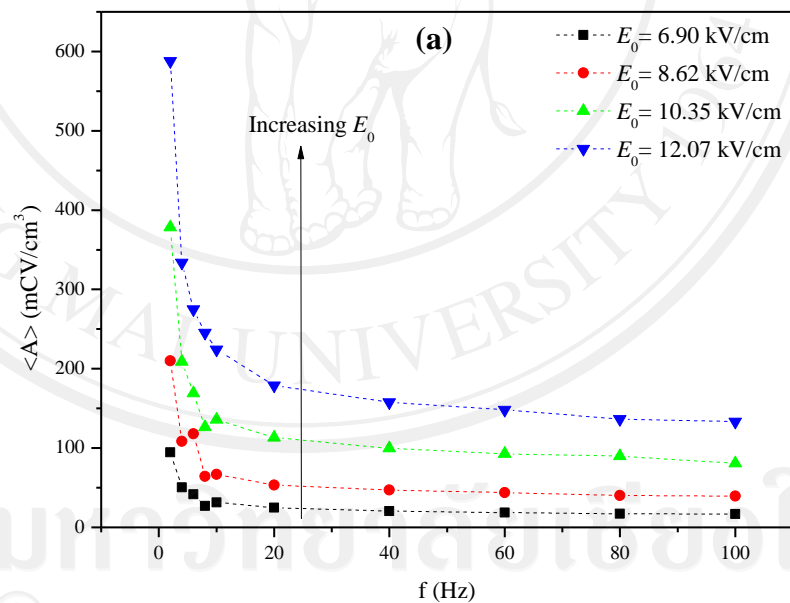
0.7PZT-0.3PZN; (x = 0.3)

The *P-E* hysteresis profiles with various frequencies *f* and field amplitude E_0 for rhombohedral 0.7PZT-0.3PZN are obtained. The hysteresis loops at different *f* but fixed E_0 (12 kV/cm) and at different E_0 but fixed *f* (10 Hz) are shown in Figure 4.32(a)-(b), respectively [129].
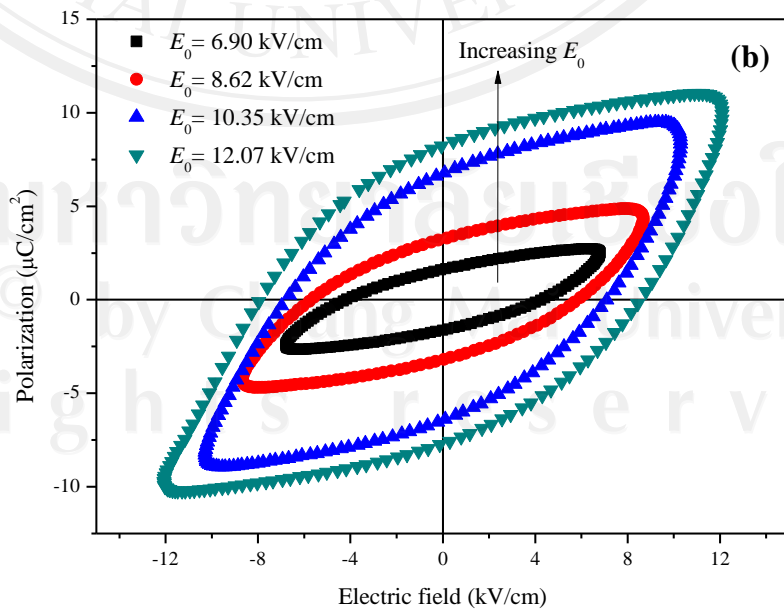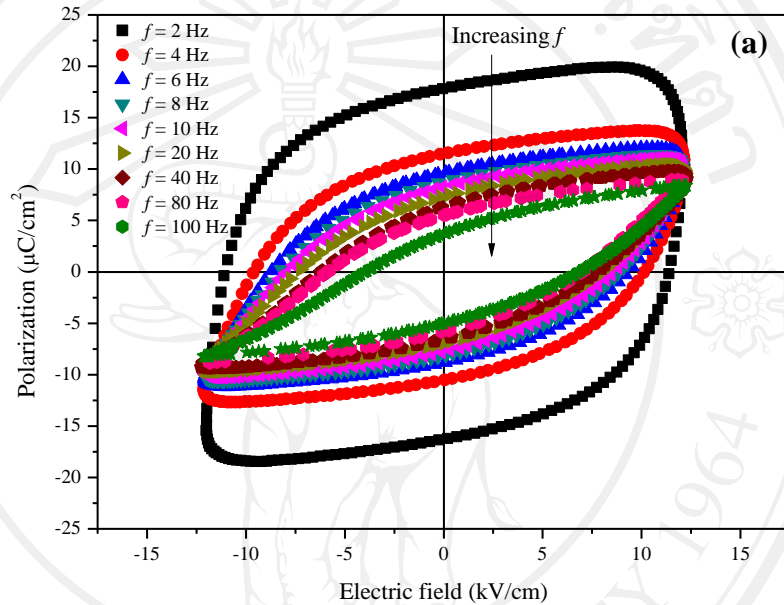
Figure 4.32 The *P-E* hysteresis loops under sub-coercive field condition for 0.7PZT-0.3PZN ceramic (a) at various f fixed E_0 = 12.07 kV/cm and (b) at various E_0 fixed f = 10 Hz [129]

The dependence of the loop pattern and hysteresis area $< A >$ on f and E are revealed. At fixed E_0, the loop area $< A >$, remnant polarization (P_r) and coercive field (E_C) decrease with an increase of frequency f, as shown in Figure 4.32(a) and 4.33(a). The dependence of the hysteresis area $< A >$ on E_0 is depicted in Figure 4.33(b). Similar observations have also been reported in the other PZT–PZN compositions as well as in soft and hard PZT ceramics [168-170].
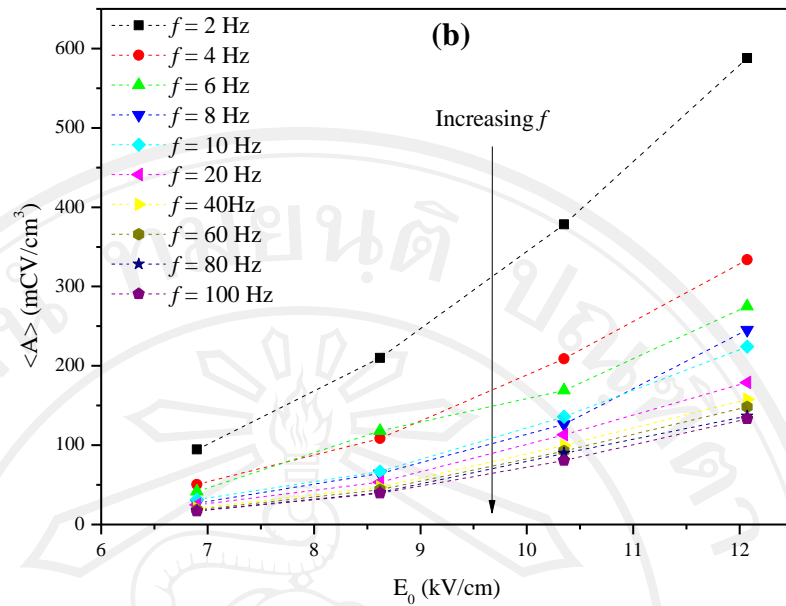
Figure 4.33 The hysteresis area $< A >$ profiles with evolutions of (a) frequency f, and (b) field amplitude E_0 under sub-coercive field condition for 0.7PZT-0.3PZN ceramic

To obtain a suitable scaling relation for the bulk ceramic, one can first follow the suggested scaling law given in Equation (4.1) to determine exponent m and n directly from the experimental data. By plotting $\log < A >$ against $\log f$ at fixed E_0, one obtains the exponent m. On the other hand, the exponent n can be obtained from plotting $\log < A >$ against $\log E_0$ at fixed f. The plotting of $\log < A >$-$\log f$ and $\log <A>$- $\log E_0$ are shown in Figure 4.34(a)-(b).
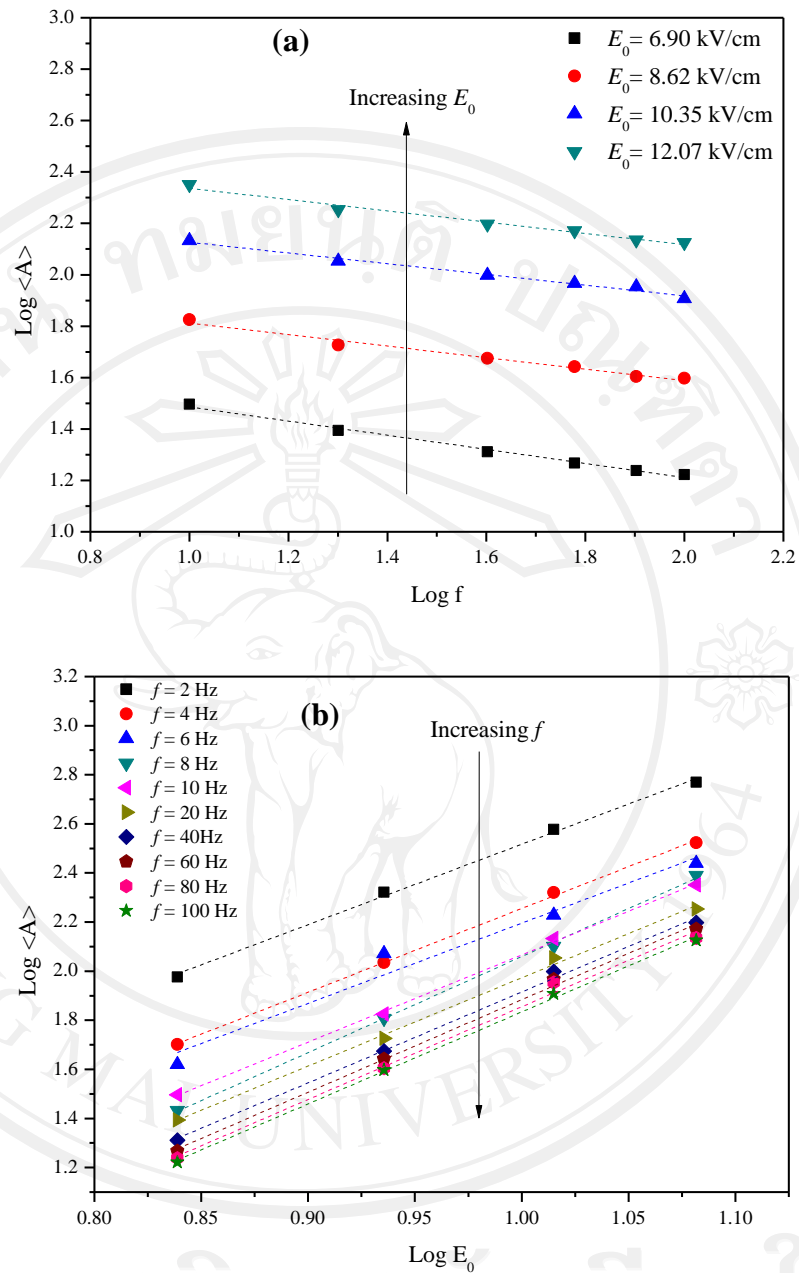
Figure 4.34 Logarithmic plots between (a) log $< A >$ and log f, and (b) log $<A>$ and log E_0 under sub-coercive field condition for 0.7PZT-0.3PZN ceramic. The dotted lines represent linear fitting

It is found that the f-exponent m depends strongly on the field amplitude E_0, while the E_0-exponent n significantly depends on the frequency f in low f-range (2-10 Hz), but more slightly depends on the frequency f in high f-range (20-100 Hz), as seen

in Figure 4.35(a)-(b). The variations of both exponents obtained here are in strong contrast to most of the previous investigations [4-5, 7-8, 10, 13, 16-18, 127, 134], in which the scaling exponents are normally treated as constant and depend only on the dimensionality and symmetry of the system, not the frequency f and field amplitude E_0.
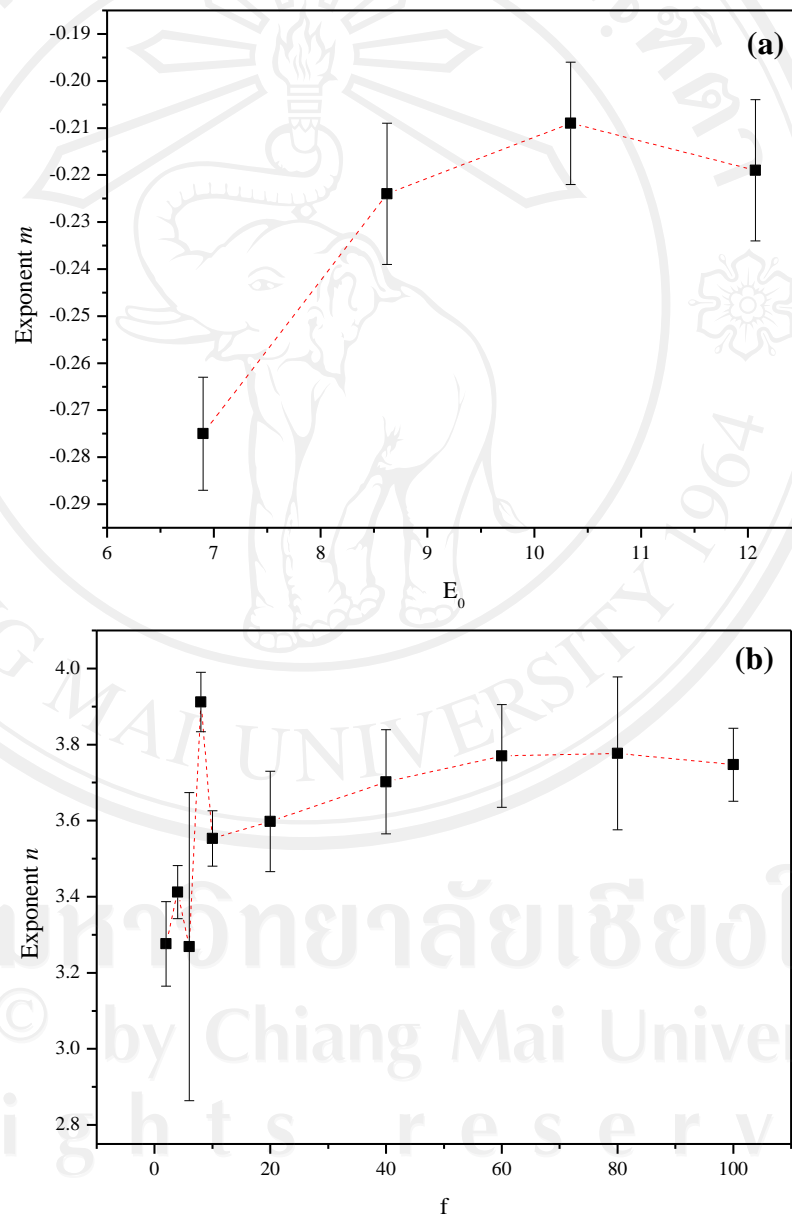
Figure 4.35 (a) Variation of f-exponent m with E_0, and (b) variation of E_0-exponent n with f under sub-coercive field condition for 0.7PZT-0.3PZN ceramic

For better illustration, the simplification to establish power-law scaling relation is constructed. Both of f-exponent m and E_0-exponent n are approximated as constant values to be representatives to conduct power-law scaling relations. Through first approximation, the f-exponent $m = -0.35$ and the E_0-exponent $n = 3.47$ are obtained for scaling relation of rhombohedral 0.7PZT-0.3PZN ceramic under sub-coercive field condition.

As plotted in Figure 4.36, it is revealed that the experimental data can be fitted (with $R^2 = 0.96$), within the measured uncertainty, by

$$< A > \propto f^{-0.35} E_0^{3.47} \tag{4.16}$$
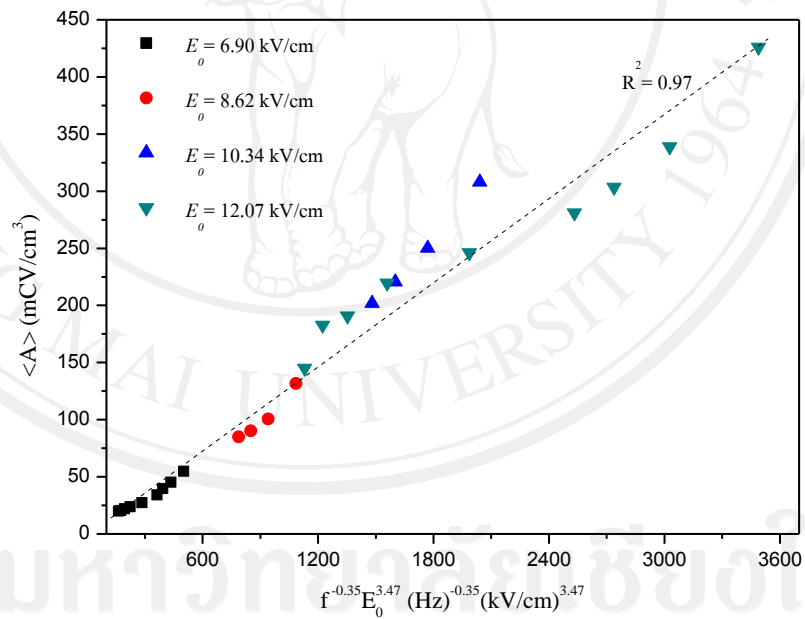
Figure 4.36 Power-law scaling relation of hysteresis area $< A >$ against $f^{-0.35} E_0^{3.47}$ for 0.7PZT-0.3PZN ceramic under sub-coercive field condition. The dotted lines represent linear fitting [129]

Here, the first interesting observation is that the minor loop scaling in PZN-modified PZT bulk ceramics is generally similar to that of the PZT thin film [6-7], as

well as that of the minor loop of PZT bulk ceramics [16-17]. As explained in our previous investigation [16], this is attributed to the fact that the polarization orientation mechanism in thin films and in sub-coercive field condition for bulk ceramics is likely from the 180° domain reversal [150-153, 172]. This explains why the scaling behavior of PZT bulk ceramics at low E-fields is similar to that of thin films. More importantly, the scaling relation obtained in Equation (4.16) indicates that $<A>$ decays slightly more quickly with f and grows more quickly with E_0 than the minor-loop scaling relations obtained earlier for commercial soft PZT bulk ceramic with $<A> \propto f^{-0.33}E_0{}^3$ [16]. This clearly indicates the ease of the polarization orientation process in rhombohedral 0.7PZT–0.3PZN ceramics that leads to faster polarization orientation kinetics, as compared with complex domain structures of commercial PZT bulk ceramics which require higher energy barrier for the polarization orientation process. Furthermore, the scaling relations obtained here also support our previous proposed hypothesis that the domain structures play a major role in controlling dynamic hysteresis behavior of ferroelectric materials [16-17].

0.6PZT-0.4PZN; (x = 0.4)

The P-E hysteresis loops at different f but fixed E_0 (10.5 kV/cm) and at different E_0 but fixed f (10 Hz) for rhombohedral 0.6PZT-0.4PZN ceramic are shown in Figures 4.37(a)-(b), respectively [130].
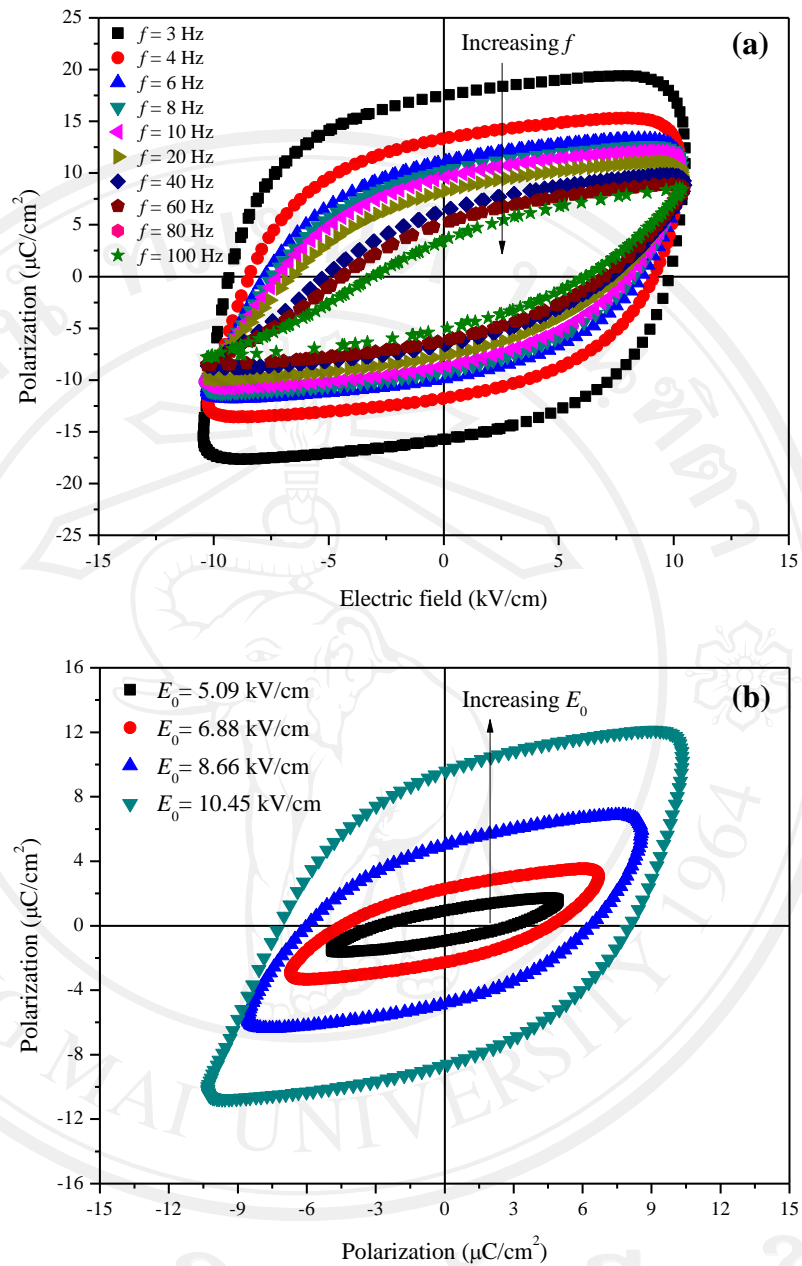
Figure 4.37 The *P-E* hysteresis loops under sub-coercive field condition for 0.6PZT-0.4PZN ceramic (a) at various *f* fixed $E_0 = 10.45$ kV/cm and (b) at various E_0 fixed *f* = 10 Hz [130]

The dependence of the loop pattern and hysteresis area $< A >$ on *f* and *E* are exposed. At fixed E_0, the loop area $< A >$, remnant polarization (P_r) and coercive field (E_c) decrease with an increase of frequency, as shown in Figure 4.38(a). The

dependence of the hysteresis area $< A >$ on E_0 is depicted in Figure 4.38(b). Similar observations have also been reported in the other PZT–PZN compositions as well as in soft and hard PZT ceramics [168-170].
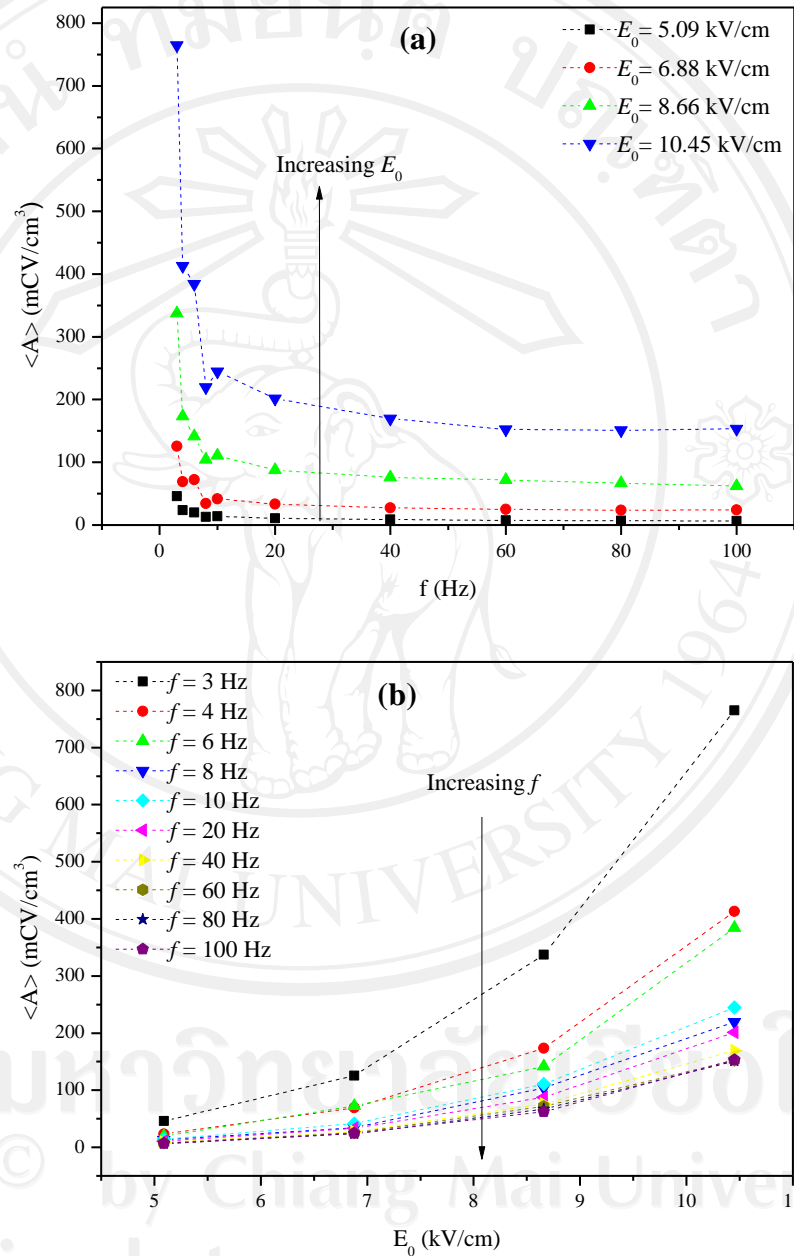
Figure 4.38 The hysteresis area $< A >$ profiles with evolutions of (a) frequency f, and (b) field amplitude E_0 under sub-coercive field condition for 0.6PZT-0.4PZN ceramic

To obtain suitable scaling relations, one can first follow the suggested scaling law given in Equation (4.1) to determine exponent m and n directly from the experimental data. By plotting $\log <A>$ against $\log f$ at fixed E_0, one obtains the exponent m. On the other hand, the exponent n can be obtained by plotting $\log <A>$ against $\log E_0$ at fixed f. In conjunction with the least-square-fitting method, the exponent m and n are obtained. The plotting of $\log <A>$-$\log f$ and $\log <A>$- $\log E_0$ are shown in Figure 4.39(a)-(b).
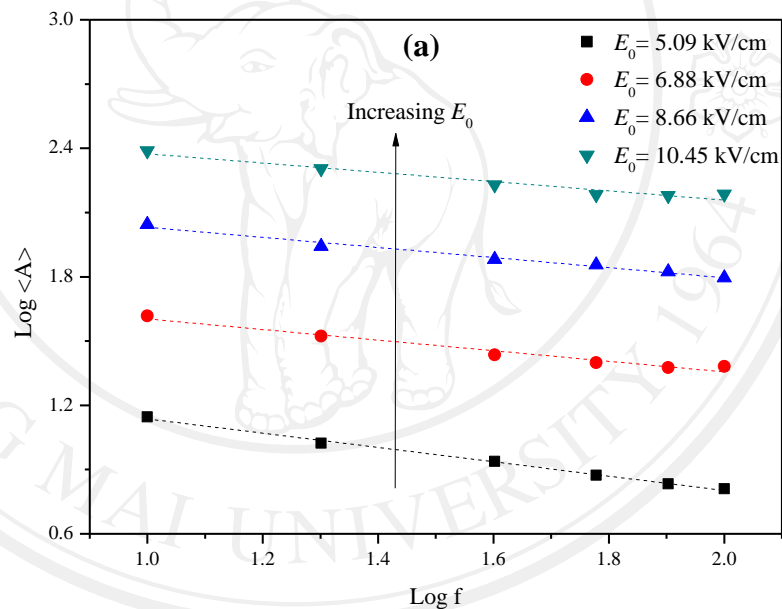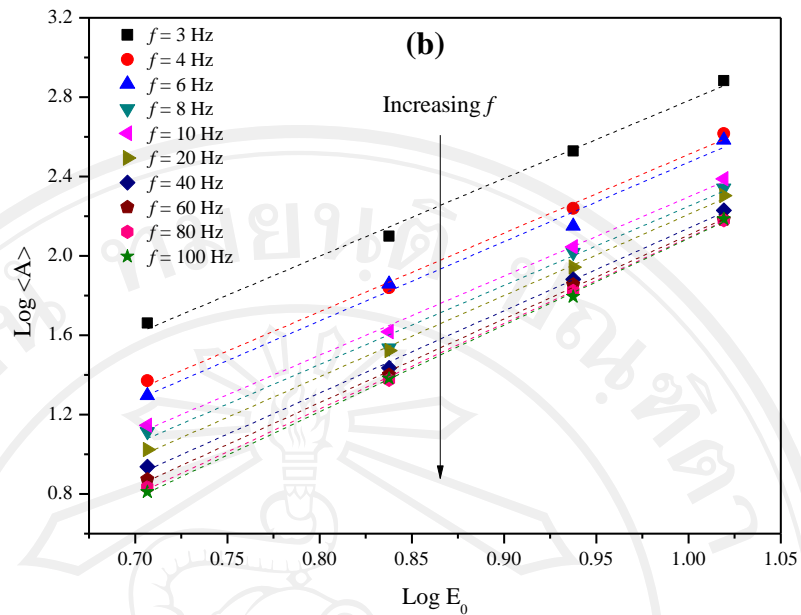
Figure 4.39 Logarithmic plots between (a) log $< A >$ and log f, and (b) log $<A>$ and log E_0 under sub-coercive field condition. The dotted lines represent linear fitting for 0.6PZT-0.4PZN ceramic

It is found that f-exponent m depended significantly on field amplitude E_0, while E_0-exponent n seems to be linear-trend with frequency f for all f-range (2-100 Hz), as seen in Figure 4.40(a)-(b). The variations of both exponents obtained here are in strong contrast to most of the previous investigations [4-5, 7-8, 10, 13, 18-19, 127, 134], in which the scaling exponents are normally treated as constant and depend only on the dimensionality and symmetry of the system, not the frequency f and field amplitude E_0.
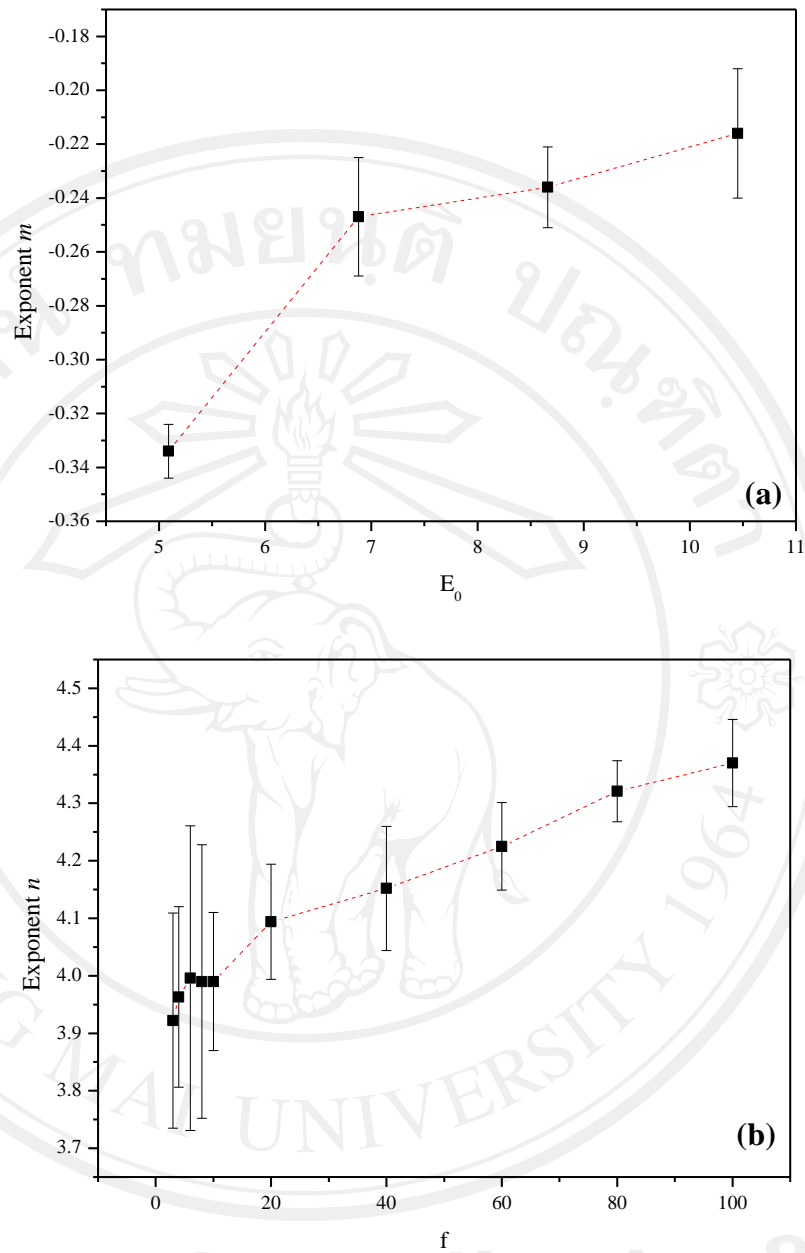
Figure 4.40 (a) Variation of f-exponent m with E_0, and (b) variation of E_0-exponent n with f under sub-coercive field condition for 0.6PZT-0.4PZN ceramic

For better illustration, the simplification to establish power-law scaling relation is constructed. Both of f-exponent m and E_0-exponent n are approximated as constant values to be representatives to conduct power-law scaling relations. Through first approximation, the f-exponent $m = -0.36$ and the E_0-exponent $n = 4.03$ are

obtained for scaling relation of rhombohedral 0.6PZT-0.4PZN ceramic under sub-coercive field condition.

As plotted in Figure 4.41, it is revealed that the experimental data can be fitted (with $R^2 = 0.99$), within the measured uncertainty, by

$$< A > \propto f^{-0.36} E_0{}^{4.03} \tag{4.17}$$
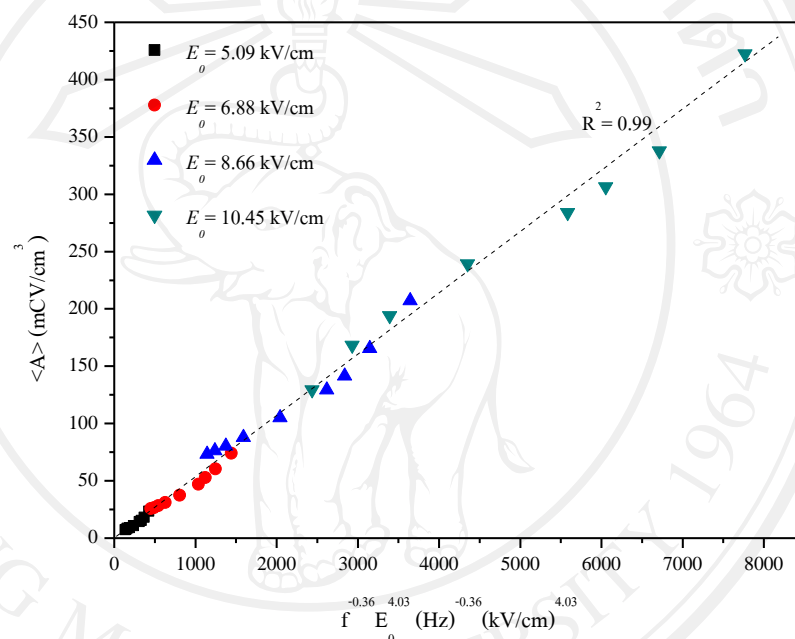
Figure 4.41 Power-law scaling relation of hysteresis area $< A >$ against $f^{-0.36} E_0{}^{4.03}$ for 0.6PZT-0.4PZN ceramic under sub-coercive field condition for 0.6PZT-0.4PZN ceramic. The dotted lines represent linear fitting [130]

Here, the first interesting observation is that the minor loop scaling in PZN-modified PZT bulk ceramics is generally similar to that of PZT thin film [6-7], as well as that of the minor loop of PZT bulk ceramics [16-17]. This is attributed to the fact that the main polarization orientation mechanism in thin-films and in sub-coercive field conditions for bulk ceramics is likely from the same reversible 180° domain

rotation (which also occurs at a much faster rate than the irreversible process), as the irreversible non-180° domain switching normally accompanied by mechanical strain occurs at a higher E-field [16-17, 150-153, 172]. More importantly, the scaling relation obtained in Equation (4.17) indicates that $<A>$ decays slightly more quickly with f and grows faster with E_0 than in commercial soft PZT bulk ceramic with $<A> \propto f^{-0.33} E_0^3$ [16]. This indicates the ease of the polarization orientation process in rhombohedral 0.6PZT–0.4PZN ceramics that leads to faster polarization orientation kinetics, as compared to complex domain structures of commercial PZT bulk ceramics which require a higher energy barrier for the polarization orientation process.

Considering the E_0 exponent of 4.03, which is approximately of the same order as that in PZT thin film [6-7], as well as those in minor loops of PZT bulk ceramics [16-17], the reversible domain wall vibration is also believed to play an additional role in the dependence of hysteresis area on E_0 at a sub-coercive field. In the nucleation and growth concept [6-7, 135] domain reversal can be characterized by simultaneous contributions from both the new domain nucleation rate and the domain boundary motion velocity, with the latter responding faster to the electric field [133-136]. Since the reversible domain wall vibration makes a greater contribution to the dependence of hysteresis area with E_0 in sub-coercive conditions, the response to E_0 occurs at much faster rate than at a higher field amplitude. It should also be noted that the E_0 exponent $n = 4.03$ agrees very well with the n value of 4 obtained from the previous simulation study using the Monte Carlo method based on the Q-state planar Potts model [13].

In addition, the f exponent of -0.36 is smaller in absolute value than that obtained theoretically from $(\Phi^2)^2$ and $(\Phi^2)^3$ models for non-saturated loops (exponent -1) [7]. The difference could be attributed to depolarizing effects from space charges on grain boundaries, induced electric field from interface layers, immobile defects etc. [141], acting as a buffer to the polarization-reversal mechanism in bulk ceramics. As a result, the hysteresis area must show a relatively weaker dependence on f than that of the theoretical models. Furthermore, the value of the f exponent is believed to be related to available domain states in the material, previously proposed in our investigations [16, 134], or growth dimension in the growth kinetics model proposed by Ishibashi and Orihara based on the Kolmogorov–Avrami model [144, 145].

0.5PZT-0.5PZN; (x = 0.5)

The P-E hysteresis profiles with various frequencies f and field amplitude E_0 for rhombohedral 0.5PZT-0.5PZN are obtained. The hysteresis loops at different f but fixed E_0 (9.6 kV/cm) and at different E_0 but fixed f (10 Hz) are shown in Figure 4.42(a)-(b), respectively [19].
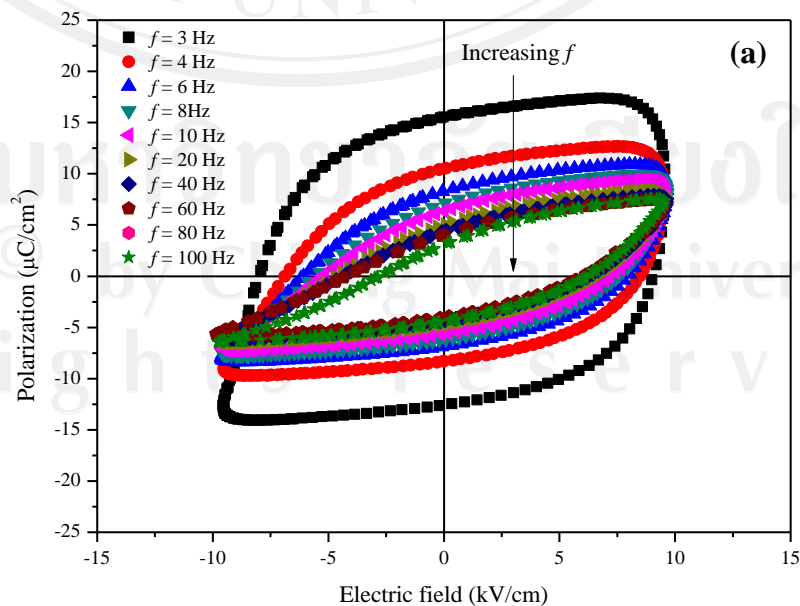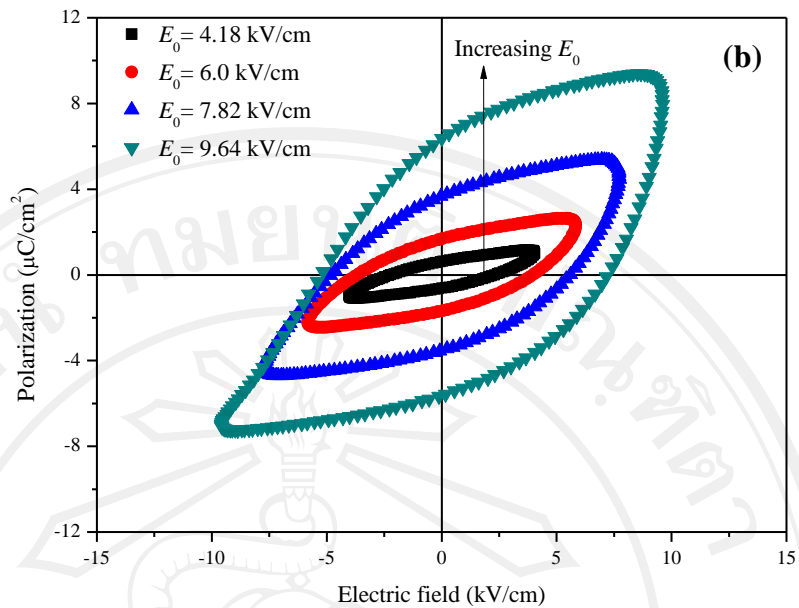
Figure 4.42 The *P-E* hysteresis loops under sub-coercive field condition for 0.5PZT-0.5PZN ceramic (a) at various f fixed $E_0 = 9.64$ kV/cm and (b) at various E_0 fixed $f = 10$ Hz.

The dependence of the loop pattern and hysteresis area $< A >$ on f and E are disclosed. At fixed E_0, the loop area $< A >$, remnant polarization (P_r) and coercive field (E_C) decrease with an increase of frequency f, as shown in Figure 4.42(a) and 4.43(a). The dependence of the hysteresis area $< A >$ on E_0 is depicted in Figure 4.43(b). Similar observations have also been reported in the other PZT–PZN compositions as well as in soft and hard PZT ceramics [168-170].
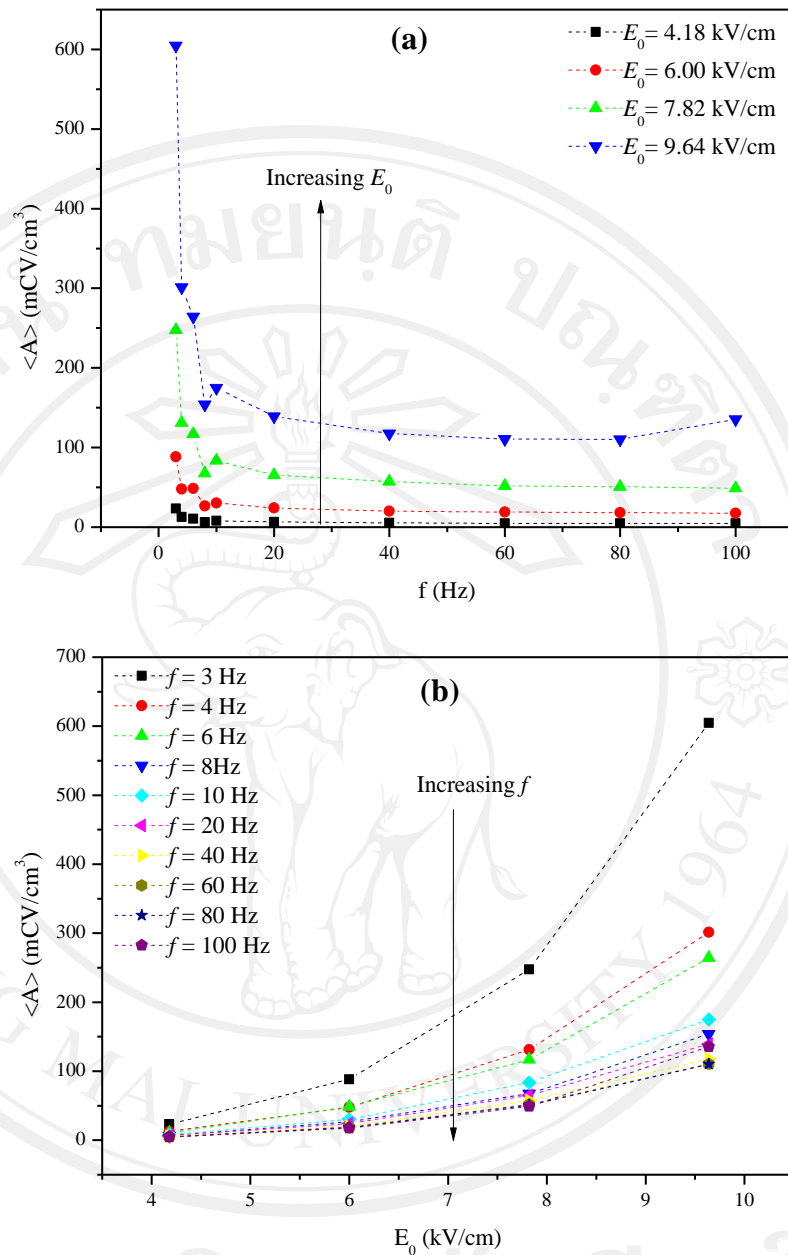
Figure 4.43 The hysteresis area $< A >$ profiles with evolutions of (a) frequency f, and (b) field amplitude E_0 under sub-coercive field condition for 0.5PZT-0.5PZN ceramic

To obtain the suitable scaling relation for the bulk ceramic, one can first follow the suggested scaling law given in Equation (4.1) to determine exponent m and n directly from the experimental data. By plotting $\log < A >$ against $\log f$ at fixed E_0,

one obtains the exponent m. On the other hand, the exponent n can be obtained from plotting $\log <A>$ against $\log E_0$ at fixed f. The plotting of $\log <A>$-$\log f$ and $\log <A>$- $\log E_0$ are shown in Figure 4.44(a)-(b).
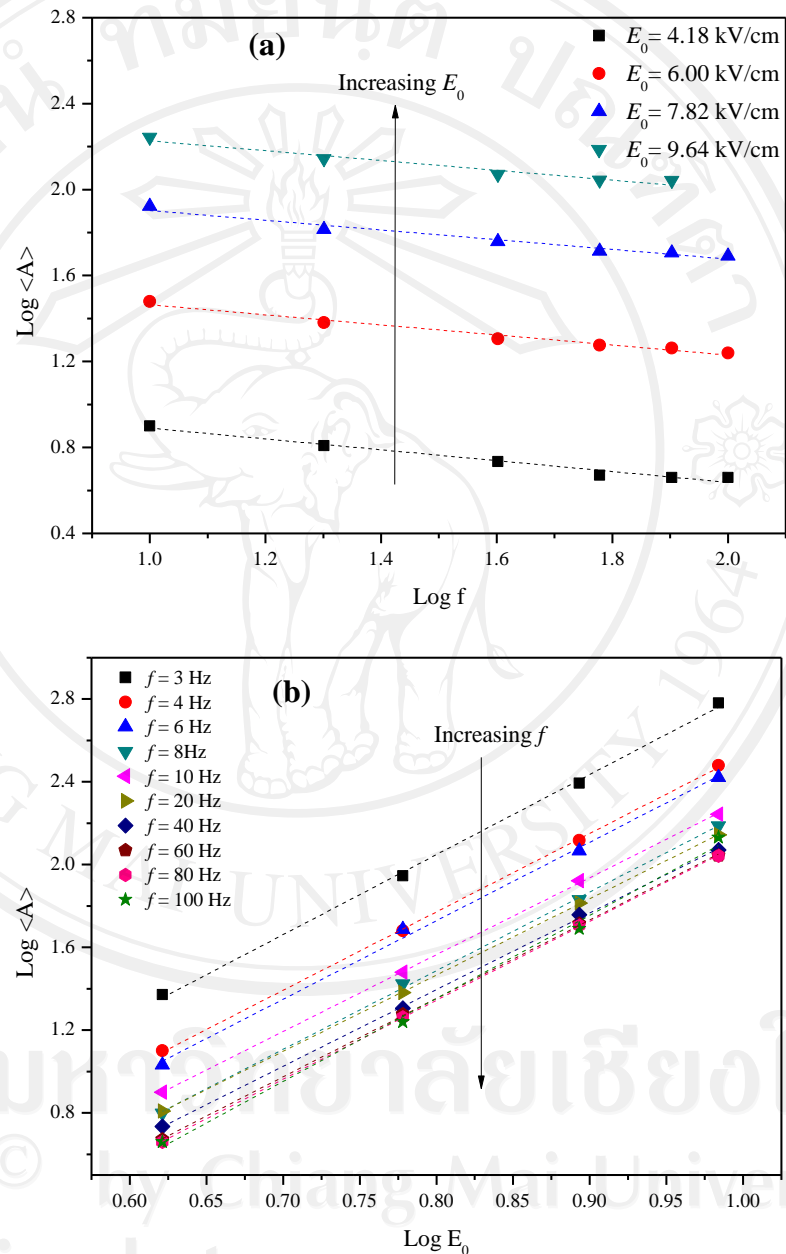
Figure 4.44 Logarithmic plots between (a) $\log <A>$ and $\log f$, and (b) $\log <A>$ and $\log E_0$ under sub-coercive field condition for 0.5PZT-0.5PZN ceramic. The dotted lines represent linear fitting

It is found that both *f*-exponent *m* and E_0-exponent *n* depended significantly on field amplitude E_0, and frequency *f*, respectively, as seen in Figure 4.45(a)-(b). The variations of both exponents obtained here are in strong contrast to most of the previous investigations [4-5, 7-8, 10, 13, 16-18, 127, 134], in which the scaling exponents are normally treated as constant and depend only on the dimensionality and symmetry of the system, not the frequency *f* and field amplitude E_0.
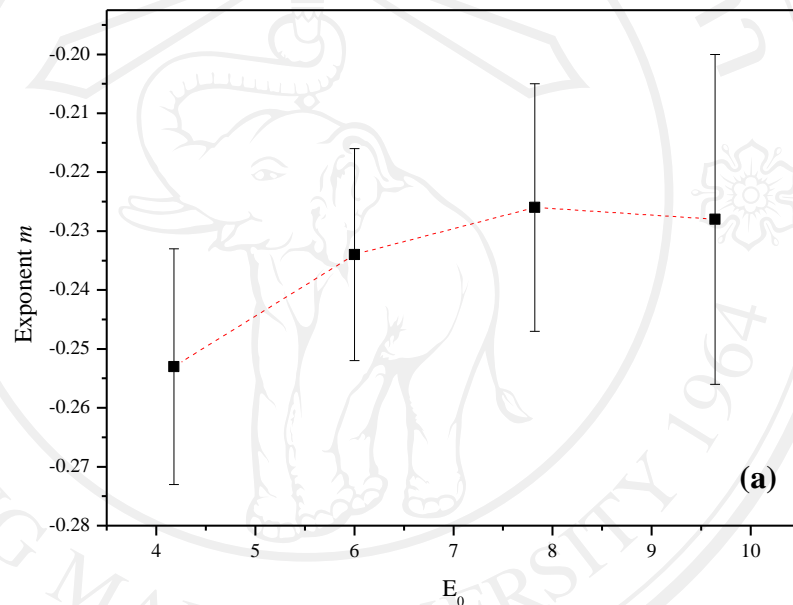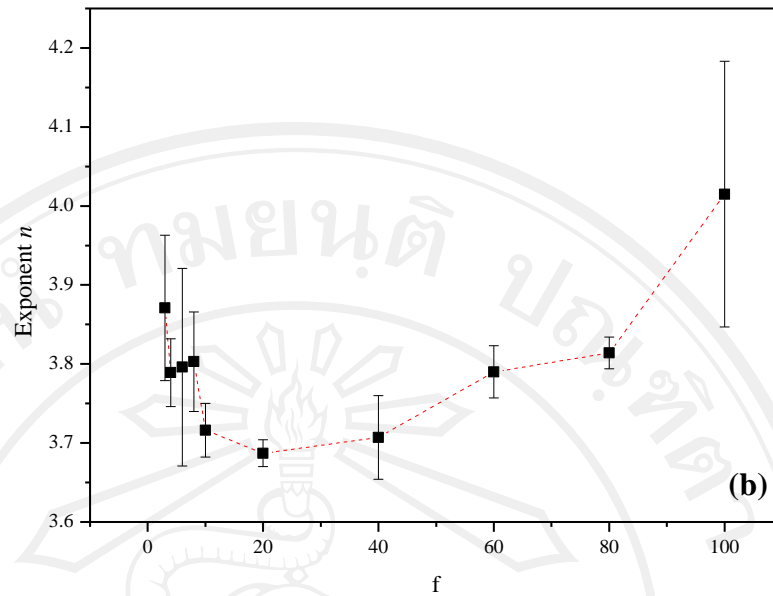
Figure 4.45 (a) Variation of f-exponent m with E_0, and (b) variation of E_0-exponent n with f under sub-coercive field condition for 0.5PZT-0.5PZN ceramic

For better illustration, the simplification to establish power-law scaling relation is constructed. Both of f-exponent m and E_0-exponent n are approximated as constant values to be representatives to conduct power-law scaling relations. Through first approximation, the f-exponent $m = -0.34$ and the E_0-exponent $n = 3.68$ are obtained for scaling relation of rhombohedral 0.5PZT-0.5PZN ceramic under sub-coercive field condition.

As plotted in Figure 4.46, it is revealed that the experimental data can be fitted (with $R^2 = 0.99$), within the measured uncertainty, by

$$< A > \propto f^{-0.34} E_0^{3.68} \tag{4.18}$$
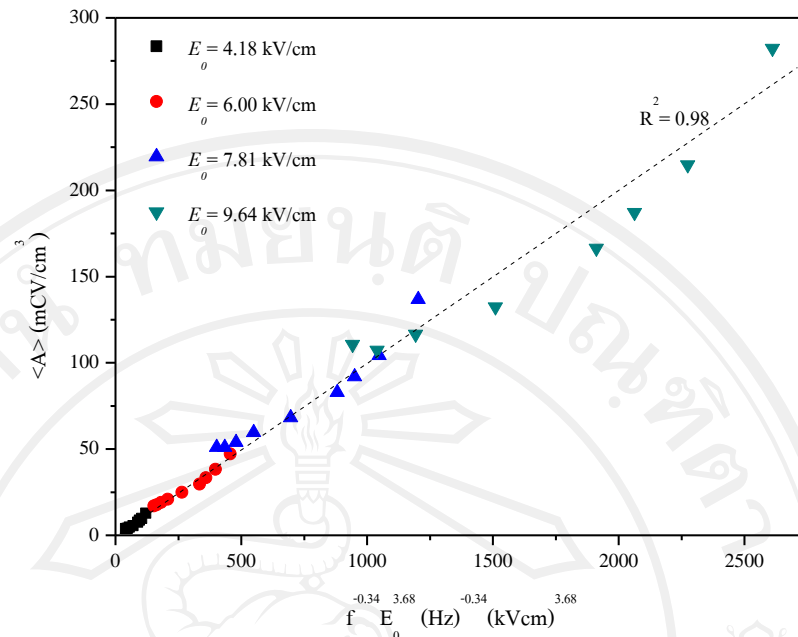
Figure 4.46 Power-law scaling relation of hysteresis area $< A >$ against $f^{-0.34}E_0^{3.68}$ for 0.5PZT-0.5PZN ceramic under sub-coercive field condition. The dotted lines represent linear fitting [19]

Here, the first interesting observation is that the minor loop scaling in 0.5PZT–0.5PZN bulk ceramics is generally similar to that of PZT thin film [6-7] as well as that of minor loop of PZT bulk ceramics [16-17]. As explained in our previous investigation [16], this is attributed to the fact that main polarization orientation mechanism in thin films and in sub-coercive field condition for bulk ceramics is likely from the 180° domain reversal [150-153, 172]. This explains why the scaling behavior of PZT bulk ceramics at low electric fields is similar to that of thin films. More importantly, the scaling relation obtained in Equation (4.18) is generally very similar to that of the minor-loop scaling relations obtained earlier for commercial soft and hard PZT bulk ceramics with $< A > \propto f^{-0.33}E_0^3$ and $< A > \propto f^{-0.43}E_0^{3.19}$, respectively [16-17]. This clearly indicates that the polarization orientation process in

rhombohedral 0.5PZT–0.5PZN ceramics with disrupted domains is similar to that in commercial PZT bulk ceramics with the same complex domain structures. Therefore, the scaling relations obtained here clearly support our previous proposed hypothesis that the domain structures play major role in controlling dynamic hysteresis behavior of ferroelectric materials [16-17].

All PZT-PZN compositions

To provide better comparison, the exponents *m* and *n* of power-law scaling relations for all PZT-PZN ceramic systems obtained from the data fitting are listed in Table 4.4.

Table 4.4 The scaling exponents *m* and *n* for PZT-PZN ceramic systems [173]

Composition	*m*	*n*
0.9PZT-0.1PZN	-0.42 ± 0.01	3.65 ± 0.01
0.8PZT-0.2PZN	-0.36 ± 0.01	3.32 ± 0.12
0.7PZT-0.3PZN	-0.35 ± 0.02	3.47 ± 0.09
0.6PZT-0.4PZN	-0.36 ± 0.01	4.03 ± 0.03
0.5PZT-0.5PZN	-0.34 ± 0.10	3.68 ± 0.04

As plotted in Figure 4.47, it is revealed that the experimental data can be fitted very well with the scaling relations obtained [173].
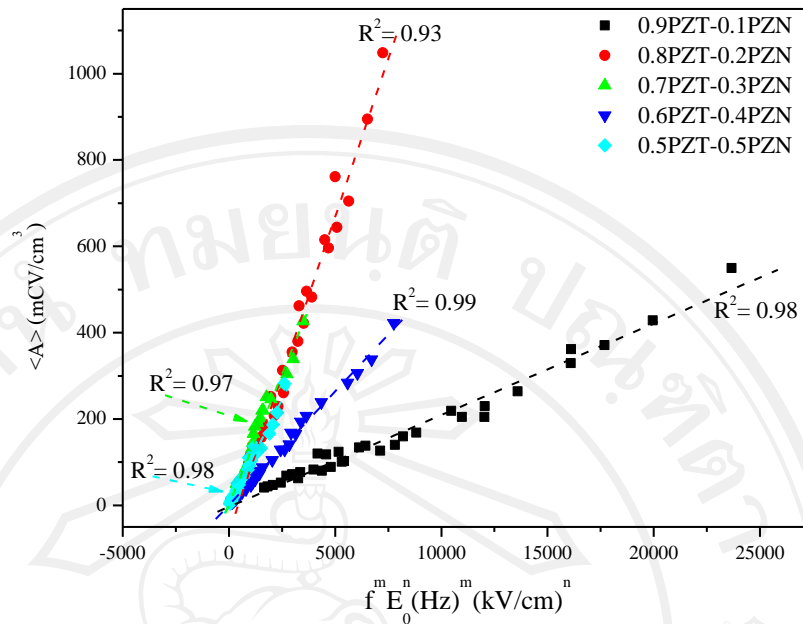
Figure 4.47 Power-law scaling relations of hysteresis area $<A>$ against $f^{m}E_0^{n}$ for PZT-PZN ceramics under sub-coercive field condition. The dotted lines represent linear fitting

Here, the first interesting observation is that the minor loop scaling in PZN-modified PZT bulk ceramics is generally similar to that of PZT thin film [6-7] as well as that of minor loop of PZT bulk ceramics [16-17]. This is attributed to the fact that main polarization orientation mechanism in thin films and in sub-coercive field condition for bulk ceramics likely is from the 180º domain reversal. As explained in our previous investigation [24], PZT ceramics generally contain 180º and non-180º domain structures [16]. The non-180º domain switching is normally accompanied with mechanical strain, it occurs at higher E field than the 180º domain reversal does. Therefore, under low E fields, one would expect the 180º domain reversal to occur first. It is also well known that the non-180º domain wall motion is typically very heavily clamped in thin films. Therefore, the main switching contribution in thin films

would be from the 180° domain reversal. This explains why the scaling behavior of PZT bulk ceramics at low E fields is similar to that of thin films [16].

More importantly, the scaling relations obtained, as listed in Table 4.4, indicate that $< A >$ decays more quickly with f and grows more quickly with E_0 than the minor-loop scaling relations obtained earlier for commercial soft PZT bulk ceramic with $< A > \propto f^{0.33} E_0^3$ [16]. This clearly indicates the ease of the polarization orientation process in PZT-PZN ceramics with a clear regular lamellar 90° domain configuration [171] that leads to faster polarization orientation kinetics, as compared to complex domain structures of commercial PZT bulk ceramics, which require higher energy barrier for the polarization orientation process. Comparing between soft and hard PZT bulk ceramics, soft PZT bulk ceramics with donor dopants contain A-site vacancies and lamella-like domain structures, while hard PZT bulk ceramics from an acceptor-doped PZT causes oxygen vacancy and disruptive-like domain structures, which are more complex than that of soft PZT bulk ceramics. Hence, hard PZT bulk ceramics require higher energy to reorient polarization.

Considering exponents m of PZT-PZN ceramic systems listed in Table 4.4, it can be seen obviously that scaling f-exponents m are controlled by domain structures. The exponents m of $(1-x)$PZT-(x)PZN where $x = 0.2, 0.3, 0.4,$ and 0.5 are very similar (in order of -0.34 to -0.36) because they are all in and near rhombohedral structure while the exponent m of $(1-x)$PZT-(x)PZN where $x = 0.1$ is so dominantly different (-0.42) due to its tetragonal structure.

For the exponents m and n obtained, they in fact have inter-correlation. However, it is too complicated to create scaling relation containing this kind of the inter-correlation. Hence, we create scaling relation by approximation. The median

values of each exponent (*m* and *n*) are chosen as the representative values. Therefore, the exponent values appeared in this work for PZT-PZN system is constant by approximation.

4.2   The dynamic hysteresis properties with temperature

4.2.1   BT bulk ceramics

Since barium titanate (BaTiO$_3$, BT) ceramics exhibit rhombohedral, orthorhombic, tetragonal and cubic phases with transition temperatures of -90 ℃, 0 ℃, and 120 ℃, respectively [174], it is then of interest to investigate dynamic hysteresis and scaling behaviors as a function of temperature in this material.

The hysteresis profiles on different *f* but fixed E_0 and on different E_0 but fixed *f* (insets) are shown for various phases, i.e., -100 ℃ (rhombohedral), -60 ℃ (orthorhombic), 25 ℃ (tetragonal) and 170 ℃ (cubic), in Figure 4.48(a)-(d). At fixed E_0, hysteresis area $< A >$, remnant polarization (P_r) and coercive field (E_C) are found to decrease with increasing *f*. All the three parameters increase with an increase of E_0 at fixed *f*. These results are consistent with previous studies [18, 21, 128, 175-177]. When measuring temperature is increased above Curie temperature (T_C), no hysteresis loop is expected [174]. However, as displayed in Figure 4.48(d), at $T = 170$ ℃ ($> T_C$), hysteresis loops are still obtained likely due to presence of charged defect movement in the as-synthesized sample [21].
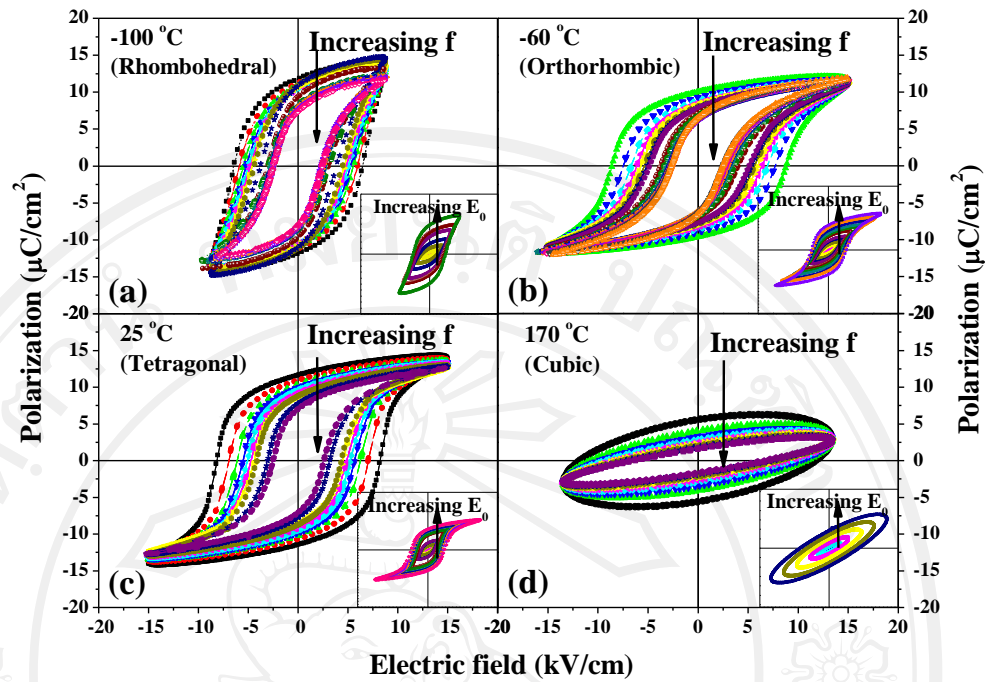
Figure 4.48 The *P-E* hysteresis loops at various frequencies f (10-100 Hz) and various electric fields E_0 (insets, up to 15 kV/cm) for $BaTiO_3$ material at different temperatures (a) -100 ℃ (rhombohedral), (b) -60 ℃ (orthorhombic), (c) 25 ℃ (tetragonal), and (d) 170 ℃ (cubic)

In order to illustrate the relations of $< A >$ to f and E_0 for various structures, results are plotted in Figure 4.49(a)-(d). It can first be seen that $< A >$ decreases with increasing f and increases with increasing E_0.
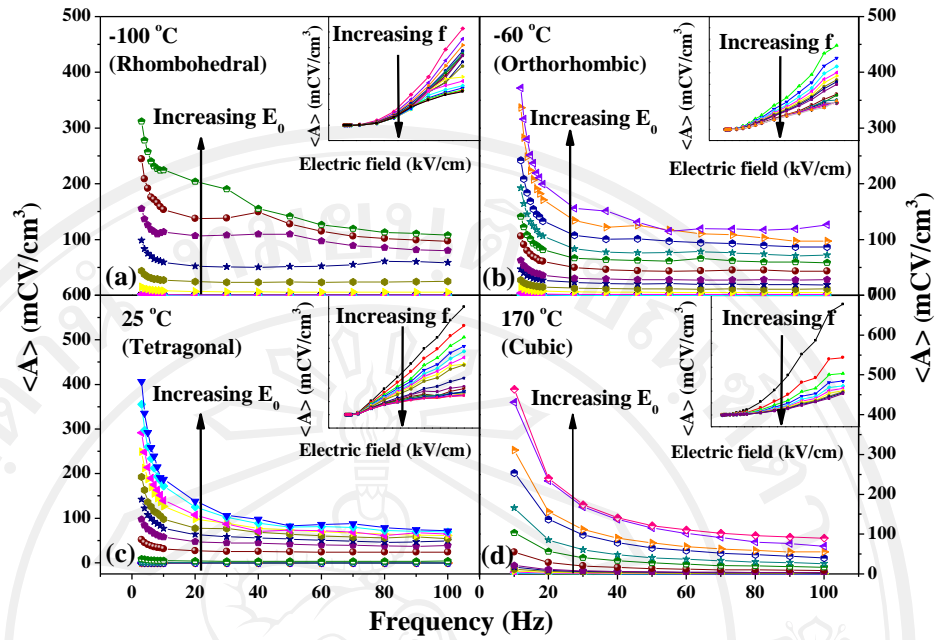
Figure 4.49 Development of hysteresis area $<A>$ as a function of f and E_0 (insets) for BaTiO$_3$ at (a) -100 ºC (rhombohedral), (b) -60 ºC (orthorhombic), (c) 25 ºC (tetragonal), and (d) 170 ºC (cubic)

Scaling relations are determined in f-range of 10-100 Hz and E_0 up to 15 kV/cm by using the data in Figure 4.49(a)-(d). Exponent m and n for all phases are extracted by using the method described in details elsewhere [177]. The scaling relations of $<A>$ against f and E_0 for various structural phases are shown in Figure 4.50(a)-(d). It is noticed that the scaling relations for orthorhombic and tetragonal structures are divided into two regimes corresponding to sub-coercive and saturated field regions (hereafter called low field and high field, respectively) [176]. In cubic phase, the scaling relations of both low and high field regimes manifested the same exponent values as shown in Figure 4.50(d). This implied that domains (if any) in both regimes experienced the same switching mechanisms which are mainly from thermal fluctuation of charged carriers [21]. The scaling relation for rhombohedral

phase is only determined in low field because for $T < -90$ °C, the silicone oil used in measurement started degrading.

The physical meaning of scaling exponent m and n has been discussed in previous study [128]. The influence of temperature on the exponents is shown in Figure 4.51 under low and high field conditions. Under low field condition, exponent n exhibits magnitude in the order 3-4 ($n \sim 3$-4) in ferroelectric phases. This can be explained based on basis of available different spontaneous polarization states regarding to each crystal structures [18, 21, 80, 175, 177]. However, with careful consideration, it is found that the exponent n gradually increased (from 3.04 to 3.49) with crystal structure change from rhombohedral to tetragonal phase (Table 4.5) which is very consistent with evolution of spontaneous polarization (P_S) along structure phase change in BT (from 8 $\mu C/cm^2$ in rhombohedral to 16 $\mu C/cm^2$ in tetragonal) [121]. So this suggests that exponent n is directly related to P_S, except in high field condition.

More interestingly, the obtained exponent n values are approximately 1 for high field and close to 3-4 for low field, similar to many previous studies [177], as seen in Table 4.5. Clearly, change in structures does not cause much change in the exponent because the mechanism of domain switching/re-orientation with field is roughly the same. So this shows universality of the scaling behavior. Significant deviation in thin-film cases is caused by clamped states in the thin-films, so switching mechanism is changed.

In cubic phase ($T > T_C$), exponent n under low field is reduced to the order 2 ($n \sim 2$) because above T_C, there is no large scale domains left, only small thermally fluctuated ones. So the P-E loop is mainly from space-charge and thermally activated

charged carrier movement, regarding to long-range movement of oxygen vacancies, resulting in thermal loss (Joule heat) [178-179]. The increase of exponent n under high field in cubic phase can also be explained in term of migration of charged carriers. This result is very consistent with previous study by Yang *et al.* ($\alpha = n \approx 2$) [21], but the present study extended the range of observed temperature, f and E_0 covering both low and high field conditions. The same exponent n values in both low and high fields in cubic phase confirmed that the polarization reversal mechanism above T_C is not related to domain switching, but it is from long-range migration of thermally activated charged defects. The difference in exponent n values between low and high field conditions in ferroelectric phases can be attributed to the induced strain originating from irreversible non-180º domain switching which is slower process.

In case of exponent m for various phases, relatively constant trends with temperature development are obtained for both low and high field conditions as shown in Figure 4.51. This suggested that for polycrystalline material f-exponent m is crystal structure-independent. In contrast, the magnitude of m rapidly decreases in cubic phase. Theoretically, domain switching time (t_0) decreases with increasing temperature (T) below Curie point (T_C) following Ishibashi's model [180-182] as $t_0 = BE^{-j}\tau^{+k}$ with empirical j and k of order 1-2 and $\tau = (T_C - T)/T_C$ which is very compatible with Scott's model [183] that proposed switching time in form of $t_s \approx A\tau/E$. Hence, rapid decrease of exponent m(convergent on $m \sim$ -1) in cubic phase, indicating very long time for switching, is arisen by the activity from long-range migrating charged defects, not from ferroelectric domains.
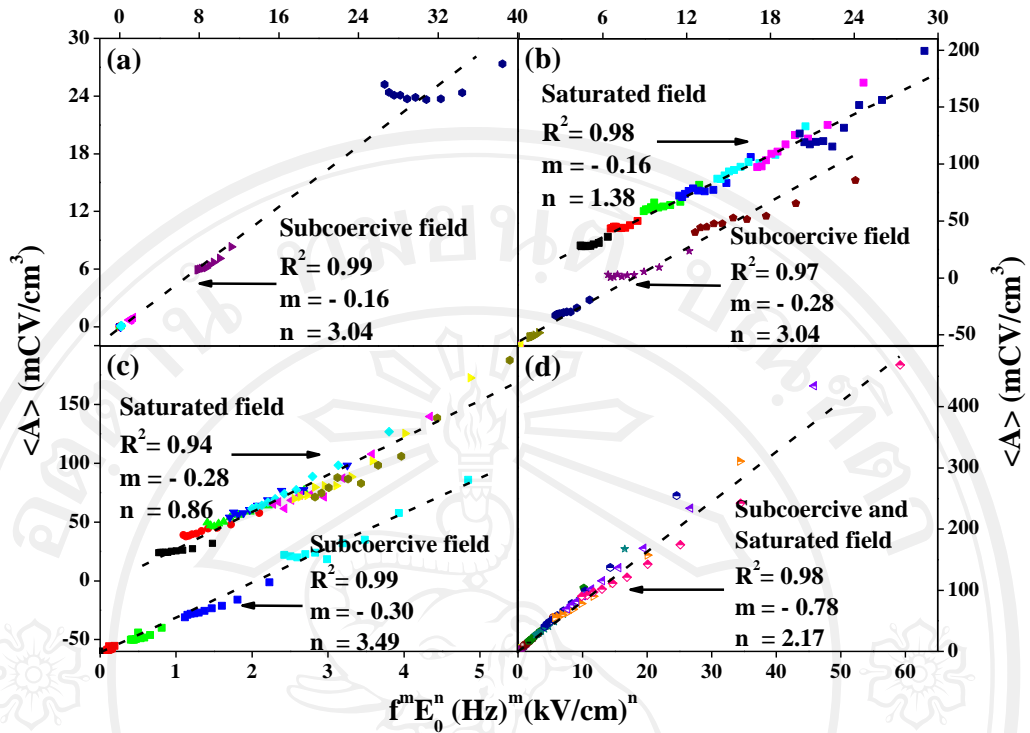
Figure 4.50 Power-law scaling relations in form of hysteresis area $< A >$ as a function of f and E_0 in various crystal phases of BaTiO$_3$ at (a) -100 °C (rhombohedral), (b) -60 °C (orthorhombic), (c) 25 °C (tetragonal), and (d) 170 °C (cubic). The frequency is varied in the range of 10-100 Hz and E_0 from 0-15 kV/cm

The exponent m in ferroelectric phases for polycrystalline BT are in order of -0.1 to -0.3 by taking into account possible deviation values. These values showed discrepancy against exponent m = -1 for three-dimensional $(\Phi^2)^2$ and $(\Phi^2)^3$ model which is probably because frequency is approaching infinity limit ($\Omega \to \infty$) [184]. In contrast, these exponent m values are much different from ones obtained by Ishibashi [144] and Scott (m = 0.145) [185] because the Kolmogorov-Avrami based model used in those studies is assumed to work properly with highly anisotropic uniaxial ferroelectrics that the domain wall motion is needlelike. This assumption is not

compatible with general polycrystalline ceramics which are normally not uniaxial ferroelectrics. This is possibly why the exponent *m* is different.
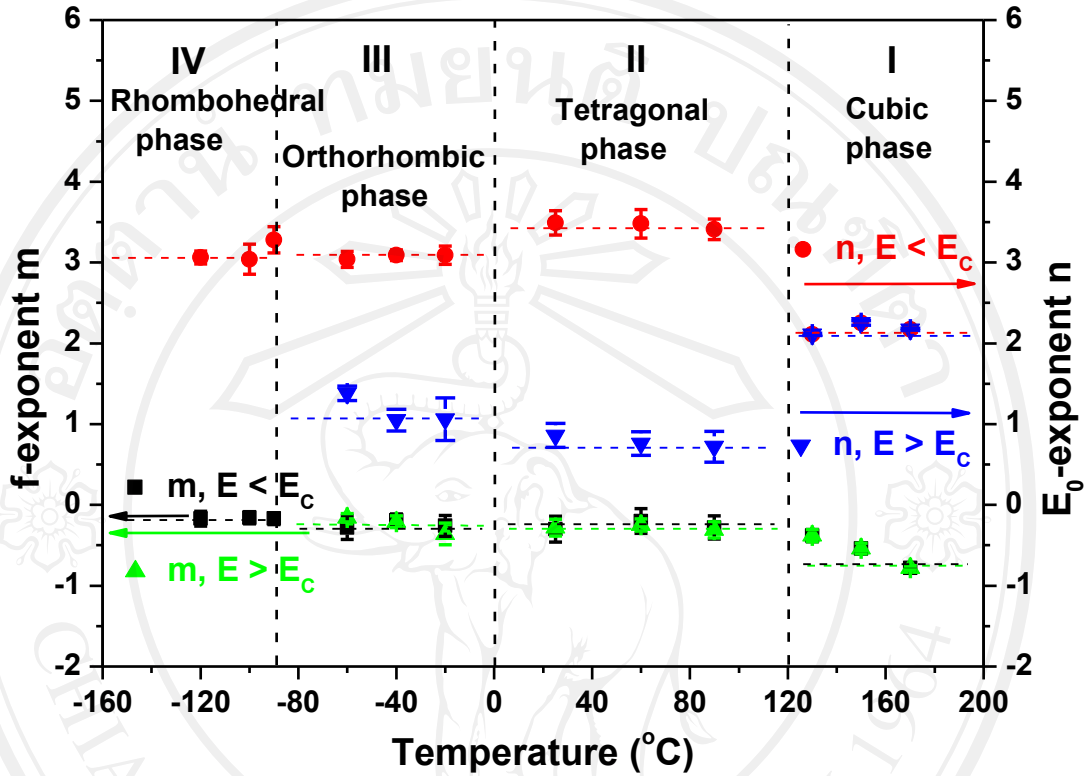
Figure 4.51 Variation of *f*-exponent *m* and E_0-exponent *n* as a function of temperature covering typical structural phases of $BaTiO_3$ bulk ceramic

Table 4.5 Power-law scaling exponents in ferroelectric systems

Temperature (°C)	Sub-coercive field		Saturated field	
	m	*n*	*m*	*n*
BaTiO$_3$ bulk ceramic				
170	-0.78±0.03	2.17±0.01	-0.78±0.03	2.17±0.01
25	-0.30±0.16	3.49±0.15	-0.28±0.10	0.86±0.15
-60	-0.28±0.15	3.04±0.10	-0.16±0.05	1.38±0.09
-100	-0.16±0.08	3.04±0.18	-	-
Soft PZT bulk ceramic				
(25°C) [177]	-0.33	3	-0.25	1
Hard PZT bulk ceramic				
(25°C) [177]	-0.43	3.19	-0.28	0.89

Above Curie temperature (T_C), ionized oxygen vacancies can move under applied electric field and result in Joule loss which can be expressed as:

$$W_{loss} = \int iv \, dt \qquad (4.19)$$

where W_{loss} is the Joule loss, leakage current for a non-ferroelectric state $i = \sigma v A/d$, σ is conductivity, v is the measured voltage, A is the area of electrode, d is the sample thickness [186], and t is the measurement time. For sinusoidal waveform, $v = v_0$ sine(ωt), where v_0 is the amplitude voltage. Hence,

$$W_{loss} = 4 \int_0^{t/4} \frac{\sigma A (v_0 sine\, \omega t)^2}{d} \, dt \qquad (4.20)$$

then,

$$W_{loss} = \frac{A\sigma v_0^2}{2df} \tag{4.21}$$

Equation (4.21) shows the Joule loss for sinusoidal signal applied voltage. It is directly proportional to quadratic power of voltage whereas inversely proportional to frequency. This also suggests that loss from charge migration can be reduced by increasing f.

With agreeable results of E_0-exponent $n \approx 2$ above T_C obtained from BT ceramics and previous study [21]; it thus can be considered as universal criterion to distinguish the artifact polarization. Similarly for f-exponent m, by convergent on -1 above T_C of BT ceramics, it suggests instinctively that f-exponent $m \approx$ -1 might be the critical criterion. Consequently, the same set of E_0-exponent $n \approx 2$ and f-exponent $m \approx$ -1 is the quantitative criterion called "universal set" to identify the artifact ferroelectric state.

4.2.2 BT single crystals

The P-E hysteresis profiles on different f but fixed E_0 and on different E_0 but fixed f (insets) of {001} BaTiO$_3$ single crystal with various structure phases, i.e., orthorhombic (-60 ℃), tetragonal (25 ℃) and cubic (180 ℃), are shown in Figure 4.52(a)-(c). At fixed E_0, hysteresis area $< A >$, remnant polarization (P_r) and coercive field (E_C) are found to decrease with increasing f. All three unique parameters increased with an increase of E_0 at fixed f. These results are consistent with previous studies [18, 21, 128, 175-177]. When measurement temperature is increased above Curie temperature (T_C), no hysteresis loop is expected [174]. However, as seen from 180 ℃ (cubic) in Figure 4.52(c), at T = 180 ℃ (> T_C), hysteresis loops are still

obtained due to presence of charged defect movement in the as-synthesized sample [21].
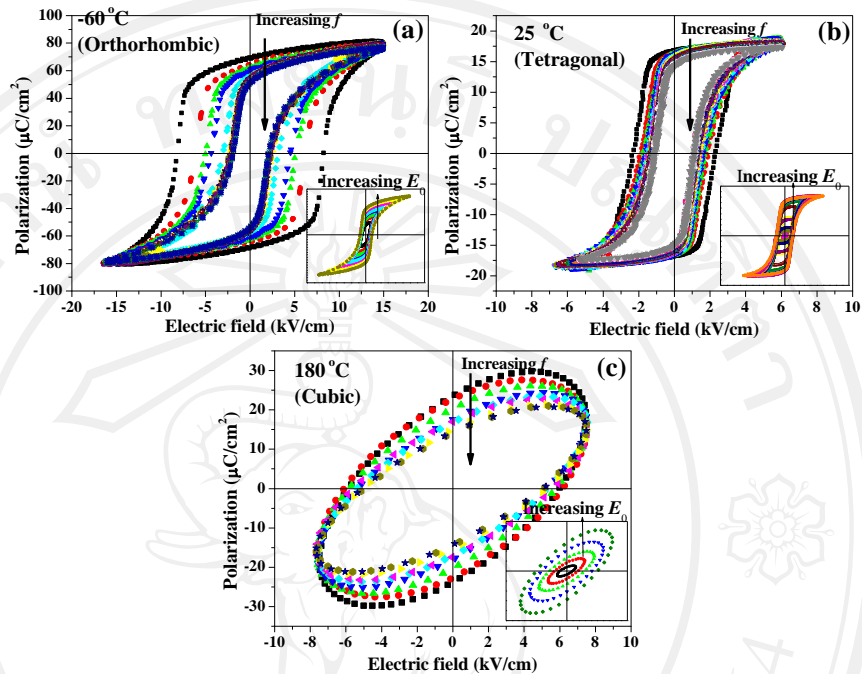
Figure 4.52 The *P-E* hysteresis loops for BaTiO$_3$ single crystal at various frequencies *f* (1-300 Hz) and various electric fields E_0 (insets, up to 15 kV/cm) (a) -60 °C (orthorhombic), (b) 25 °C (tetragonal), and (c) 180 °C (cubic)

In order to illustrate the relations of $< A >$ to *f* and E_0 for various crystal structures, results are plotted in Figure 4.53(a)-(c). It can be seen more obviously that $< A >$ decreased with increasing *f* and increased with increasing E_0.
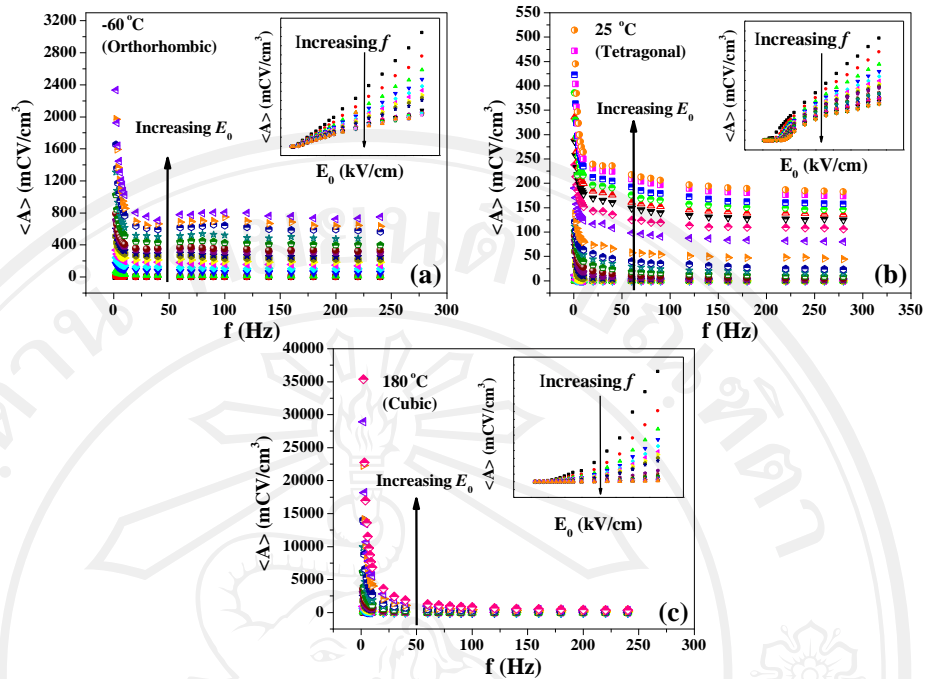
Figure 4.53 Development of hysteresis area $< A >$ as a function of f and E_0 (insets) for BaTiO$_3$ single crystal at (a) -60 ºC (orthorhombic), (b) 25 ºC (tetragonal), and (c) 180 ºC (cubic)

The magnitude of exponent m and n are determined in scaling relations under low and high field conditions for the three phases, i.e., orthorhombic, tetragonal, and cubic, as shown in Figure 4.54.

Scaling relations are determined in f-range of 1-300 Hz and E_0 up to 15 kV/cm (depending on observed temperature) by using the data in Figure 4.53(a)-(c). Exponents m and n for all crystal phases are extracted by using the method described in detail elsewhere [177]. The scaling relations of $< A >$ against f and E_0 for various structural phases are shown in Figure 4.54(a)-(c). Notice that the scaling relations for orthorhombic and tetragonal structures are divided into two regimes corresponding to sub-coercive and saturated field regions (hereafter called low field and high field, respectively) [176]. In cubic phase, the scaling relations of both low and high field

regimes manifest the same exponent values as shown in Figure 4.54(c). This implies that domains in both regimes experienced the same switching mechanisms which are mainly from thermal fluctuation of charged carriers (i.e. oxygen vacancies) [21].
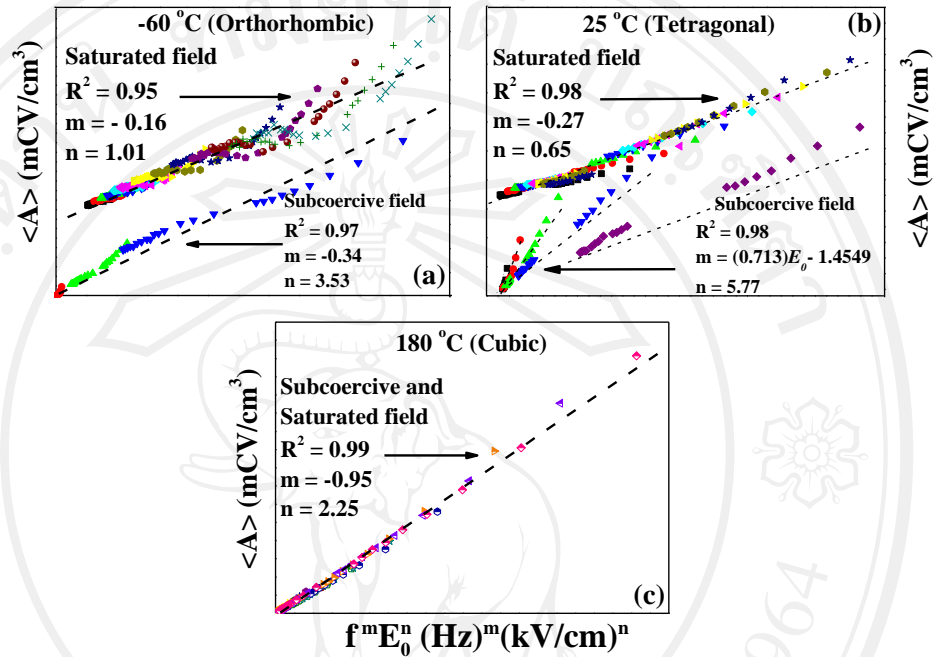
Figure 4.54 Power-law scaling relations in form of hysteresis area $< A >$ as a function of f and E_0 in typical crystal phases of BaTiO$_3$ single crystal at (a) -60 ℃ (orthorhombic), (b) 25 ℃ (tetragonal), and (c) 180 ℃ (cubic). The frequency is varied in the range of 1-300 Hz and E_0 from 0-15 kV/cm. The dotted lines represent linear fitting

The evolution of exponents m and n with temperature exhibits similar trends as of BT bulk ceramic but the magnitude is significantly different. Exponent n value under low field condition for BT single crystal is 3.53 at -60 °C and 5.77 at 25 °C. These values are clearly larger than that of BT bulk ceramic which exhibited 3.04 at -60 °C and 3.49 at 25 °C. This can be explained in term of much more concentration of grain boundaries in polycrystalline ceramics which normally suppress domain

switching and migration. Table 4.6 lists the values of m and n for bulk and single crystal BT for various temperatures and field conditions.

Surprisingly, exponents n under high field condition for BT single crystal (1.01 at -60 °C and 0.65 at 25 °C) exhibit lower values than that of BT bulk ceramic (1.38 at -60 °C and 0.86 at 25 °C). This is because, above E_C, available domain states for BT ceramic previously constrained by energy barriers are significantly enhanced. Similar exponent behaviors can be found on comparison between soft PZT and BT single crystal [24]. Moreover, in cubic phase, exponent n for BT single crystal is also about ~2.

In case of exponent m under high field, the magnitudes for ceramic and single crystal are quite similar, i.e., -0.16 at -60 °C and -0.27 at 25 °C for single crystal and -0.16 at -60 °C and -0.28 at 25 °C for bulk ceramic. This is expected as the dynamic hysteresis behavior is mainly governed by the availability of domain states above E_C [17]. The magnitudes of exponent m under low field condition for BT bulk ceramic (-0.28 at -60 °C and -0.30 at 25 °C) showed significantly higher values than that of BT single crystal (-0.34 at -60 °C and -0.74 at 25 °C). This is probably due to two factors. The first is BT bulk ceramic and BT single crystal are observed in different f-ranges which f-range 10-100 Hz is for BT bulk ceramic and f-range 1-300 Hz is for BT single crystal. In previous study, the difference of observed f-ranges resulted in discrepancy of scaling exponents [17]. The other one can be explained by taking into account the fact that the boundary defects in ceramic are overwhelming and effectively prevent domain rotation. Then even f increases, the delayed domain response does not change so much because of initial difficulty of movement. This effect is further amplified in materials with higher defect volume [187].
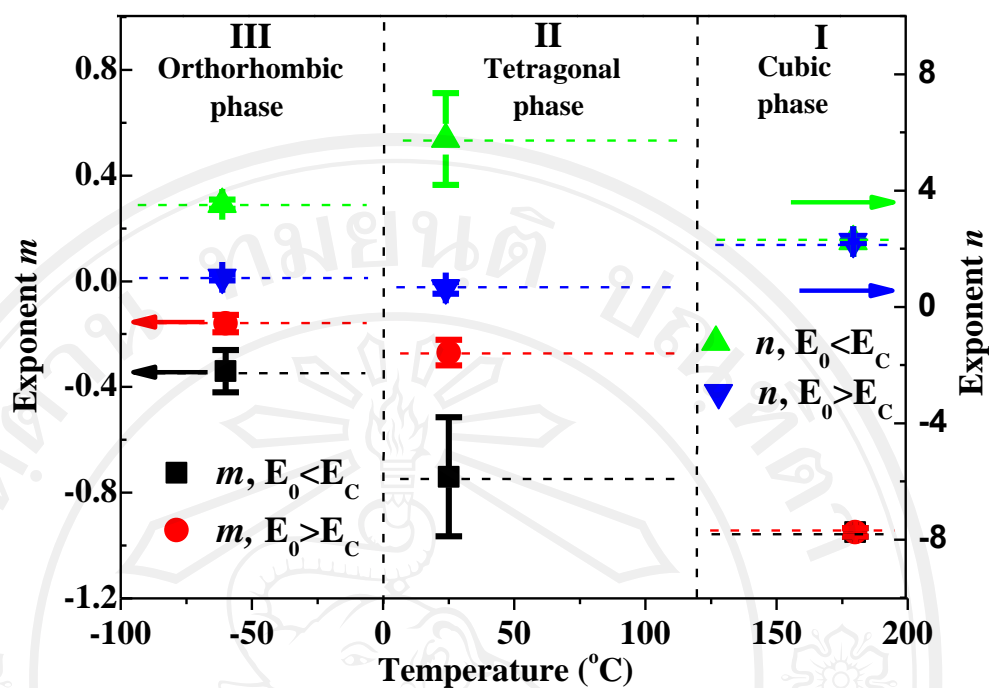
Figure 4.55 Variations of *f*-exponent *m* and E_0-exponent *n* as a function of temperature covering typical structural phases of BaTiO$_3$ single crystal

Table 4.6 Power-law scaling exponents for BT systems in typical phases

Temperature (°C)	Sub-coercive field		Saturated field	
	m	*n*	*m*	*n*
BaTiO$_3$ single crystal				
180	-0.95±0.02	2.25±0.02	-0.95±0.02	2.25±0.02
25	(0.713)E_0- 1.4549	5.77±1.58	-0.27±0.05	0.65±0.20
-60	-0.34±0.08	3.53±0.16	-0.16±0.03	1.01±0.10
BaTiO$_3$ bulk ceramic				
170	-0.78±0.03	2.17±0.01	-0.78±0.03	2.17±0.01
25	-0.30±0.16	3.49±0.15	-0.28±0.10	0.86±0.15
-60	-0.28±0.15	3.04±0.10	-0.16±0.05	1.38±0.09
-100	-0.16±0.08	3.04±0.18	-	-

The exponent *m* in low and high field conditions for BT single crystal revealed obviously different values. Generally, switching time decreases as field amplitude increases. Switching time (t_s) in BaTiO$_3$ can be expressed as $t_s = a(d - d')e^{\alpha/E}$ suggesting the direct proportion to sample thickness (*d*) and inverse proportion to field amplitude (*E*) [188]. Thus, lower decaying rate of domain response with increasing frequency in high field can be expected.

With agreeable results of E_0-exponent $n \approx 2$ above T_C obtained from BT ceramics, BT single crystal and previous study [21], thus, it can be considered as universal criterion to distinguish the artifact polarization. Same for *f*-exponent *m*, agreement of convergent on -1 above T_C for both BT ceramics and BT single crystal suggested instinctively that *f*-exponent $m \approx -1$ is the critical criterion. Consequently, the same set of E_0-exponent $n \approx 2$ and *f*-exponent $m \approx -1$ is the quantitative criterion called "universal set" to identify the artifact ferroelectric state.

4.3   The dynamic hysteresis properties with electric field-waveform

In previous study of dynamic hysteresis behaviors for 0.7PMN-0.3PT single crystal conducted by sinusoidal field-waveform application at room temperature, the dynamic *P-E* hysteresis profiles with sinusoidal waveform applied at different E_0 (up to 15 kV/cm) but fixed *f* = 50 Hz and different *f* (range of 1-200 Hz) but fixed $E_0 = 15$ kV/cm are shown again in Figure 4.56(a)-(b), respectively.
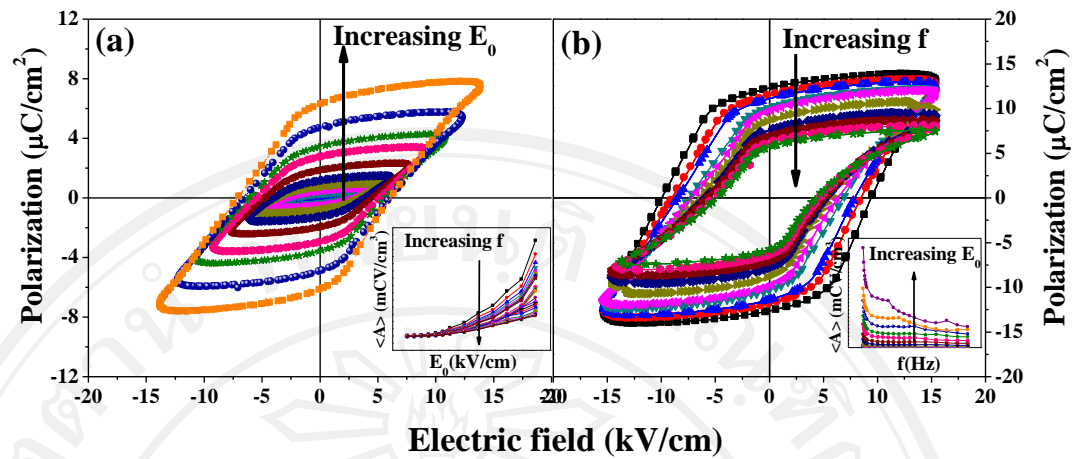
Figure 4.56 The sinusoidal-waveform *P-E* hysteresis loops of 0.7PMN-0.3PT
single crystal for (a) various E_0 but fixed f = 50 Hz, and (b) various f but fixed E_0 = 15
kV/cm

The power-law scaling relations determined in f-range of 1-200 Hz and E_0 up
to 15 kV/cm are shown in Figure 4.57. The scaling relations of $<A>$ against f and E_0
for sinusoidal waveform are divided into two regimes corresponding to sub-coercive
and saturated field conditions which possess different domain switching mechanisms.
The reversible 180º domain switching mechanism is active in low field condition
whereas the irreversible non-180º domain switching is active in high field condition
[16].
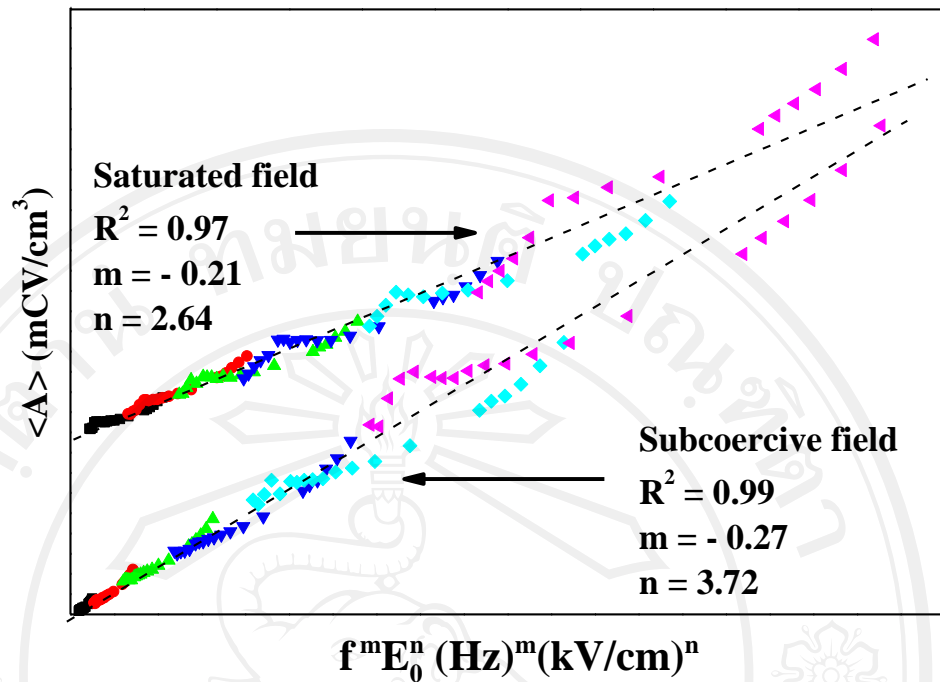
Figure 4.57 Power law scaling relations in form of hysteresis area $<A>$ as a function of f and E_0 for low and high field conditions with sinusoidal-waveform for 0.7PMN-0.3PT single crystal

By comparing at saturated field condition, E_0-exponent n of 0.7PMN-0.3PT single crystal is 2.64 while that of 0.7PMN-0.3PT film is 0.67 [21]. These exponents are very different, possibly because the maximum field applied of 15 kV/cm does not produce fully saturated P-E loops. Besides the difference in observed E_0-ranges and material forms (single crystal and film), one interesting issue which should be taken into consideration is applied field-waveform. In our investigation, the electric field sinusoidal waveform is used in conducting hysteresis measurement while triangle-waveform which is generally the basic setting for automatic hysteresis measurement employed in previous study [21]. Hence, to determine influence of field-waveform on hysteresis characteristics and scaling relations, the dynamic hysteresis and scaling behaviors conducted by triangle field-waveform should be carried out.

Hysteresis traits and scaling relations for 0.7PMN-0.3PT single crystal conducted by triangle waveform achieved by the same methodology as of sinusoidal waveform are shown in Figure 4.58(a)-(b) and 4.59, respectively.

Figure 4.58 The triangle-waveform P-E hysteresis loops of 0.7PMN-0.3PT single crystal for (a) various E_0 but fixed $f = 50$ Hz, and (b) various f but fixed $E_0 = 15$ kV/cm
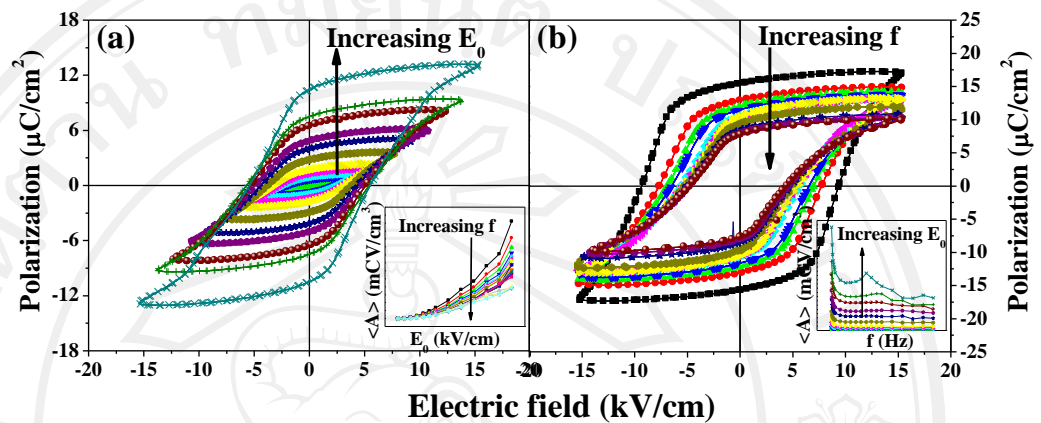
By comparison, E_0-exponent n obtained from sinusoidal waveform for both low and high field conditions are higher than those obtained from triangle waveform whereas f-exponent m are lower in both regimes, as shown in Table 4.7. In order to explain the cause of difference in exponents obtained from sinusoidal and triangle waveforms, the waveform characteristics must be considered. As shown in Figure 4.60, Triangle waveform-hysteresis loop exhibited higher remnant polarization (P_r) with approximately equal coercive fields (E_C) resulting in larger hysteresis area $< A >$ compared with results obtained from sinusoidal waveform-hysteresis loop. Generally, triangle-voltage waveform typically used in ferroelectric analyzers can be described by

$$V = 4V_a ft, \tag{4.22}$$

where V, V_a, f and t are measured voltage, maximum voltage, measured frequency and measured time, respectively, whose slope is $4V_a f$ [158]. The sinusoidal waveform which is typically $V = V_a \sin \omega t$ and the slope can be written as; $\omega V_a \cos \omega t$. The electric field (directly related to voltage) applied by triangle waveform increases uniformly with constant rate (slope) reaching to maximum at $t/4$, whereas the electric field of sinusoidal waveform reaches maximum at $t/4$ with non-uniform increasing rate, as seen from inset of Figure 4.60. The triangle waveform has more uniformity. This enables domains to easily rearrange their directions along applied field compared to less uniform sinusoidal waveform. So this explains why P_r and $<A>$ of hysteresis loop from triangle waveform are higher than those of sinusoidal waveform.
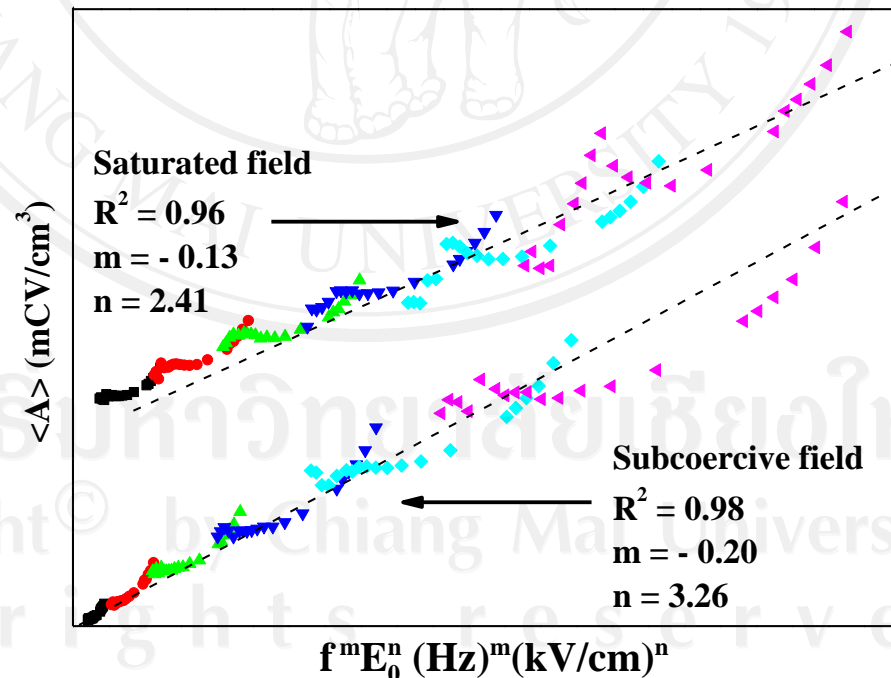
Figure 4.59 Power-law scaling relations for 0.7PMN-0.3PT single crystal in form of hysteresis area $< A >$ as a function of f and E_0 for low and high field conditions with triangle waveform

The higher exponent n for low and high field conditions of sinusoidal waveform as compared to triangle waveform can be explained based on electrical driving force strength. Sinusoidal waveform generates electric field reaching maximum in $t/4$. Within this period, field strength of sinusoidal waveform is always higher than that of triangle waveform. Domains get instantaneously strong forced by driving field and become switching easier. So increasing rate of polarization and $<A>$ of sinusoidal waveform grows faster and results in higher exponent n.

On the other hand, exponents m obtained by sinusoidal waveform is lower than that obtained by triangle waveform for both low and high field conditions. This is attributed to the uniformity. Triangle waveform provides uniform electric field which is more comfortable for domains to gradually rearrange the direction. Then higher exponent m can be expected.
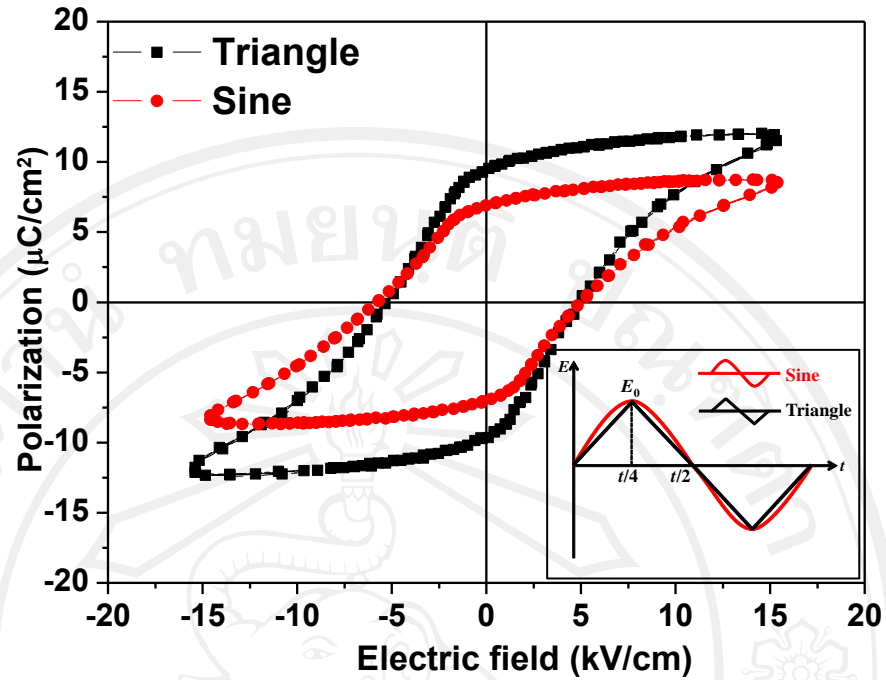
Figure 4.60 The *P-E* hysteresis loops of 0.7PMN-0.3PT single crystal obtained by applying sinusoidal and triangle electric field-waveforms. Inset shows waveform characteristics

Table 4.7 The exponents of power-law scaling relation for ferroelectric systems

System	Sub-coercive field		Saturated field	
	m	n	m	n
PMN-PT single crystal				
Sine waveform	-0.27±0.05	3.72±0.27	-0.21±0.03	2.64±0.16
Triangle waveform	-0.20±0.05	3.26±0.26	-0.13±0.03	2.41±0.13

Although the waveform of applied electric field affected the hysteresis characteristics and scaling relations, when compared with previous work of 0.7PMN-0.3PT film [21] the E_0-exponent n are still too much different. For this investigation,

exponent *n* for high field condition of sinusoidal waveform is 2.64 and triangle waveform is 2.41, while that of 0.7PMN-0.3PT film is 0.67. This can be presumed that the main cause of discrepancy is likely from observed E_0-range being far away from fully saturated field state.

With taking into account the deviation value (error bar), the exponents *m* and *n* obtained from both sinusoidal and triangle electric field-waveforms overlapped in some range. For example, under low field condition, exponent *m* of sinusoidal waveform is -0.27±0.05 and that of triangle waveform is -0.20±0.05. These values are found to overlap in the range of -0.22 to -0.25 and range of 3.45-3.52 for exponent *n*. Therefore, it can be said that while the different waveforms produce a variation in the exponents *m* and *n*, this cannot be accounted for the difference in the exponents between thin films and bulk forms.

4.4   Summary of influencing factors

The factors which impact on dynamic hysteresis and scaling exponents include;

1. The modeling conditions: the conditions applied in theoretical models do not fully cover the real behaviors in nature while the experimental models do, as seen from the difference between exponent *n* of $BaTiO_3$ single crystal and that of theoretical $(\Phi^2)^2$ and $(\Phi^2)^3$ model. A qualitative explanation for the difference may come from the polarization-interaction terms as considered in the $(\Phi^2)^2$ and $(\Phi^2)^3$ models, in which the polarization flip just has one contribution, i.e., polarization reversal [4-5].

2. The switching mechanism: as seen from several materials in this study, the exponents *m* and *n* between sub-coercive and saturated field conditions of the same material were obviously different while exponents obtained from sub-

coercive field ceramics were very similar to those obtained from thin films. This is attributed to the fact that the main polarization orientation mechanism in thin films and in sub-coercive field condition for single crystals and bulk ceramics is likely from the reversible 180° domain rotation (which also occurs at much faster rate than the irreversible process), as the irreversible non-180° domain switching is normally accompanied with mechanical strain, it occurs at higher E-field than 180° domain rotation does. Therefore, under low E-fields, one would expect the 180° domain rotation to occur first [23, 139-143]. This explains why the scaling behavior of the single crystals and bulk ceramics at low E fields is similar to that of thin films and why the response to E_0 at sub-coercive field occurs at much faster response than that at higher field amplitude.

3. Defect concentration: as seen from comparison between exponents obtained from $BaTiO_3$ single crystal and bulk ceramic, exponents for $BaTiO_3$ single crystal were higher than those for bulk ceramic due to less defect concentration.

4. Observed range of f and E_0: we can see from $BaTiO_3$ bulk ceramic characterization at room temperature section, the scaling exponents obtained from f-range 1-100 Hz and f-range 20-100Hz were obviously different. For instance of different observed E_0-range we can see from 0.7PMN-0.3PT single crystal section. Exponent n obtained for saturated field condition in this study was quite far from that obtained in 0.7PMN-0.3PT thin film [21] because applied field in this study does not provide full saturation state.

5. Random field: as seen from the difference in scaling exponents between normal ferroelectric BaTiO$_3$ single crystal and relaxor ferroelectric material 0.7PMN-0.3PT single crystal, the exponents of scaling relations for 0.7PMN-0.3PT single crystal were lower than those for BaTiO$_3$ single crystal due to existence of random field.

6. Crystal structure: this can be seen obviously in PZT-PZN ceramic system section. The exponents were varied with composition.

7. Temperature: this one can also be seen clearly in temperature dependence of hysteresis properties and scaling relations in BT system section. Variations of exponents with temperature were revealed.

8. Waveform: this can be seen from the latest section of field-waveform dependence of dynamic hysteresis and scaling behaviors in 0.7PMN-0.3PT single crystal. The exponents slightly changed with field-waveform.

Table 4.8 Summarized scaling exponents for ferroelectric materials at room temperature

Systems	m	n
Nd-doped $Bi_4Ti_3O_{12}$ thin film	-0.33	2
$SrBi_2Ta_9O_4$ thin film	-0.33	3
$Pb(Zr,Ti)O_3$ thin film	-0.33	1
$PbTiO_3$/polymer composite	-1	2
Soft PZT bulk ceramic		
Saturated Loops	-0.25	1
Minor Loops	-0.33	3
Hard PZT bulk ceramic		
Saturated Loops	-0.28	0.89
Minor Loops	-0.43	3.19
PZT-PZN bulk ceramic(Minor loop)		
0.9PZT-0.1PZN	-0.42	3.65
0.8PZT-0.2PZN	-0.36	3.32
0.7PZT-0.3PZN	-0.35	3.47
0.6PZT-0.4PZN	-0.36	4.03
0.5PZT-0.5PZN	-0.34	3.68
$Na_{0.5}Bi_{0.5}TiO_3$ ceramic		
Minor Loops	-0.39	2.63

Table 4.8 (continued) Summarized scaling exponents in ferroelectric materials at room temperature

Systems	m	n
{001}-BaTiO$_3$ single crystals		
Saturated Loops	-0.195	0.95
Minor Loops	$(1.667)E_0$-2.804	4.157
BaTiO$_3$ bulk ceramic (20-100 Hz)		
Saturated Loops	-0.25	0.82
Minor Loops	-0.32	3.68
BaTiO$_3$ bulk ceramic (1-100 Hz)		
Saturated Loops	-0.39	1.06
Minor Loops	-0.55	3.40
P_r-scaling relations of BaTiO$_3$ bulk ceramic (1-100 Hz)		
Saturated Loops	-0.18	0.47
Minor Loops	-0.43	1.73
E_C-scaling relations of BaTiO$_3$ bulk ceramic (1-100 Hz)		
Saturated Loops	-0.33	0.46
Minor Loops	-0.27	1.35

Table 4.8 (continued) Summarized scaling exponents in ferroelectric materials at room temperature

Systems	m	n
0.7PMN-0.3PT single crystals		
Sinusoidal waveform		
Saturated Loops	-0.21	2.64
Minor Loops	-0.27	3.72
Triangle waveform		
Saturated Loops	-0.13	2.41
Minor Loops	-0.20	3.26